# SPATIAL AND TEMPORAL SCALES OF COASTAL CURRENTS IN THE ST HELENA BAY - CAPE COLUMBINE REGION.

A thesis presented by Clive John Holden to the
University of Cape Town, for the degree of Master
of Science, March 1986.

# SCOPE

This thesis presents the results of a current meter experiment performed in the St Helena Bay-Cape Columbine region during winter 1982. The work, which forms part of the shelf dynamics programme undertaken by the Sea Fisheries Research Institute, attempts to identify the important time and spatial scales within the coastal currents and to investigate the relationship between the sub-inertial flow and low frequency variations in the coastal winds.

Oeanographic Reseacher
Sea Fisheries Rsearch Institute
Private Bag X2
Roggebaai

# CONTENTS

## NOTATION

Throughout the thesis mathematical notion are used to describe various functions. Where possible, these notation conform to that adopted by the standard reference works quoted in the text.

| | |
|---|---|
| autocovariances | $c_{1,1}(k)$ |
| cross covariances | $c_{1,2}(k)$ |
| auto correlations | $r_{1,1}(k)$ |
| cross correlations | $r_{1,2}(k)$ |
| autospectra | $C_{1,1}(f)$ |
| cross spectra | $C_{1,2}(f)$ |
| coincident spectra | $L_{1,2}(f)$ |
| quadrature spectra | $Q_{1,2}(f)$ |
| phase spectra | $F_{w,2}(f)$ |
| coherence spectra | $K_{w,2}(f)$ |
| impulse response function | $h_k$ |
| squared frequency response function | $H^2(f)$ |
| phase response function | $G(f)$ |
| degrees of freedom | $v$ |
| standerdized spectral bandwidth | $b_1$ |
| frequency | $f$ |
| Nyquist frequency | $F$ |
| maximum lag | $m$ |
| number of data points | $N$ |
| time | $t$ |
| spectral window weights | $w(k)$ |

## LIST OF MAJOR ABBREVIATIONS

| | |
|---|---|
| acf | auto correlation function |
| acvf | autocovaiance function |
| ccf | cross correlation function |
| ccvf | cross covariance function |

# 1. INTRODUCTION.

One of the principal tasks required of fisheries management is that of establishing annual fishing quotas to optimize the balance between conservation and commercial exploitation, thus ensuring perpetuity of the resource, and fostering economic stability in the fishing and linkage industries. In establishing quotas, two major problems confront management. The first is the difficulty of acquiring an accurate stock assessment. The second is in estimating the inherent variability in fish populations caused by environmental anomalies. On this issue, Bakun and Parrish (1980) illustrate some of the problems arising in trying to incorporate environmental perturbations in fisheries management models, and list, what they consider to be, the four most important physical properties imparting a decisive impact on stock recruitment. These properties are: a) horizontal advection b) vertical stability c) water temperature and d) vertical advection associated with surface convergence and divergence.

Of the above properties, horizontal advection clearly exerts the greatest influence on the range and distribution of marine plant and animal life. Consequently, it has been studied intensively in the biologically productive upwelling regions of the World's oceans and in particular in the four major eastern boundary currents (i.e., the Benguela Current off western Southern Africa, the California Current off western North America, the Canary Current off western North Africa and the Iberian Peninsula and the Peru or Humboldt Current off western South America -

Wooster and Reid 1963, Bakun and Parrish 1980). Current determination in the four regions, prior to direct current meter measurements, were derived mostly from isopycnal analysis and direct surface observation, based on data accummulated from repeated hydrological surveys, such as those obtained in the Californian system during field programmes like the California Cooperative Fisheries Investigations initiated in 1949 (Reid et al 1958). These data enabled scientists to describe the large scale circulation patterns and, where sufficient data permitted, to recognise mean seasonal variations in both the geostrophic flow and surface Ekman transport (Wyllie 1966, Hickey 1979, Parrish et al 1981). A digest of the early work undertaken in the eastern boundary currents can be found in Wooster and Reid (1963), Bakun and Parrish (1980) and Parrish et al (1983).

Beckoned by the Fisheries's needs for more detailed studies in the shallow coastal waters, the emphasis on large scale oceanic programmes took a turn during the 1960's towards small scale, geographically specific surveys and direct current meter studies, eventually culminating into such programmes as the Coastal Upwelling Experiments CUE-1 and CUE-2 off Oregon during 1972-1973 and the Coastal Upwelling Ecosystem Analysis (CUEA) studies conducted off Oregon in 1973, North West Africa in 1974 and Peru in 1977 (e.g., Halpern 1976, 1977; Brink et al 1980).

In the southern Benguela system, the urgent need for environmental information developed during the late 1940's, prompted by a dramatic boom in the west coast pelagic fishery - pilchard then being the major contributor (Clowes 1950). To secure fish and environmental statistics for management purposes, the Sea Fisheries Research Institute (SFRI) in 1950 (then Divison of Fisheries under the Department of Commerce and Industries), embarked on a programme of stock assessment and environmental monitoring, focusing particular attention on the biologically productive St Helena Bay region that lies at about 32° 40′S, some 160 km north of the Cape Peninsula, Fig (1).

The Pilchard Research Programme, like that of contemporary studies was largely based on the results of repeated ships surveys, with emphasis falling on conditions within the upper 50 m layer (Clowes 1954). Analysis of these data rendered information on the spatial distribution of the physical and chemical properties, together with an indication of seasonal trends and annual anomalies (Clowes 1954; Buys 1957, 1959; Duncan 1964; Shannon 1966, 1985 and De Decker 1970). Current measurements at this time were confined to ships observations (Clowes 1950, 1954) and drift card experiments (Duncan and Nel 1969). Consolidation of these data revealed a surface current pattern in which the direction of flow tended to follow the lines of bathymetry, being predominantly northwards during summer and southward along the inshore region during winter in response to seasonal shifts in the prevailing winds. Although, some evidence was accumulated to suggest nearshore tidal motions near Elands Bay, and local cyclonic rotation in St Helena Bay during summer months, information on the important time and spatial scales in the coastal currents was confined to that associated with seasonal features exhibited in the primary flow. This status applied equally to the sub-surface layers, where currents were mainly determined from isopynal analysis and the distribution of water properties, such as, temperature salinity and dissolved oxygen (Clowes 1954, Shannon 1966, 1985; De Decker 1970 and Bang 1973, 1976). Although generally good agreement was found between surface and sub-surface currents, the occasional summer appearence of an oxygen depleted bottom layer was interpreted as a nearshore poleward under current, identified by De Decker (1970) as the Deep Compensation Current postulated by Hart and Currie (1960) and a general characteristic of eastern boundary current systems (Wooster and Reid 1963, Parrish et al 1983).

With the deployment of moored current meters by the National Research Institute for Oceanology (NRIO) at the head of the Cape Point valley in 1978, and by the SFRI along the Cape Peninsula onward of 1980, a number of interesting feature emerged demonstrating the tremendous variability in the shelf zone on time and spatial scales beyond the resolution afforded by previous studies. Of particular interest were the display of fairly regular longshore current reversals, near the bottom, exhibiting close visual correlation with directional shifts in the local winds (Nelson 1985). These findings tended to suggest the presence of coastally trapped shelf waves similar to that observed in current meter records in each of the other eastern boundary current systems. Off Oregon, for example, detailed observations of the poleward undercurrent showed near barotropic fluctuations (Smith 1974) having an off-shore decay scale of about 15-20 km (Kundu and Allen 1976, Huyer et al 1978), a longshore coherence of about 200 km or more (Huyer et al 1975) and displaying significant correlation to changes in the local sea level and wind stress (Smith 1974). Interestingly, the study also showed that the transition in the coastal flow from the typical winter situation to the typical spring/summer regime brought about a marked change in the shelf wave characteristics, decreasing its off shore scale (Huyer et al 1978) and causing the dominant barotropic mode to change from first to third mode (Hsieh 1982). Shelf waves with periods of between 5 and 10 days, in response to variations in the wind were also evident off North West Africa, (Badan-Dagon 1980). Moreover, periodic events of between 5 and 7 days occasionally appear independently of the wind (Mittelstraedt 1983). Huthnance (1978), in applying his model of continental shelf waves to the region found that the effect of topography and stratification combined to produce predominantly barotropic waves, with energy concentrated over the upper slope and shelf. In contrast to the Californian and North West African systems, continental shelf waves reported off Peru, during the CUEA programme, showed no correlation with local wind stress (Brink 1983). These, instead, displayed the characteristics of free internal Kelvin waves in balance with fluctuations in the longshore pressure gradient (Allen and Smith 1981). Subsequent examination of

Peruvian current meter records between 5°S and 15°S by Romea and Smith (1983) suggested that these fluctuations originated in the equatorial wave guide.

In addition to the possible shelf waves perturbations, the initial current meter records off the Cape Peninsula indicated significant energy contributions from inertial and sem-diurnal tidal motions. Of particular note, inertial motions were found to exist well below the surface mixed layer, demonstrating a vertical component in the inertial wave, indicative of an small increase in the local inertial frequency. During the CUEA studies of Peru, Johnson (1981) showed that intermittent inertial motions occurred in the upper 10 metres corresponding to the onset of strong wind events. A similar tendency was observed of Oregon in 1973 (Hayes and Halpern 1976, Kundu 1976), although inertial motions, there, also extended well into the sub-surface layers, more akin to the situation found in current meter data for the Benguela system. In current meter records off North West Africa, internal semi-diurnal tides were found to dominate the sub-inertial range in the near bottom layer over areas of steep topography (Horn and Meincke 1976, Fahrback 1976, Gordon 1978). From consideration of the temporal hydrographic variations, seaward of the North West African continental slope, Defant (1937) assumed the onshore propagation of large amplitute internal tides, and suggested that the breaking of these waves, further up the shelf, could cause the destruction of the coastal stratification and form a pre-requisite for upwelling (Defant 1949). Although the recent measurements of Horn and Meincke (1976) and Gordon (1978) confirm the presence of large internal tidal motions, the disruptive influence on the stratification that they cause and their importance in priming the region for upwelling is uncertain (Brink 1983).

In response to the current meter work along the Cape Peninsula and the developments observed in the other eastern boundary currents, the Sea Fisheries Research Institute began a programme of current meter experiments in the St Helena Bay-Cape Columbine region in winter 1982, in line with Fisheries management objectives. The first experiment, reported here, utilized three current meter moorings, instrumented at 25 m and 100 m, deployed approximately along the 180 m isobath, close to the inner shelf break. Although these mooring were maintained in position for three months, poor batteries resulted in data returns of between only 14 and 53 days. Concurrent meteorological measurements covering this period were obtained from the SFRI's automatic weather station, situated at Stompneus Point on the northern tip of the Cape Columbine peninsula.

The principal objectives of this work were to identify the important time and spatial scales in the coastal currents, to describe their physical characteristics, and to observe whether or not a functional relationship exists between the sub-inertial flow to local wind stress.

This thesis presents the results and interpretations derived from the winter 1982 experiment. In attempting to do so, substantial application has been made of the various time series analysis techniques available for oceanographic use. These techniques, which include rotary spectral analysis and complex demodulation, together with digital filtering, are presented below in Chapter 2. Chapter 3 covers the issue of data acquisition and, with regard to the current records, two important aspects of data quality, namely the effect of mooring motion and instrument tilt. The processed data and results of the spectral analysis are presented in Chapter 4. Here, the data from each mooring are first analysed individually to determine the important time and vertical scales motion at the three different locations. This is followed by a coherence and phase anaylsis between current meters at the outer moorings to establish a measure of the horizontal scales involved in the low frequency flow. Concluding the section is a cross analysis of winds stress and currents at the northern most site. In the Discussion, which forms Chapter 5, the results and a description of the individual processes identified in the previous section, with further analysis where necessary to highlight important features, are presented. In closing the discussion, the work is examined to see to what extent the original objectives have been met, and in which areas future research effort is required.

# 2. DATA ANALYSIS TECHNIQUES.

## 2.1 Digital filtering.

It is often desirable to filter out certain frequency components from the data either to avoid aliasing, or to visually enhance certain features of immediate interest. This can generally be accomplished by using one of the family of linear digital filters, as for example, the difference filter (high-pass) or the three point running mean (low-pass). These and other simple filters are easy to apply and have extensive application wherever time series observations are encountered. Ideally, we would like the filter to remove all unwanted frequencies, leaving the phase and amplitute of the remaining components unaltered. In practice this cannot always be achieved although the condition may be closely approximated for filters with a large number of weights (Bloomfield 1976).

## 2.2 The frequency response function.

Before applying a digital filter to data, it is first necessary to examine the frequency response function. This curve shows which group of frequencies will be removed and the degree to which the filter will taint remaining components. Chatfield (1980) shows that if we consider a series of observations $x_t$ taken at equal time intervals, then a new series $y_t$ can be formed from the linear transformation of the set$\{x_t\}$.

$$y_t = \sum h_k x_t \quad \ldots\ldots\ldots\ldots\ldots\ldots\ldots\ldots\ldots\ldots \quad 2.2.1$$

where the summation is performed over a finite number of weights $h_K$.

The frequency response function H(f), or transfer function as it is sometimes called, is then defined by

$$H(f)=\sum_{k} h_{k} e^{-2\pi i f k} \tag{2.2.2}$$

H(f) is a complex function having real and imaginary parts and can thus be expressed in the form

$$H(f)= G(f)e^{i\phi} \tag{2.2.3}$$

where G(f) is the gain function and $\phi$ is the phase shift.

If k is odd, then

$$H(f)= \sum_{k} h_{k}\cos(2\pi fk) \tag{2.2.4}$$

$$= G(f) \tag{2.2.5}$$

and there is no phase shift. Filters with this property are known as symmetric filters. In the analysis ahead, symmetric filters are used exclusively.

## 2.3 The cosine-Lanczos filter

A filter that has gained favour among oceanographers in recent years is the cosine-Lanczos filter (Lanczos 1961). Though fairly complicated in appearance, the filter is easily tuned to meet the user's demands and, for a sufficiently large number of weights, has a response function that closely approximates that of the ideal filter. The overshoots on either side of the transition band (the Gibb's phenomena) associated with this type of filter are greatly supressed by the cosine taper. The algorithm for the filter weights V is given by

$$V_{k}= U_{k}/(1+2\sum_{i=1}^{M-1} U) \tag{2.3.1}$$

where

$$U_{k}= t_{k}(\sin(\pi Fk)/F\pi k) \; ; \quad t = 0.5(1+\cos(\pi k/m)) \qquad k=0,1\cdots M-1$$

m = the number of filter weights in one wing, including the central weight; and F is the frequency of the quarter power point measured in Nyquists (Schumann 1976).

## 2.4 Removal of linear trend.

One of the pre-requisits for good spectral analysis is that the data should be rid of linear trend (Jenkins and Watts 1972). Although this may be accomplished in a number of different ways, it is, perhaps, best achieved using the method of least squares. In this approach, a best-fit line, having the form

$$Y=a_0 +a_1 X \quad \ldots\ldots\ldots\ldots\ldots\ldots \quad 2.4.1$$

is fitted to the data $(y_t)$ where the coefficients are given by

$$a_0=((\Sigma y)(\Sigma x^2)-(\Sigma x)(\Sigma xy))/(N\Sigma x^2-(\Sigma x)^2) \quad \ldots\ldots\ldots \quad 2.4.2$$

and

$$a_1=((N\Sigma xy)-(\Sigma x)(\Sigma y))/(N\Sigma x^2-(\Sigma x)^2) \quad \ldots\ldots\ldots \quad 2.4.3$$

By subtraction, a new data set $\{Y_t\}$ is formed having zero trend and mean, where

$$Y_t=y_t-Y \quad \ldots\ldots\ldots\ldots\ldots\ldots \quad 2.4.4$$

To perform the above filtering operation on wind and current data, a number of computer programs were written in FORTRAN 5 (see Appendices I to V ).

## 2.5 Spectral analysis techniques.

The spectral analysis techniques applied to the data essentially follow the methods of Gonella (1972) and Brundrit (1980). Some differences, however, occur in the way that the basic spectral sets, i.e. the single and bi-variate energy densities are produced. Both Gonella and Brundrit derive these statistics by transforming the original data series over a range of frequencies. Here, the basic functions are defined in terms of the transformed auto- and cross-covariance functions as suggested by Jenkins and Watts (1972), Chatfield (1982) and others.

## 2.6 Univariate spectra.

The auto covariance function (acvf) is defined as

$$c_{1,1}(k)=1/N(\sum_{t=1}^{N-k}(x_t-\overline{x})(x_{t+k}-\overline{x})) \quad \text{for } k=0,1,2...p; \quad p<N-1 \qquad 2.6.1$$

and provides a measure of correlation between observations at different time intervals. Where parameters expressing changes in different processes are compared, as for example between temperature and pressure, the acvf is usually nomalized by dividing through by the product of the variances for each record. This produces the generally more useful statistic, the autocorrelation function

$$r_{1,1}(k)=c_{1,1}(k)/c_{1,1}(0) \quad \text{for } k=0,1,2...p; \quad p<N-1 \qquad 2.6.2$$

The smoothed spectral density function, or energy spectrum, is estimated from the transform of the truncated acvf

$$C_{1,1}(f)=2(c_{1,1}(0)+2\sum_{k=1}^{M}c_{1,1}(k)w(k)\cos(2\pi fk)) \quad \text{for } 0\leqslant f\leqslant 0.5 \qquad 2.6.3$$

where w(k) is the lag window. A similar expression for $C_{1,1}$ (f) can be found by transforming the acf. To make allowance for the fact that the precision of the $c_{1,1}(k)$'s decrease with increasing k, the acvf and the acf are smoothed by a suitable lag window w(k). A number of windows are presented in the literature, the Parzen and the Blackman-Tukey windows perhaps being the most popular. Jenkins and Watts (1972) show that provided the window has a reasonable shape, the particular choice of window is unimportant since

Bandwidth*Variance=Constant.

Chatfield (1980), however, comments that although the Parzen and Blackman-Tukey windows produce very similar results, the Parzen window has a slight advantage in that it cannot produce negative spectral estimates. The weights of the Parzen window are given by

$$w(k)=\begin{cases} 1-6(k/m)^2+6(k/m)^3; & 0\leqslant k\leqslant m/2 \;\ldots\ldots\ldots\ldots \quad 2.6.4 \\ 2(1-k/m)^3; & m/2\leqslant k\leqslant m \;\ldots\ldots\ldots\ldots \quad 2.6.5 \end{cases}$$

The spectal window is the Fourier transform of the lag window. Its properties are illustated in Table 1.

<u>Table 1.</u>

| Spectral window | Variance ratio I/N | Degrees of freedom $\nu$ | Standerdized bandwidth $b_1$ |
|---|---|---|---|
| $3/4m(\sin(\pi fm/2)/(\pi fm/2))$ | 0.539m/N | 3.71N/m | 1.86 |

There are no hard and fast rules written on how to select a suitable truncation point. A small value of m produces a spectrum with low variance, but high bias (poor resolution). If m is too small important features may be smoothed out, while if m is too large the spectrum may become erractic, creating difficulty in distinguishing between real and spurious features. Ultimately, the choice is a compromise between resolution and variance. As a rough guide, Chatfield (1980) suggests trying $m=2/(N)^{1/2}$, while Jenkins and Watts (1972) advocate taking two extreme values to get a feel for the spectrum, then suggest seeking a compromise value which produces spectral estimates that make physical sense. In real terms, this means that the number of degrees of freedom for the window should lie roughly in the range 15 to 30. After some experimentation with one of the longer current meter record containing distinct inertial and tidal frequencies, it was found that m based on 24 degrees of freedom produced a physically realistic spectral density function, with an acceptable balance between resolution and variance.

## 2.7 Confidence limits

Confidence limits for the spectral estimates are approximately distributed as $X_\nu$ , where the $100(1-\alpha)\%$ confidence interval is given by

$(\nu C_{1,1}(f))/(X_\nu \alpha/2)$ to $(\nu C_{1,1}(f))/(X_\nu (1-\alpha/2))$. ..... 2.7.1

As can be seen, the confidence interval applies to one particular frequency only. This inconvenience is usually circumscribed by plotting the spectral estimates on a logarithmic scale such that the transformed confidence interval becomes

$\log(\nu/(X_\nu(1-(\alpha/2)))$ to $\log(\nu/(X_\nu(\alpha/2)))$ .......... 2.7.2

and can, therefore, be represented by a singe vertical line.

The bandwidth is a function of the spectral window and is constant over the linear frequency range. For the Parzen window, the bandwidth is given by

$$b=1.86/m \qquad \text{2.7.3}$$

Replacing m in terms of the number of degrees of freedom (see Table 1) in (2.7.3) gives

$$b=0.5v/N \qquad \text{2.7.4}$$

With v=24 the expression for the bandwidth approximates to

$$b=12/N \qquad \text{2.7.5}$$

## 2.8 Bi-variate spectra.

The cross spectrum is the natural tool for examining the frequency relationship between two time series. Akin to the auto spectrum, it is determined by the Fourier transform of the truncated cross covariance function (ccvf)

$$c_{1,2}(k)=\frac{1}{N}\sum_{t=1}^{N-k}(x_t-\bar{x})(y_{t-k}-\bar{y}) \quad \text{for} \quad k=0,1,2...p \qquad \text{2.8.1}$$

or, if the normalized cross spectrum is required, by the transform of the cross correlation function (ccf)

$$r_{1,2}(k)= c_{1,2}(k)/(c_{1,1}(0)c_{2,2}(0)) \quad \text{for} \quad k=0,1,2...p \qquad \text{2.8.2}$$

Unlike the auto spectrum, $C_{1,2}(k)$ is a complex valued function

$$C_{1,2}(f)= L_{1,2}(f) -iQ_{1,2}(f) \qquad \text{2.8.3}$$

having real and imaginary spectral estimates. The set of real estimates are given by the coincident spectra

$$L_{1,2}(f)= 2w(0)r(0)+ \sum_{k=1}^{m} w(k)(r(k)+r(-k))\cos(2\pi fk) \qquad \text{2.8.4}$$

and the imaginary set are given by the quadrature spectra

$$Q_{1,2}(f)= 2 \sum_{k=1}^{m} w(k)(r(k)-r(-k))\sin(2\ fk) \qquad \text{2.8.5}$$

As with the auto spectra, the cross spectral estimates are smoothed using a suitable lag window based on a selected number of degrees of freedom.

## 2.9 Vector spectral analysis

If a two dimensional vector time series is resolved into a pair of orthogonal components (u) and (v), then the basic spectral sets $C_{1,1}(f)$, $C_{2,2}(f)$, $L_{1,2}(f)$ and $Q_{1,2}(f)$ can be determined for any choice of co-ordinate axes. Of these, only the coincident spectrum is invariant with axes rotation. Further invariant sets can be created, however, which fully describe the vector properties. From Gonella (1972), these further sets are

the total spectrum

$$S_T = C_{1,1}(f)+C_{2,2}(f) \quad \ldots\ldots\ldots\ldots\ldots \quad 2.9.1$$

the clockwise spectrum

$$S_- = 0.5(C_{1,1}(f)+C_{2,2}(f))+Q_{1,2}(f) \quad \ldots\ldots\ldots\ldots \quad 2.9.2$$

the anticlockwise spectrum

$$S_+ = 0.5(C_{1,1}(f)+C_{2,2}(f))-Q_{1,2}(f) \quad \ldots\ldots\ldots\ldots \quad 2.9.3$$

Together, these spectra give information about the mean spectral energy distribution and the partition of energy into clockwise and anticlokwise rotation. The total spectrum is the vector equivalent of the scalar spectral density function and gives the total energy associated with the flow at a particular frequency. The rotary spectral components are an unique property of vector analysis and provide insight into the physical processes involved. From these spectra, a number of important parameters can be derived. A measure of rotation is given by the rotary coefficient

$$C_{R_\sigma} = (-2Q_{1,2}(f))/(C_{1,1}(f)+C_{2,2}(f)) \quad \ldots\ldots\ldots\ldots\ldots\ldots \quad 2.9.4$$

or, alternatively by the ellipse eccentricity

$$\varepsilon = 1 - \left| C_{R_\sigma} \right| \ldots\ldots\ldots\ldots\ldots\ldots\ldots\ldots\ldots\ldots \quad 2.9.5$$

where the latter lies between 0 (circular motion) and 1 (unidirectional flow).

The ellipse orientation $\emptyset$, given by the equation

$$\tan 2\emptyset = (2L_{1,2}(f))/(C_{1,2}(f)-C_{2,2}(f)) \quad \ldots\ldots\ldots\ldots\ldots\ldots \quad 2.9.6$$

and the ellipse stability by

$$E = (R/(C_{1,1}(f)+C_{2,2}(f)) \; -4Q^2_{1,2}(f)) \quad \ldots\ldots\ldots\ldots\ldots\ldots \quad 2.9.7$$

where

$$R = (C_{1,1}(f)+C_{2,2}(f)) \; -4(C_{1,1}(f)C_{2,2}(f)-L^2_{1,2}(f))^{1/2} \ldots\ldots\ldots \quad 2.9.8$$

give the preferred flow direction and stability of the preferred axis. The ellipse orientation is not an invariant quantity and $\emptyset$ is measured in the clockwise sense about the y component axis as shown in diagram 1.

DIAGRAM 1.

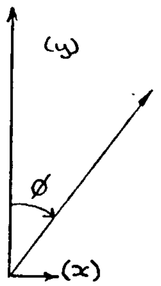

In considering the relationship between two vector quantities, two further statistics prove to be very useful. These are the vector coherence and phase functions, both of which are invariant under co-ordinate rotation. If two vectors

$w = u_1 + iv_2$

$z = u_3 + iv_4$

are considered, then the vector product takes the form

$w . z = u_1 u_3 + v_2 v_4 + i(u_1 v_4 - v_2 u_3)$ .................... 2.9.9

From this we can derive a complex sum of complex cross spectral densities that is invariant under co-ordinate rotation. For the two vectors w and z above, the sum is given by

$\overline{C_{w,z}}(f) = L_{1,3}(f) + L_{2,4}(f) + Q_{1,4}(f) - Q_{2,3}(f)$

$+ i(L_{1,4}(f) - L_{2,3}(f) + Q_{1,3}(f) + Q_{2,4}(f))$ ......... 2.9.10

Adapting the expression for coherence between two vectors, Brundrit (1980), we get

$K_{w,z}(f) = ((|\overline{C_{wz}}(f)|)/(S_\pm * S_\pm))$ ..................... 2.9.11

which is evaluated for positive and negative Q's.

The phase relationship is given by

$F_{w,z}(f) = -(|\mathrm{Im}\ \overline{C_{wz}}(f)|)/(S_\pm * S_\pm)$.

As with the auto- and cross-spectral densities, it is convenient to transform the coherence estimates to obtain a simple expression for the confidence interval which is applicable over the whole frequency range. For coherence, Jenkins and Watts (1972) suggest the transformation

$Y_{w,z}(f) = \mathrm{arctanh}(|K_{w,z}(f)|)$ ........................ 2.9.12

$= 0.5 \ln((1 + |K_{wz}(f)|)/(1 - |K_{wz}(f)|))$ .......... 2.9.13

With this transformation, the 100(1-$\alpha$)% confidence limits are given by

$Y_{w,z}(f) = \mp \eta (1 - \alpha/2)(I/2N)^{1/2}$ ......................... 2.9.14

for $v=24$

$Y_{\omega,z}(f) = \mp \eta(1-{}^{\alpha}/_{2})(0.204)$ ........................ 2.9.15

( $I/2N = 0.5*$ variance ratio. See Table 1).

Confidence intervals for the phase spectrum are more difficult to obtain than for the coherence estimator and must be calculated for each f. Therefore, for convenience, confidence intervals are often read directly from appropriate graphs, such as, that for the 95 percent confidence interval reproduced in Appendix (VI) from Jenkins and Watts (1972).

## 2.10 Complex Demodulation.

In the Fourier approach to time series analysis, it is assumed that the amplitude and phase of the constituent frequency components remain constant throughout the record. Complex demodulation, which may be thought of as a local form of harmonic analysis, is more accommodating in this sense in that it allows both the signal amplitude and phase to vary in the neighbourhood of t, (Bingham, Godfrey and Tukey, 1967), thus rendering the method useful for looking at time-vaying changes in the waveform in response to external influences.

If we consider data written in the form

$x_t = A_t \exp(i(\lambda t+\phi))$ ............................ 2.10.1

then Bloomfield (1976) shows that the extraction of $\{A_t\}$ and $\{\phi_t\}$ are trivial for all $t$. This result, he shows, holds equally true for the demodulated series, which is expressed as

$y_t = x_t \exp(-i\lambda t)$ ................................ 2.10.2

$$=A_t \exp(i\phi_t) \qquad \ldots\ldots \qquad 2.10.3$$

giving $A_t=|y_t|$ and $\exp(i\phi_t)=y_t/|y_t|$.

If, however, (2.10.1) is written as the sum of two complex terms, i.e.,

$$x_t=0.5\ A_t[\exp(i(\lambda t+\phi_t))+\exp(-i(\lambda t+\phi_t))] \qquad \ldots\ldots \qquad 2.10.4$$

and demodulated in the same way as above, then it can be simply shown that

$$y_t=0.5\ A_t\exp(i\phi_t)+0.5\ A_t\exp(-i(2\lambda t+\phi_t))+z_t\exp(-i\lambda t) \qquad \ldots \qquad 2.10.5$$

This indicates that the demodulated series not only contains information about the term in $\lambda$, but also includes the effect of the first harmonic and noise component $z_t$. In applying complex demodulation, therefore, it is essential to filter the transformed time series to remove the term in $2\lambda$ and $z_t$ before proceeding with further analysis. The width of the filter window determines the neighbourhood in which the demodulation takes place. For example, if we demodulate at f=7.6 10 cph (T=5.5 days) and it takes a filter with, say, 70 weights to remove the term in $2\lambda$, then the demodulated series will give a mean amplitude and phase for a period of 70 hours.

A number of FORTRAN 5 programs have been written to apply the spectral analysis techniques to both current and wind data. These, together with a flow chart for the analysis, are give in Appendices (VII to XVI).

# 3. DATA

## 3.1 Data aquisition.

Current observations presented in this study were obtained from a line of sub-surface moorings deployed on the continental shelf adjacent to Elands Bay, Cape Columbine and Abrahamskraal, (see Fig 2). Each mooring supported two Aanderaa RCM-4 current meters which recorded average speed, current direction, water temperature and hydrostatic pressure. Details of the instruments and moorings are summerized in Table 3.

Table 3.

| Mooring position Lat,Long | Water depth m | current meter depth m | sampling interval min | dates |
|---|---|---|---|---|
| 32 21S 17 40E | 175 | 75 | 15 | 7 Jul-24 Aug '82 |
| | | 150 | 15 | 7 Jul-27 Jul '82 |
| 32 47S 17 38E | 192 | 92 | 15 | 7 Jul-22 Jul '82 |
| | | 167 | 15 | 7 Jul-11 Aug '82 |
| 33 15S 17 45E | 170 | 70 | 15 | 7 Jul-31 Jul '82 |
| | | 145 | 15 | 7 Jul-29 Aug '82 |

Concurrent meteorological observations, in the form of hourly wind measurements, atmospheric pressure and air temperature, were obtained from the Stompneus Point weather station until 28 August '82. Supplementing this data, for interpretive purposes, were the daily synoptic weather charts produced by the South African Weather Bureau.

In addition to the above data, collected by the Sea Fisheries Research Institute, a brief record of sea surface elevations at Lamberts Bay, for the period 19 July to 24 August '82, was supplied by Beverly de Cuevas of the University of Cape Town. This data, acquired originally through the Fisheries Development Corporation, had been corrected for the inverse barometer effect in the atmospheric pressure fluctuations (Gill 1982).

## 3.2 Data processing.

The current meter and weather station data collected during the course of the experiment were processed to produce a set of time series observations suitable for visual interpretation and statistical analysis. Stage 1 entailed translating the raw data into scientific units, while various editing routines checked for data integrity and on the instrument's electrical status. In addition, current meter data were averaged to form a series of hourly observations compatible with the series of sea surface elevations and coastal winds. In stage 2, the translated data sets were plotted and inspected for any spurious points missed by the initial editing procedure. Where bad data were encountered these were over written by interpolated values. Subsequently, the cleaned up records were used to produce some elementary statistics, ie., histograms, stick vectors and progressive vector diagrams. The final processing stage entailed filtering the data to remove high frequency noise and to prevent aliasing. In order that the Nyquist and higher frequency components were attenuated, a cosine-Lanczos filter with five weights in one wing and a quarter power point of 0.375 cph (0.75 Nyquists - 1 Nyquist=0.5 cph) was chosen. The response function for the filter is given in Appendix (XVII).

### 3.3 Data quality.

Before analysing the data, the accuracy and resolution of the various instruments were considered in order to assess the precision with which the various parameters were recorded. This was achieved by examining the performance characteristics for both the current meter and the weather station sensors presented in Tables 4 and 5 respectively below.

TABLE 4 (current meter sensors).

| sensor | range | accuracy | resolution |
|---|---|---|---|
| current speed | 2.5 to 250 cm.s$^{-1}$. | ± 1cm.s$^{-1}$ or 2% of actual speed, whichever is greater | * |
| current direction | 0° to 360° degrees | ±7.5° for speeds within 2.5 to 5cm.s$^{-1}$; or 100 to 200cm.s$^{-1}$.<br>±5° for speeds within 5 to 100cm.s$^{-1}$. | 0.35 |
| temperature | -2.46°C to 21.48°C | ±0.05°C | 0.1% of range |
| pressure | 68 bar | ±1% of range | 0.1% of range |

TABLE 5 (weather station sensors)

| sensor | range | accuracy | resolution |
|---|---|---|---|
| wind speed | 0 to 76m.s$^{-1}$ | ±2% | * |
| wind direction | 0° to 360° | ±5 | * |
| air temperature | -8° to 41° C | ±0.20° C | * |
| pressure | 720 to 1070 mbar | ±0.6% FSR | 0.34 mbar |

* information not supplied by manufacturer

Diagram 2

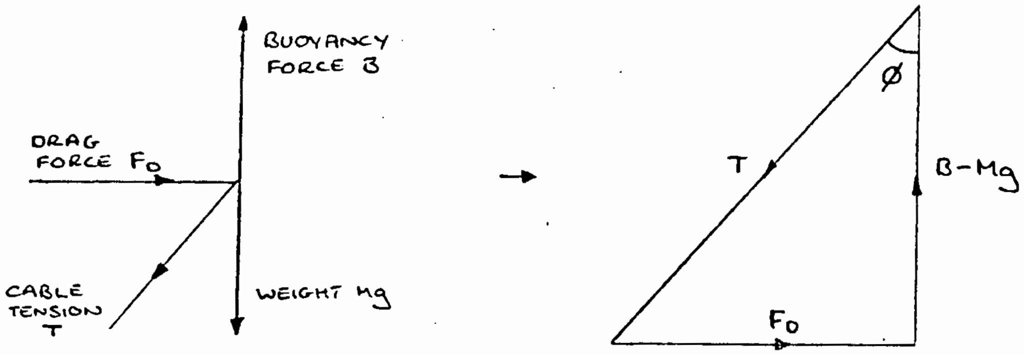

From the triangle of forces we see that

$T\cos\phi_T=B-Mg$ .................................... 3.4.1

and

$T\sin\phi_T=F_D$ .................................... 3.4.2

where T=tension along the mooring line - assumed to be constant along its length; B=the buoyancy force; Mg=the total weight of the mooring in water; and $F_D$=the hydrodynamic drag force given by the expression

$F_D=0.5p_wC_DAU^2$ .................................... 3.4.3

($p_w$=density of sea water; $C_D$=the constant drag coefficient - Knox and Session (1979) quote $C_D=2$ as a conservative estimate; A=the cross sectional area of the current meter, mooring line, flotation packages etc, perpendicular to the current; and U=the horizontal component of current speed).

By combining equations (3.4.1) and (3.4.2) we see that the wire angle $\phi_T$ is given by

$\phi_T=\arctan(F_D/(B-Mg)$ ............................ 3.4.4

Taking typical values: (B-Mg)=650 Newtons and $F_D=1500*U^2$Newtons. Equation (3.4.4) reduces to

$\phi_T=\arctan(2.31U^2)$ ............................ 3.4.5

Fig(3) shows the plot of $\phi_T$ against U for speeds in the range $0 \leqslant U \leqslant 60$ cm.s$^{-1}$. Consideration of this curve, prior to deployment, indicated that the mooring would operate effectively in currents up to about 45 cm.s$^{-1}$- the speed at which the wire angle reaches 27 degrees. Beyond this speed the current meter was expected to tilt, reaching the critical value of 12 degrees in a current of about 60 cm.s$^{-1}$.

On recovery of the mooring, a re-estimation of the wire angle was acquired empirically from the pressure sensor data and the results compared to the theoretical solution generated above. The relationship between wire angle and water pressure is demonstrated in diagram 3.

Diagram 3.

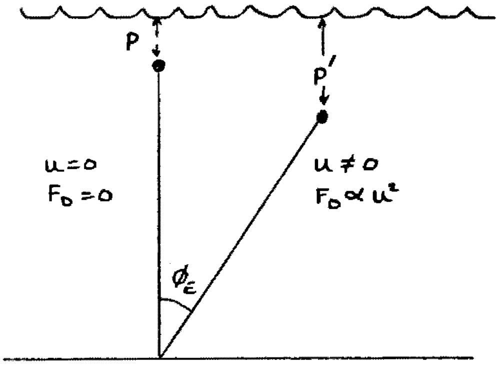

At zero current speed the instrument records a head of water h corresponding to a pressure reading P (1 dbar approximates to the height of 1 m of water). As U increases the instrument and mooring wire are deflected from the vertical and a new head of water $h' \propto P'$ is recorded, where $h' > h$. By approximating the mooring catenary to a straight line, the tilt angle $\phi_E$ can be found from

$\phi_E = \arccos(1-(h'-h)/L)$ .............................. 3.4.6

where L= the length of the mooring line.

The plot of $\phi_E$ against current speed for a short section of the upper current meter record at 32° 47'S 17° 38'E was compared to the theoretical curve in Fig(3). A least square parabola, given by

$\phi_E = 0.4 + 0.39U + 0.006U^2$ .............................. 3.4.7

was fitted to the data and clearly showed that $\phi_E > \phi_T$ for all U in the range $0 \leqslant U \leqslant 60$ cm.s$^{-1}$. Examination of the empirical results showed that at low current speeds ($<20$ cm.s$^{-1}$) the wire angle remained small, lying between 0 and 7 degrees. The fairly large scatter in $\phi_E$ in this region could be attributed to two factors. The first was due to the large fractional error in $h'-h$ given by

$\Delta h = 2*dh/(h'-h)$ .................................. 3.4.8

where dh=0.72 m (see Table 4 for resolution of pressure sensor). (Clearly, h decreases as $h'$ increases).

The second factor stemmed from the fact that $\{\phi_E\}$ were calculated from a set of discrete depths (pressures), while {U} were a set of averaged current speeds based on a process of continous sampling. As a result, it followed that the scatter depended on the level of turbulence within the sampling period and would tend to decrease with increasing current uniformity.

The clustering of points about the line over the speed range $20 \leqslant U \leqslant 50$ cm.s$^{-1}$, indicated that the mooring responded smoothly to changes in current speed. As can be seen, the critical wire angle of 27 degrees occurred at a current speed of about 42 cm.s$^{-1}$. Nevertheless, the continued clustering of points about the line at slightly higher speeds indicated that good current data could be assumed for wire angles of up to about 34 degrees ( intrument tilt of 7 degrees).

Beyond speeds of 50 $cm.s^{-1}$ the parabolic relationship between current speed and wire angle appeared to change. In this region, wire angles ranging from 31 to 43 degrees seemed to lie more along a vertical axis centered at a speed of about 55 $cm.s^{-1}$. This tended to imply that the current meter operated ineffectively at speeds over 1knot (50 $cm.s^{-1}$), with a consequent deterioration in data quality as a result. Although little practical correction could be applied to the available data sets, an attempt to reduce the wire angle of successive moorings, during periods of high current speed, was made by increasing the buoyancy of the flotation package by 25 percent.

### 3.5 Mooring motion.

The second source of error, which was considered likely to taint the quality of current data, was that of mooring line motion due to the semidiurnal tide (Knox and Sessions 1979). Visual inspection of the data at the three mooring sites indicated that maximum curent speeds associated with tidal oscillations were about 10-15 $cm.s^{-1}$. From Fig(3), it was inferred that at this speed the cable angle ($\phi_{\epsilon}$ ), at one of the upper current meters, would have been about 8 degrees. At any other depth, an estimate of the off-vertical angle could be found from the expression

$$d\phi_{\epsilon}/ds=0.5p_{w}C_{D}U^{2}D/(B-Mg) \text{ (degrees } m^{-1}) \text{ ................ } 3.5.1$$

progressive vector diagrams shown in Fig(6 and 7).

Inspection of data in the upper layer revealed a current pattern of inertial motions, semi-diurnal tides and a contingent of irregular low frequency flows. Evidence of the semi-diurnal tides appeared in both temperature and velocity records, with maximum expression occurring towards the middle and end of sampling. Inertial motions flourished during the first 20 to 25 days of recording as illustrated by the parade of anticlockwise loops in the progressive vector diagram, (see Fig 6). Their presence was equally well noted in the corresponding component series, where an especially clear example was observed between days 3 and 10 (see Fig 4). Beyond the middle of the record, their presence noticeably declined in the face of strengthening longshore flow. Current speeds associated with inertial and tidal motions were estimated to lie in the range 5 to 15 $cm.s^{-1}$, consistent with the findings of surface current studies in the region reported by Clowes (1954) and Holden (1985). The third, and by far the most pronounced signal observed, was that of a large amplitude, low frequency, oscillation with peaks at about 5, 11, 19, 26, 29, 36, 41 and 45 days. In appearance, this feature resembled a longshore wave-type motion having an average period of about 5 to 6 days. Strongest flow resulted in the equatorward direction, with speeds occasionally reaching 35 $cm.s^{-1}$. In general, currents speeds during poleward reversals remained below 15 $cm.s^{-1}$. However, one notable exception occurred on day 14 when southward speeds increased to about 25 $cm.s^{-1}$.

The associated temperature record revealed two pronounced features. The first was a very low frequency cycle with temperature fluctuations of between 10° C and 11° C degrees. The second, illustrated the daily temperature response to the semi-diurnal tides. No visual consistency was found between the low frequency temperature and currents oscillations, although certain similarities were often evident in isolated stretches of data. Clearly, in this region, noted as a site of intensive upwelling and within close proximity of the oceanic front, the undulating temperature fluctuations reflected a complex response to both local water movements and the advection and mixing of water types with remote origin. On average, tidal temperature oscillation showed an amplitude of about half a degree. However, much larger variations, as much as one degree, sometimes occurred, demonstating the temporal variability of the vertical temperature stratification.

Having acquired a brief visual appreciation of the important features in the upper layer, a more detailed examination of the velocity data followed, using the spectral analysis techniques outlined in Chapter 2. The rotary spectra, shown in Fig(8), provided a measure of the turbulent kinetic energy as a function of frequency, plotted in the range 0 cph to 0.3 cph. As expected, prominent peaks occurred at frequencies associated with the semi-diurnal tides, inertial motions and that of the longshore 5 to 6 day cycle. All three peaks were found to be statistically significant at the 80 percent confidence level, while 99 percent confidence was attached to peaks at the tidal and inertial frequencies. The 5 to 6 day cycle showed almost equal energy in the clockwise and anticlockwise spectra. Elsewhere, substantially greater energy was associated with the anticlockwise polarization, reflecting the natural tendency for currents to be deflected to the left in the southern hemisphere.

Examination of the ellipse orientation, stability and ellipticity, Fig(9), revealed that both the 5 to 6 day cycle and the semi-diurnal tides had stable preferred axes orientated at 15 and 60 degees respectively, (angles taken anticlockwise about true north). Values close to 1 in the ellipticity spectra revealed that the 5 to 6 day cycle was highly unidirectional, typical of motion generally associated with a continental shelf wave (Schumann and Perrins 1982). Semi-diurnal tidal sets were indicated as having rounded orbits, while, not surprisingly, circular motion was depicted at the inertial frequency.

Like currents in the upper layer, those measured near the bottom showed the presence of strong inertial and tidal motions superimposed on a large amplitude, low frequency, longshore oscillation, with peaks at about 5 and 12 days. Moreover, events towards the end of the record showed a rise in equatorward flow, suggesting the emergence of a third peak on day 19, corresponding to that apparent in the upper layer. On the whole, northward current speeds tended to be fractionally slower than that above, while some increase was observed during southward current reversals. This feature was more clearly evidenced in the progressive vector diagrams (see Figs 6 and 7) which showed a net southward in the upper layer. With respect to the ellipticity spectra, further similarities existed between various frequency components at the two depths. Of particular interest were the high values obtained at the 5 to 6 day cycle, again indicating predominantly unidirectional flow. In contrast, however, the ellipticity obtained for the lower tidal current suggested a substantially more circular or rounded ellipse than that observed in the upper layer.

Further details expressing the connection between the upper and lower currents followed with the examination of the cross correlation function (ccf) and determination of the vector coherence and phase relationships. The ccf was computed from equation 2.8.2 for the N/S speed components in the upper and lower layers. The cross correlogram for k=0, 1, ...., 40 is shown in Fig(12). From the graph it was established that the dominant peak occurred at k=-5. Considering the order in which the data were entered, this result indicated that certain frequency events at the bottom current meter led those above by about 5 hours. To discover whether the delay applied to the entire frequency range or to a specific frequency band only, more detailed information was elicited from the vector coherence and phase diagrams shown in Fig(13). From the coherence spectra it was noted that a high correlation existed between the series at low frequencies (-0.02 to 0.02 cph), with maximum coherence corresponding to the 5 to 6 days cycle. Strong coherence was also obtained at the frequency of the semi-diurnal tides and to a lesser extent at the inertial frequency. In all cases the coherence was statistically significant at the 95 percent confidence level. Inspection of the phase diagram showed that the two current meter records were in phase in the coherent low frequency band, signifying a predominantly barotropic motion in the sub-inertial range. At higher frequencies, a least squares fit indicated evidence of strong linear trend, with the lower currents exhibiting a constant phase lead of about 5 hours i.e., the dominant feature picked up by the ccf. As a consequence, the ccf was not considered a good tool for examining the delay between low frequency current components and, therefore, except in special circumstances (discussed later), greater reliance was placed on the use of the vector phase diagram in subsequent analyses.

### 4.2 Mooring B (32° 47'S 17° 38'E).

Only 14 days data were collected from the upper current meter at this location making it the shortest of all the records obtained. Despite its length, well defined peaks were found in the N/S current series (Fig14) at about 5 and 11 days, symbolic of the long period cycle observed at mooring A to the north. Southward current reversals dominated the record, with speeds reaching 40 $cm.s^{-1}$ . Northward flow tended to be rather slow (15 $cm.s^{-1}$) and limited to 3 short events, each lasting no more than a couple of days (see the progressive vector diagram, Fig 15). As at the more northern site, the data showed marked tidal oscillations and some indication of weak inertial motions. Temperature fluctuations over the period fell between 9° C and 10.5°C. Tidal effects typically accounted for temperature variations of about 0.5° C. But, several instances of tidally related movements occurred in which temperatures varied by more than 1°C.

Too few data were available from which to seriously quantify the energy contributions associated with tidal, inertial and lower frequency signals. Nevertheless, the rotary spectra (Fig16) did manage to convey the impression that tidal and inertial currents contributed nearly equal amounts of energy, the greater portion of which was associated with anticyclonic rotation. At extremely low frequencies, greater parity occurred between the two polarisations, with even a slight suggestion of more energetic flow associated with the clockwise component.

Axis orientation, stability and ellipticity are shown in Fig(17). High stability was indicated over a, broad, low frequency band (0 to 0.2 cph), but elsewhere rather poor values were obtained. In the stable region, the axis orientation and ellipse eccentricity showed a preference for unidirectional flow in the longshore direction typical of a coastal wave.

The near bottom current measurements extended over a period of 35 days, (Figs 18 and 19). The velocity series depicted the familiar low frequency cycle with peaks at about 5, 11, 19, and 29 days, similar to that observed at mooring A and in the layer above. Furthermore, current speeds during southward flow frequently exceeded those in the upper layer, at times reaching speeds of 50 study the relationship between the upper and lower velocity time series. Excellent coherence was obtained between the series at sub-inertial frequencies, with a maximum occurring at about 8 days. Coherence was also observed over a fairly narrow frequency band in the anticlockwise coherence spectra centered at the semi-diurnal frequency. Elsewhere, a poor correlation was observed. A least squares line fitted to the phase estimates established a gradient of about 1 hour, (corresponding to the peak in the ccf at lag k=-1). Clearly, this trend did not apply to the frequency region -0.02 to 0.02 cph. There, the phase gradient was approximately zero, implying an in phase relationship between upper and lower low frequency components. It should be noted that within this region a constant positive phase angle of about 16 degrees was obtained. The non-zero phase at f=0 arose because a small component of non-linear trend persisted in one or both of the records. No attempt, however, was made to remove this by the usual filtering techniques, as to do so would have been too costly in terms of the number of data points lost.

## 4.3 Mooring C (33° 15'S 17° 45'E).

The upper current meter at this site recorded data for a total of 23 days. Figs(23 and 24) show the times series measurements and progressive vector diagrams for the period. Inspection of the velocity components revealed strong longshore oscillations with peaks in the equatorward flow at about 5, 11, and 19 days. As found at mooring B, prolonged periods of southward flow occurred at the upper meter, with an major surge evident on day 14. Both velocity components exhibited a rather ragged band of high frequency components, providing indication of inertial motions and semi-diurnal tides. These features, as in previous cases, tended to be more conspicuous in the E/W series where lower frequency components were less obtrusive. Current speeds associated with the longshore, low frequency, flow varied considerably, ranging from 35 cm.s$^{-1}$(northwards) to 45 cm.s$^{-1}$(southwards). Despite these high speeds, an almost equal balance of northward and southward flow resulted in a net longshore current displacement of about 14 km (see Fig 24). From Fig(23) it was estimated that the upper speed limit for inertial motions lay in the region of 10 cm.s$^{-1}$. The corresponding upper speed estimate for the semi-diurnal tides proved more difficult to ascertain because of the fragmentary appearance of uninterrupted tidal sequences. After some consideration, an upper estimate of 10 cm.s$^{-1}$ was reached, based on the small group of tidal oscillations observed between days 9 and 11.

Much greater similarity appeared in the low frequency fluctuations between longshore currents and water temperatures at this site than at any sampled depth further north. A visual comparison of the current and temperature time series indicated that cold water conditions resulted during southward current reversals, while invasions of warm water appeared to be connected with Equatorward flow. The absolute temperature range spanned about 3° C, althougth the range appropriate to the low frequency response was perhaps somewhat less: closer to 1.5° C. Very large tidal temperature fluctuations occurred throughout most of the record, with associated peak to trough temperature differences of up to 3° C being recorded. On the whole, largest tidal spikes occurred during, northward, warm water flow, possibly as a result of enhanced vertical temperature stratification. Conversely, muted tidal oscillations generally appeared when the background temperatures were at their lowest.

The penalties of working with short data sets were again apparent in the rotary spectral estimates, Fig(25). Large energy contributions occurred over the narrow low frequency band, but too few data prevented the emergence of a statistically significant peak. A peak was present, however, in the anticlockwise rotary component at about 0.049 cph (20.4 hours), signifying a strong input from inertial motions, which at this latitude have a period of 21.8 hours. At the semi-diurnal tidal frequency, a rather subdued peak appeared. The apparent lack of energy caused some surprise, considering the large tidal period oscillations evident in the temperature record.

From the diagram of ellipticity, axis stability and orientation (Fig26), it was observed that stable flow was confined to currents with periods greater than a couple of days. Within the stable low frequency band, the spectra of axes orientation depicted predominatly longshore flow, while values of ellipticity indicated high directionality associated with motion typical of a coastally trapped wave.

The lower current meter functioned for 53 days, recording the longest data set of the experiment. The velocity time series (Fig 27) showed 3 prominent features. The most conspicuous of these was the ubiquitious 5 to 6 day cycle with peaks in the equatorward flow at approximately 5, 11, 19, 26, 29, 41 and 45 days (compare with the upper record at mooring A). Several long periods of southward flow occurred, the most notable being that on day 14 when speeds in excess of 40 $cm.s^{-1}$ were recorded. Bursts of speed such as this were infrequent features of both northward and southward flow. More typically, much slower speeds were recorded with only the few exceptions rising much above 20 $cm.s^{-1}$. The result of continual current switching was observed in the progressive vector diagram shown in Fig(28). Despite early domination by southward flow, a net northward current displacement of nearly 80 km had accrued by the end of the record. The two other features of note were the strong oscillations associated with inertial motions and the semi-diurnal tides.

The majority of the water temperature measurements collected at this depth ranged between 8°C and 9.5°C. Little low frequency variation was present here as in the upper layer, although temperatures did tend to decline slightly during the second half of the record. Contrary to conditions observed in the upper layer, very little evidence, if any, could be given in support of tidally generated temperature fluctuations.

Depicted by the rotary spectra (Fig 29) were peaks at about

8 days, at the inertial period and at the period of the semi diurnal tides. The low frequency cycle just emerged at the 80 percent confidence level, with the clockwise rotary component taking the ascendency. Much greater statistical confidence was attached to the two higher frequency peaks, both of which were dominated by energy levels associated with the anticlockwise spectra.

Examination of Fig(30) revealed a highly stable ellipse orientation of about -10 degrees for frequencies in the range 0 to 0.015 cph, consistent with that observed in the upper layer. Over this frequency band the flow was also found to be highly elliptic, suggesting unidirectional longshore motion. Good stability occurred at the semi-diurnal tidal frequency. Here the major ellipse axis had an angle of 63 degrees (anticlockwise about true north), while the ellipticity indicated the ellipse to be well rounded.

Once again, the relationship between the upper and lower records were examined using the vector coherence and phase diagrams shown in Fig(31). Very high coherence was depicted over the frequency range -0.02 to 0.02 cph, with a maximum at about 0.008 cph (5.2 days). At higher frequencies, coherence estimates fell dramatically, showing poor correlation at the tidal and inertial frequencies. In the low frequency band, the phase diagram indicated an in-phase relationship and predominantly barotropic conditions. Over the spectrum as a whole, however, there was a linear component with a negative slope of 3 hours corresponding to the off-set of the dominant obtained peak in the cross correlation function.

## 4.4 Longshore coherence and phase in the sub-inertial current.

In sections 4.1 to 4.3, results showed that strong coherence existed between upper and lower current measurements at sub-inertial frequencies, with maximum coherence occurring at a period of about 5 to 6 days. In addition, higher spectral estimates indicated that these fluctuations exhibited traits usually associated with costally trapped waves. To investigate the spatial continuity of these phenomenon, a coherence and phase analysis was performed using the longer current records at moorings A and C, Fig(32). As suspected from a visual inspection of the data, high coherence was depicted in the coherence spectra at a period of 5 to 6 days. Elsewhere in the spectra, poor coherence was observed.

In the coherent frequency band, the phase estimates showed a southward propagation, with a delay of 5 ±1 hours. With a separation distance between moorings of close to 100 km, the propagation speed of the wave was therefore estimated to be about $5.5 \pm 1 m.s^{-1}$.

## 4.5 Functional relationship between Stompneus Point winds and off shore currents.

Part of the original project aims was to determine to what extent sub-surface currents respond to local weather conditions.

In order to help answer this question, direct meteorological measurements, comprising atmospheric pressure, air temperature and wind velocity were obtained throughout the experiment from Stompneus Point weather station, located at the northern tip of the Cape Columbine Peninsula. These data were subsequently processed and plotted to provide a means of visual comparison with the various offshore current meter records. An initial view of the progressive wind vector diagrams, Figs(33a and 33b), showed that, during the study period, the region fell under the influence of moderate to near gale force southeasterly winds and brief northwesterlies reversals which culminated in a net north--northwest wind displacement of nearly 8 000 km. Inspection of the corresponding time series, (Fig 34), with wind velocity components resolved along conventional N/S and E/W axes, showed that a strong visual correlation existed between the low frequency winds and the changing pattern of atmospheric pressure. No such obvious connection appeared between winds and air temperature at low frequencies, but a clear similarity in the two records at the diurnal frequency was observed, providing evidence of a well developed land-sea breeze cycle.

The spectral energy distribution for Stompneus Point winds, Fig(35), depicted peaks at 12 and 24 hours. Clearly the diurnal peak reflected the energy input associated with the land-sea breeze cycle. The peak at 12 hours, however, posed slightly more problems in interpretation. Some contribution to the spectral density by atmospheric tides was expected at about this frequency, but not with the energy intensity observed (M Jury pers. comm.). Considering this, the peak was probably partly due to a contribution from the first harmonic of the diurnal cycle. In the low frequency band, no single frequency component emerged as statistically significant, albeit that a weak hump appeared at about 8 days in the anticlockwise spectra.

From the estimated spectra of ellipse orientation, stability and eccentricity, Fig(36), highly directional winds were inferred in the low frequency range zero to 0.01 cph, with the preferred axes lying between 120 and 130 degrees (clockwise about true north). At the diurnal frequency, low directional stability was encountered, implying a near circular pattern of land-sea breezes. In order to acquire a better time series impression of the low frequency wind cycle, N/S - E/W wind speeds were rotated through -55 degrees (anticlockwise), thus forming a new set of wind components with coordinate axes N'/S' - E'/W', Fig(37). (A Fortran 5 program to rotate the coordinate axes is given in Appendix XVIII). Additional improvement was provided by filtering the series still further to attenuate signals with periods shorter than 10 hours. Details of the filter window and response function are given in Appendix (XIX). The new time series revealed a more abrupt switch in the southeast/northwest wind direction and visually re-affirmed the presence of the strong, regular, pulse of the land-sea breeze. As expected, an excellent visual correlation appeared between the N'/S' wind component and the pattern of atmospheric pressure. Owing to the cleanness of both series, the phase delay between wind and pressure could be closely approximated by manually aligning the two records and noting the apparent off-set value on the time axis. In this way, wind fluctuation with periods longer than a few days were found to lag corresponding pressure variations by about 12 hours, Fig(38).

Despite the statistical absence of a dominant low frequency wind component, a comparison between winds and upper currents at mooring A showed a number of clear similarities among gross features, hinting at a possible functional relationship between the two parameters. Particularly clear was the association displayed between northwesterly wind events and the relaxation and reversals in the northward currents. Notable examples appeared at about days 14, 21, 32 and 46. To quantify the relationship, a vector coherence and phase analysis was conducted between wind stress (proportional to $|W|.W$) and current velocity V. On first attempt, poor spectral estimates were obtained owing to the presence of low frequency non-linear trend in the time series of wind stress. This problem was largely resolved by band pass filtering both data sets prior to spectral analysis (the filter window and response function is given in Appendix XX). Unfortunately, filtering created a slight problem of its own by reducing the number of data points by nearly 26 percent and, in doing so, it increased the bandwidth by about 40 percent. With trend largely suppressed, the resulting coherence spectra (Fig(39)) displayed a strong correlation at low frequencies, with a peak clearly identfied at between 4 and 8 days. The frequency at which the peak appeared coincided with that shown to be statistically significant in the current data. High coherence between the synoptic scale winds and sub-surface currents at this frequency, therefore, clearly suggested that wind stress might have played a major role in generating the southward propagation of barotropic shelf waves, though the exact mechanism by which this occurred would need to be sought elsewhere.

The phase relationship between wind stress and currents was derived by obtaining the gradient of the phase diagram within the coherent frequency band. Using the method of least square, winds events were found to lag behind those exhibited in the current record by approximately 5 hours. In contrast to the relatively smooth phase relationships encounted previously for currents, phase angles between wind stress and currents in the coherent band were less well behaved. This apparent non-linearity, together with the broad bandwidth, inevitably casted doubt on the accuracy of the interpretation. Thus, to gain better faith in the result, the phase relationship was alternatively approximated by filtering out all the high frequency components in the original data and computing the cross correlation function between the N/S currents and the N'/S' wind stress, Fig(40). (The filter window and its response function are given in Appendix XXI). With all periods beyond about 5 days suppressed, it was assumed that the position of the peak in the ccf would give the time delay between the dominant low frequency components i.e., the 5 to 6 day cycle. Consequently, the appearence of a peak at k=-5 indicated that the interpretation of the phase diagram was indeed correct.

The coherence and phase analysis established a significant statistical relationship between the current, wave-type, oscillations and local winds. To examine this connection in the time domain, both the N/S current and the N'/S' wind stress components were demodulated at 0.0076 cph (approximately 5.5 days) using the complex demodulation technique described in section 2.10, Fig(41). As seen, three distinct periods emerged in the demodulated wind series in which the amplitude of the 5.5 day cycle showed a substantial increase, with local maxima forming at about 14, 21 and 32 days. The corresponding series for the demodulated N/S current component showed slightly more structure and a visible, overall, lead of several hours. A comparative look at the rotated time series of winds (Fig 37) and the daily weather maps (South African Weather Bureau) showed that during periods of low amplitude in the 5 to 6 day cycle, as for example on days 17, 27 and 34, southerly to southeasterly winds prevailed, associated with the, dominant, regional influence of the South Atlantic high pressure cell, Fig(42). In terms of the sub-surface current response at mooring A, Fig(4) showed that these periods were synomynous with a rapid increases in northward flow. Conversely, wind reversals were clearly associated with the three main periods of maximum amplitude in the demodulated series. During each of these periods, the northward currents abated and a spell of southward flow subsequently ensued. Consideration of the synoptic weather conditions accompanying these occasions, Figs(43 to 45) unaminously revealed northwesterly winds along the west coast associated with the procession of frontal systems which penetrated deep into the sub-tropical zone. Elsewhere in the current record, lesser perturbations in the northward current relaxation could be tied to weaker frontal systems propagating at more southerly latitudes and occasionally to wind conditions accompanying the occurrence of low pressure troughs.

# 5. DISCUSSION.

## 5.1 The St Helena Bay-Cape Columbine experiment.

Since 1950, various studies have been conducted to examine the possible linkages between commercial fish stock fluctuations and environmental variability. In the beginning, environmental studies focused on the routine acquistion of hydrological data in areas of commercial interest. Information obtained from ships stations, revisited monthly over a period a many years, slowly evolved into rudimentary time series, illustrating some of the important time and spatial scale events comprising the Benguela system.

An area that received particular attention was that surrounding St Helena Bay, Elands Bay and the Cape Columbine peninsula. Here, seasonal and annual fluctuations in the water characteristics became the topic of a number of publications (e.g., Clowes 1954; Buys 1957, 1959; Duncan 1964; Shannon 1966, 1985 and De Decker 1970), generating a better awareness of the tremendous variability existing there.

Direct current measurements throughout the 1950's and early 1960's were confined to ships' drift observations and drift card experiments. In the lower layers, water movements were inferred from isopycnal analysis and the distribution of water properties, such as, temperature, salinity and dissolved oxygen. Together, these methods presented a unified picture of generally northward flow parallel to the bottom contour during summer, and current reversals close inshore during winter. On a local scale, some evidence accrued suggesting a cyclonic eddy within St Helena Bay, while the restricted appearance of oligoxic bottom water, along the coast in summer, was taken to indicate the intrusion of a poleward undercurrent (De Decker 1970).

During the 1970's, renewed scientific interest in the coastal dynamics saw a resurgence in current measurements, with current meters being used along the peninsula and at the mouth of Saldanha Bay for the first time. Near bottom currents from the head of the Cape Canyon were of particular interest as oscillatory longshore flow was described, with currents and surface wind generally showing close visual correlation. In 1980, the SFRI commenced a programme of current metering off the Cape Peninsula to the south and observed much the same results. In the light of these findings, it was decided to take a much closer look at the current characteristics in the St Helena Bay region, and to attempt to re-evaluate the important time and spatial scales of motion inherent in the coastal flow. The results of this study, performed in winter 1982, forms the contents of this thesis.

In considering the suitability of various current meter sites, cognizance was taken of the scientific merits of the proposed locations, together with the need to avoid areas of hazardous topography and intense fishing activity. Consultation with Prof Dingle of the Department of Geology (UCT) lead to the belief that boulderous conditions along the Cape Columbine peninsula, inshore of the 100 m isobath, would imperil mooring recovery. Subsequently, discussions with the major fishing companies, further established that mooring safety in the near shore region (<100 m depth), within St Helena Bay, would be jeopardized by the purse-seine fishing fleets, while beyond the 200 m contour, trawling was envisaged to be an even greater threat. In heeding this advice, the area in which current meter moorings could be deployed and recovered with relative safety was narrowed to a longshore corridor demarcated by the 100 m and 200 m isobaths. At its narrowest point, west of the Cape Columbine peninsula, this corridor barely measured 10 km in width.

In July 1982, three current moorings were deployed along the 180 m contour, within the decreed safety zone, at sites west of Elands Bay, Cape Columbine and Abrahamskraal. Each mooring comprised two Aanderaa RCM-4 rotor-and-vane-type current meters equipped to record current speed and direction, water temperature and hydrostatic pressure. The current meters were attached to the mooring line at 25 m and 100 m from the bottom, each being set to record at 15 minute intervals. Although nearly three months of data were originally anticipated, poor batteries resulted in a recovery of much shorter record lengths of between 14 to 53 days. On collection, data were translated from voltage outputs to scientific units, edited and subsequently averaged to form a time series of hourly incremented values. Readings of hydrostatic pressure enabled mooring motion and instrument performance to be evaluated, thus giving some indication of the data quality, and to provide confidence in the interpretive results.

Mooring motion, associated with the periodic forcing of the semi-diurnal tides, was found to produce errors in current speed measurements of about 0.2 $cm.s^{-1}$, well within the accuracy of the speed sensor (1 $cm.s^{-1}$). Examination of the mooring line inclination, on the other hand, showed that excessive wire angle and resulting instrument tilt occurred at current speeds above about 50 $cm.s^{-1}$ , raising doubt about the accuracy of speed measurements exceeding 1 knot. Fortunately, such conditions were confined briefly to mooring B (32° 47′S 17° 38′E), on day 14 and, as such, were considered unlikely to have a marked effect on the ensuing analysis and interpretation. Indeed, the major dissatisfaction in the data was confined to the brevity of the records.

In conjunction with the current measurements, hourly winds, air temperatures and atmospheric pressures were acquired from the Sea Fisheries Research Institute's automatic weather station at Stompneus Point, situated at the extreme northern tip of the Columbine peninsula. These data, as for currents, were subjected to critical editing and pre-analysis preparation. Coastal sea surface elevations, corrected for atmospheric pressure, were subsequently obtained from B. de Cuevas of the University of Cape Town. Where appropriate, recourse was made to hydrological data collected in the region by the SFRI.

## Outline of objectives.

The current metering experiment in the St Helena Bay - Cape Columbine region was planned with three scientific objectives in mind. These were:

a) to determine the important time scales in the coastal currents, and to identify the physical processes that related to these time scales.

b) to estimate the vertical and horizontal coherence in the coastal flow, thus yielding typical spatial scales associated with the prominent advective processes identified in (a).

c) to determine the extent to which the sub-inertial currents respond to synoptic scale weather events.

## 5.2 The determination of the important time scales using spectral analysis techniques.

Quite often, the periods of individual current components can be visually estimated from a time series by averaging the time taken between successive peaks or troughs. This technique works well when applied to fairly 'clean' records that contain one or two dominant signals. More often, however, the problem of separating the important frequency contributions from the miscellany of background noise is one that requires assistance from a branch of statistics called time series analysis.

Time series analysis may be divided into main categories: harmonic analysis and spectral analysis. The former is essentially Fourier analysis applied to discrete data, and is the natural tool for examining periodic components. In contrast, the latter, comprising the conventional Fourier method (Jenkins and Watts 1972), the maximum entropy method (MEM) (Anderson 1974) and the maximun likelihood method (MLM) (Lacoss 1971) is the more appropriate technique for examining non-periodic functions. Usually, a record will contain both periodic and aperiodic events, and the choice of which technique to use will, therefore, hinge on the particular information required. Of the different spectral analysis techniques, the conventional method, described in some detail in Section 2, is by far the most flexible and widely used. It is, however, worth noting that the other methods (MLM and the MEM) do have certain advantages in dealing with very short records, i.e., where less than about ten complete cycles are present.

The basic spectral sets used in the vector analysis of current and wind data, throughout this thesis, comprise the Total and the Rotary spectral density functions, all of which are invariant under coordinate rotation. The total spectra provides an estimate of the total variance (mean kinetic energy) at each frequency in the range $0>f>0.5$cph, while the rotary spectra partitions the total energy into clockwise and anti-clockwise components, indirectly providing information about the manner in which the current (or wind) vector rotates, and extending insight into the physical processes it describes. To appreciate the value of the analysis, however, we have to be constantly aware of the technical limitations imposed by the sampling interval and the record length. At the top end of the spectrum, no information is possible about frequencies greater than $1/2\Delta t$, (the Nyquist or Folding frequency). For hourly readings, therefore, the highest frequency component that can be described is f>0.5 cph. The problems that arise from working with a finite record length are a little more complicated due to the need to compromise between the bandwidth and the variance. Put simply, this means that if we narrow the bandwidth, to center on a certain frequency, we automatically increase the variance in the associated spectral estimate, and consequently reduce confidence in the peak. Alternatively, we can increase confidence in the spectral estimate by broadening the bandwidth, but in doing so we sacrifice some resolution. In practice, a balance is usually reached by choosing the number of degrees of freedom for the spectrum (Section 2.5), such that the resolution is fine enough to distinguish the known frequency components, and then tuning the bandwidth gradually until distortion in the principal peaks visibly occurs. In the analysis performed here, best overall results were realised using 24 degees of freedom. A particular case, in which only 5 degrees of freedom were used, will be covered later, when the important time scales have been established and the individual processes are discussed.

Visual inspection of the filtered time series of currents (eg., Figs 4, 18 and 27) showed intermittent evidence of semi-diurnal tides and inertial motions, together with the undulating cycle of a long period wave (5 to 6 days), prominent at all three sites. Spectra, for individual current meter records, clearly confirmed the presence of tidal and inertial motions, but only depicted the 5 to 6 day cycle with statistical confidence in the two long time series at moorings A and C (see Figs 8 and 30). Within the bounds of resolution, no other major time scales were apparent. Because of the closeness of the diurnal and local inertial frequency at mooring A, the possibility of a diurnal time scale could not be totally excluded. Although very little energy was, in fact, expected to be contributed by the diurnal tides (following the results of an harmonic analysis of tide gauge records at Lamberts Bay - B. de Cuevas and Shipley pers comm.), it was not known to what extent the near coastal flow responded to the land-sea breeze, which was apparent in the wind record (Fig 37) throughout the study.

Due to the clarity of the filtered data, the prominent time scales of motion were clearly visible in most of the records on initial inspection. The importance of the individual processes, however, remained to be quantified through the associated spectra. In all cases, the greatest energy was concentrated in the sub-inertial range, indicating a broad cascade of turbulent energy dissipation (Monin 1977). Within this range lay the 5 to 6 day cycle which tended to dominate the spectrum (where record length permitted), indicating it to be the most important component present during the study period. At the inertial and semi-diurnal frequencies, comparable energy levels were obtained at most sites, implying that these processes probably shared equal importance as advective processes.

In conclusion, therefore, it was found that there were three main time scales of motion in the coastal currents during winter

1982 that stood apart from the general broad band of low frequency flow. These were:

a) current fluctuations having a time scale of 5 to 6 days.

b) near inertial motions, with periods slightly greater than the local inertial frequency f.

c) semi-diurnal oscillations associated with the barotropic and baroclinic semi-diurnal tides.

### 5.3 Semi-diurnal tides.

Tide gauge records at Lamberts Bay and other monitoring sites along the west coast of South Africa show small tidal elevations of about 1,5 m (South African Tide Tables). Accordingly, barotropic tidal components normal to the coast must be expected to be fairly low, except near the entrance to bays and inlets where high velocities may occur. Furthermore, the fact that there is no appreciable time lag between the times of high water at sites along the west coast, indicates negligible longshore velocities. (NRIO 1976).

In view of this, very few tidal current observations have been made in this region. Clowes (1954), reported some evidence from ships' records of anticlockwise tidal sets near Elands Bay during calm weather conditions. Subsequently, NRIO (1976) attempted to investigate the magnitude of the semi-diurnal tidal currents off Cape Columbine during two consecutive days in November 1975, using drogues and a Savonius-type current meter. Weather and sea conditions at station Z (32 54,1S 17 49,9E) were reported to be favourable, permitting measurments at 5 m depths between the surface and 25 m. Results showed a pattern of weak flow, with speeds of about 10 cm.s , but no clear tidal influence. During a brief interlude of calm winds, zero currents were recorded. From these results, scientists concluded that " tidal effects may be neglected in the area (except, of course, near the entrance of Saldanha Bay)". Further north, near Hondeklip Bay, Schumann and Perrins (1982) examined current meter data at depths of 29m, 79m, 159m and 239m in 255 m of water during May-June 1981. The result of their analysis showed that currents in the inertial and semi-diurnal bands contributed substantially to the current variance of the system, causing them to remark that, "It is therefore clear that there are regions where such currents cannot be ignored".

Examination of the filtered current time series at moorings sites in the St Helena Bay - Cape Columbine region during 1982, revealed ample visual evidence of semi-diurnal tides. At mooring A, these features were particularly clear in the upper record, with tidal currents occasionally showing a total variation in the E/W component of 10 cm.s$^{-1}$and more. Similar condition were observed in the lower current records at moorings B and C. But, in the upper layers there, tidal prominence was visibly subdued, particularly at mooring B. Significantly, perhaps, this location was very close to station Z, visited by NRIO in 1975.

An estimate of the semi-diurnal frequency contribution to the total current variance was given for each record by the total energy spectra, Figs(8, 10, 16, 20, 25 and 29). All, except two, showed clearly defined peaks at the appropriate frequency: the exceptions being those for the upper time series at moorings B and C, as expected. Table (5) shows the magnitude of the spectral energy for the 12 hour and 5 to 6 day cycles, providing a comparative measure of the energy associated with the tides and the dominant current component. Also given are the ratios of the two spectral estimates and their square roots, the latter describing the ratio of the respective mean speeds.

TABLE 5.

| Mooing ID | F1 Energy at 0.008 cph | F2 Energy at 0.081 cph | F2/F1 | $(F2/F1)^{1/2}$ |
|---|---|---|---|---|
| A (upper) | 6323 | 759 | 0.23 | 0.48 |
| A (lower) | 3350 | 446 | 0.13 | 0.36 |
| B (upper) | 7516 | 459 | 0.06 | 0.25 |
| B (lower) | 26977 | 1014 | 0.04 | 0.19 |
| C (upper) | 10209 | 378 | 0.04 | 0.19 |
| C (lower) | 10544 | 609 | 0.06 | 0.24 |

Examination of the above table indicated that the semi-diurnal tides were significantly important at mooring A, with speeds approaching 50 per cent of that associated by the principal current component. Further south, at mooring B and C, this ratio dropped to between 20 and 30 per-cent, despite greater tidal energy overall at the near bottom depth (155 m). As an advective process, therefore, the semi-diurnal tides could be said to relatively strong in St Helena Bay, but relatively weak along the Cape Columbine Peninsula, relegated in importance there by the overwhelming increase in the primary flow. Whether tidal movements along the peninsula can be treated quite so dismissively in terms of their affect on the regional biology remains to be discovered.

Although, advection-wise, some doubt may exist about the transportive importance of the semi-diurnal tides along the peninsula, there can be little question about their efficacy in generating internal wave motions. This facet can be clearly seen in the upper temperature records at each mooring location, and most markedly at mooring C, where temperature variations frequently exceeded 2° C, rising to 3° C on occasions. In order to translate temperature oscillations into vertical displacements required a knowledge of the in-situ temperature gradients. Unfortunately, suitable data for this purpose were not collected during the current study period, and thus recourse was made to CTD data obtained during subsequent visits to the area in 1983 and 1984. These data were collected at different times of the year and under different meteorological conditions, thereby demonstrating temporal variation in the structure, Fig(46).

Profile A (25/02/83) showed a well stratified upper 50 m layer, with several step-like features at about 10 m intervals. Temperature in this region decreased from 16.5° C at the surface to about 11° C at the base of the thermocline. Below, water temperatures decreased uniformly at a rate of about 0.028° C.m$^{-1}$, falling to 8.5° C at a depth of 150 m. Profile B (24/05/83) depicted a well mixed surface layer of some 20 m depth, having an average temperature of about 16.2° C. Immediately below, the thermocline stretched down to about 70 m, disrupted by a single step-like feature between 40 and 50 m. Thereafter, the profile tended to parallel that of A, maintaining a constant temperature difference of about 0.5°C. Finally, profile C (30/10/84) described a well mixed, homogeneous surface layer, with a temperature of about 14.3°C, extending to a depth of 60 m.

In comparing these profiles it was noted that although quite different structures were in evidence, certain basic features remained common to all. For example, at the 150 m depth, all profiles showed water temperatures close to 9°C. This temperature was also consistently observed throughout the lower current meter record at mooring C (see Fig 27). Secondly, all profiles showed uniform stratification below the thermocline, indicating that a linear profile could be assumed between upper and lower current meters. At the surface, quite contrasting differences were apparent between profile C and profiles A and B. The high surface temperature in the latter profiles almost certainly reflected the onshore movement of the thermal front, pressed shoreward under the action of northwesterly winds - such were the wind conditions during much of the current study. Close comparison between the upper temperature records at mooring C and the profiles in Fig (46) strongly suggested that either profile A or B could, in fact, be considered typical of conditions prevailing during the study period and, as such, could be used to estimate the vertical displacements associated with the observed temperature fluctuations.

If the vertical displacements of the internal tides occurred entirely over the lower sections of profiles A or B, vertical displacements, associated with a temperature fluctuation of say $2^\circ$ C would be between 60 m and 70 m. On the other hand, if the thermocline lay close to the upper current meter - as profiles A and B strongly suggest - then contact with the upper layer would reduce the vertical displacement to about 20 m. Correspondingly, a $3^\circ$ C temperature cycle would be associated with a vertical rise and fall of about 30 m. Under these conditions we might conceive enhanced cross pycnocline exchange of microscopic biological material, with upward diffusion from the cold nutrient rich lower layer into the upper euphotic zone. Regretably, suitable temperature profiles were not available for the northern region to assess conditions at mooring A. However, in view of the commensurate levels of tidal energy at the three sites, a healthy internal wave climate could be anticipated over the entire region, the scale of vertical motion depending on the position and strength of the thermocline.

When examining the coherence and phase of the tides, it is usual to first separate the barotropic and baroclinic components, and to spatially compare the properties of the two components independently. To achieve this, use is made of the fact that the depth integral of the baroclinic internal tide is zero (Holloway 1984). Accordingly, the depth-averaged in-situ current measurements equal the barotropic component, and the residuals represent the baroclinic component. Usually, tidal sea surface elevations at the coast are due to a barotropic type of Kelvin wave, (Schumann and Perrins 1982). These waves are independent of stratification, and in narrow shelf regions are relatively insensitive to shelf topography. In contrast, the baroclinic tides depend critically on stratification and respond to small scale topographic features. Where measured tidal currents exhibit a strong time dependence, it can generally be assumed that the baroclinic tides dominate (Schumann and Perrins 1982).

In order to separate the barotropic and baroclinic tides, current measurements are required at as many depths as possible, the minimum permissible number being three. With only two current meters, the residual currents, after subtracting the depth average, are equal and opposite, and thus only represent a special case. In view of this, it was not possible to separate the two tidal components for comparative purposes, using the data collected during the study period. However, some indication of the relative importance of the barotropic and baroclinic components was attempted by band pass filtering the original data to extract the tidal signal, and then examining the time dependence of the resulting record (filter details and response function given in Appendix XXII), Figs (47, 48 and 49). (These figures show the total speed plotted along the preferred ellipse axis. Speeds take the sign of the N'/S' component, where N'/S' is the preferred axis orientation given in Section 4). Inspection showed that tidal speeds fluctuated considerably, with absolute values ranging from just a few $cm.s^{-1}$ to 10 $cm.s^{-1}$. Evidence of the barotropic tides could be seen in the pattern of springs and neaps associated with different phases of the moon. This was most clearly observed in the filtered records at mooring A (Fig 47). Further south, at sites along the Cape Columbine Peninsula, the response to the lunar cycle appeared to be generally less pronounced, permitting the baroclinic component to be detected. One such example was depicted at site B (Fig 48), where current speeds near the beginning of the record, when the moon was in its last quarter, exceeded those during the following period of spring tides. As such, no decisive conclusions about the relative importance of the barotropic and baroclinic tidal components could be reached and quantification on this issue was left as the subject for further studies.

Elliptic properties for the combined barotropic and baroclinic tides were examined at each of the three moorings to illustrate spatial differences in the vertical structure, and to draw comparisons between the longshore sites, particularly between those along the peninsula and at mooring A, further north. Spectra derived in Section 4 established the preferred direction of the principal ellipse axis, the axis stability and the ellipse eccentricity over the frequency range 0<f<0.3. Table (6) presents the relevant details for the semi-diurnal tides.

TABLE 6.

| Mooring ID | Axis orientation | Axis stability | Ellipse eccentricity |
|---|---|---|---|
| A (upper) | 59 | 0.90 | 0.78 |
| A (lower) | 62 | 0.75 | 0.46 |
| B (upper) | 175 | 0.28 | 0.37 |
| B (lower) | 40 | 0.78 | 0.45 |
| C (upper) | 178 | 0.27 | 0.74 |

|  |  |  |  |
|---|---|---|---|
| C (lower) | 59 | 0.61 | 0.19 |

By way of explanation, Eulerian measurements of rotary currents, such as tides, tend to describe elliptical current patterns. The form and orientation of the ellipse is, therefore, essential to the understanding of the flow. The axis orientation is the angle, taken to be positive in the clockwise sense about true north, of the principal ellipse axis, giving the preferred current direction at frequency f. The axis stability ranges between 0 and 1, and broadly speaking tells us how much confidence that we can attach to the axis orientation. A stability of 1 would, by definition, indicate perfect axis stability, while 0 would signify non-directionality. Finally, the ellipse eccentricity defines the shape of the ellipse in terms of the lengths of the major and minor axes. Like the stability, the eccentricity lies between 0 and 1, with 1 indicating unidirectional flow and 0 defining a circle. Used collectively, these estimates can be used to describe particular flow characteristics, and in many cases may be helpful in interpreting the physical processes involved.

Inspection of the ellipse properties in table (6) above, showed that stable ellipse axes could be assumed in the bottom layer at all three mooring locations, with highest stability being observed at mooring B. In the upper layer, however, preferential axis orientation was exclusively restricted to the northern location. As observed, the principal tidal currents in the lower layer tended to lie between 40 and 60 degrees. Considering this feature, it is clear that, in the absence of strong cross shore currents, semi-diurnal tides could exert an important influence in the cross shelf diffusion of chemical and biological properties. This would have been particulaly true at mooring A, during the study period, where the preferred ellipse axis at both depths were predominantly onshore. Of those ellipses with stable axes, most exhibited a well rounded shape, and only tidal currents in the upper layer at mooring A exhibited anything approaching unidirectional motion.

In examining the vertical coherence and phase relationships established in Section 4, it was found that good coherence was indicated between the upper and lower tidal components at mooring A, and that the phase angles, corresponding to the clockwise and anticlockwise components, lay close to zero. Further south, at mooring B, coherence was only indicated in the anticlockwise sense, with the lower tides leading those at 80 m by about 0.6 hours. At mooring C, peaks, as such, were evident in the coherence spectra, but not at a statistically significant level.

Finally, tidal speeds in the upper and lower layers at each of the three moorings were found to be of comparable magnitude, where, in fact, slower speeds near the bottom might have been expected due to frictional retardation. Wunsch (1969) and others have shown theoretically, that tidal motion may be bottom intensified where the internal wave characteristic, or aspect ratio, given by

$$c=\pm((\omega^2-f^2)/(N^2-\omega^2))^{1/2} \quad \ldots\ldots\ldots\ldots\ldots\ldots\ldots\ldots\ldots 5.3.0$$

where N= the buoyancy frequency, see below.

equals the slope of the bottom topography. Observations of the baroclinic tides in the shelf zone off northwest Africa (Horn and Meincke 1976; Huthnance and Baines 1982), west of Florida (Leaman 1980) and off Oregon (Torgrimson and Hickey 1979) show good agreement with this prediction. To discover whether frictional losses along the study region were being offset by a process of bottom intensification, an approximation of the aspect ratio and the bottom slope were obtained at mooring C. The buoyancy frequency N, defined by

$$N=(-g/\rho \, d\rho/dz) \tag{5.3.1}$$

and re-written in terms of the temperature gradient giving

$$N=(g\mu \, \partial t/\partial z) \tag{5.3.2}$$

where $\mu$=the expansion coefficient ($\mu=1/\rho \ \partial\rho/\partial t) \simeq 2\times10^{-4}$) was estimated from the temperature profiles A and B in Fig (46).
At the lower current meter depth, N was estimated to lie between $7.5\times10^{-3}$ $s^{-1}$ and $8.2 \times 10^{-3}$ $s^{-1}$ (mean value=$7.85 \times 10^{-3}$ $s^{-1}$). Since $\omega <<N^2$, equation (5.1.0) reduced to

$$c=\pm((\omega^2-f^2)/N^2) \tag{5.3.3}$$

giving an aspect ratio of about $1.3 \times 10^{-3}$.

The slope of the bottom topography was calculated from bathymetric charts along a line bearing 60 degrees (axis orientation of the tidal current). This resulted in a slope angle of approximately $2.8 \times 10^{-3}$ degrees, indicating a super-critical ($\alpha>c$) condition (Holloway 1985), and one that was not theoretically conducive to not bottom intensification (Holloway 1985). Comparable tidal speeds at the upper and lower current meter depth, within the uniformly statified layer, therefore, seemed to suggest that bottom frictional affects were negligible at 25 m off the bottom.

## 5.4 Inertial motions.

Inertial oscillations, like those of the semi-diurnal tides, were conspicuous in the current records throughout the study period, with maximum expression being observed at Mooring A. A relative measure of the inertial energy and the importance of inertial currents as a source of local advection, with respect to the 5 to 6 day cycle (the dominant current component) is given in Table (7).

TABLE 7.

| Mooring ID | F1 Spectral estimate at 0.008 cph | F2 Spectral estimate at f | $(F2/F1)^{1/2}$ |
|---|---|---|---|
| A (upper) | 6624 | 1330 | 0.45 |
| A (lower) | 3350 | 1318 | 0.63 |
| B (upper) | 7516 | 562 | 0.27 |
| B (lower) | 26977 | 363 | 0.12 |
| C (upper) | 10233 | 1023 | 0.32 |
| C (lower) | 10544 | 372 | 0.19 |

Examination of the above data showed that the average speeds of inertial motions at mooring A were about 45 to 63 percent of the dominant current component. At moorings B and C, the percentages were rather lower (between 10 and 30 per cent), with the lowest values being recorded near the bottom, as expected. Like the tides, therefore, inertial motions were indicated to be of relatively greater consequence to the region north of the Cape Columbine peninsula.

Spectral analysis revealed that the inertial peaks occurred at slightly higher frequencies than that of the local inertial frequency f, (where $f=2\Omega\sin\phi$). Work by Day and Webster (1965), Gonella (1971), Leaman (1975), Kundu (1976) and others, have shown this to be the rule, with the measured 'near inertial' frequency $f'$ generally being higher than f by between 3 and 20 percent.

The significance of this fact can be found in the solution of the dispersion relationship for internal waves (Gill 1982). For motion with frequency f, the group velocity ($c_g$), and hence the energy flux (F), is horzontally polarized and no vertical energy propagation can occur. For true inertial motions, therefore, energy is constrained to the surface mixed layer. At the density interface, current shear between the upper and lower layers may create turbulent instability, promoting cross pycnocline mixing in the form of Kelvin-Helmholtz billows (Gill 1982). If, however, the frequency of the oscillation is greater than f (it is assumed here that $f'$ and f are both << the buoyancy frequency N), then vertical energy propagation will occur, the direction of propagation being opposite to that of the vertical component of the phase velocity vector. The relationship between the group velocity and the phase velocity is illustrated below in diagram (5).

Diagram 5

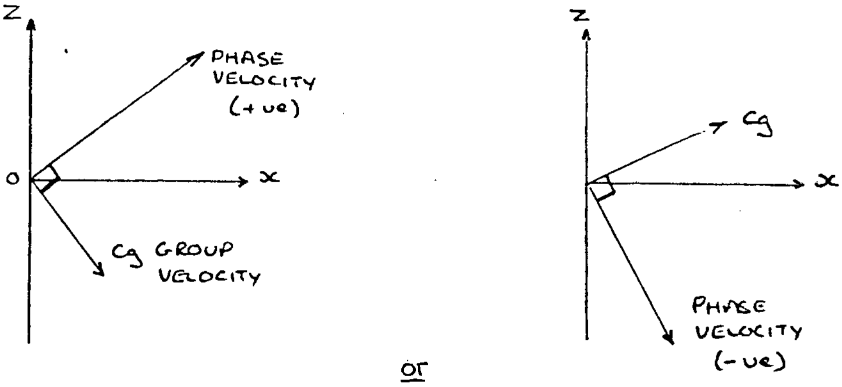

As can be seen, whether the group velocity (and hence the energy flux) has a vertical upward or downward component depends on the the sign of the phase velocity. For positive phase (z positive upwards), currents in the lower layer must lead those above. Additionally, it can also be shown that, in the southern hemisphere, a positive phase velocity is associated with anti-cyclonic motion in the horizontal plane (looking from above), (Kundu 1976, Gill 1982). From the analysis of current meter data at each of the three mooring sites, an upward phase velocity at the near inertial frequency was confirmed both by the rotary spectra (anticyclonic currents) and by the vector phase relationships shown in Figs (13, 22 and 31). Consequently, the associated vertical component of the group speed was found to be directed downwards, showing that inertial motions were able to propagate into the lower layers, and exert an influence on the near bottom flow.

In order to investigate the practical importance of the near inertial flow in the subsurface layer, it was necessary to improve on the initial estimate of $f'$. To achieve this, the spectral bandwidth was narrowed by reducing the number of degrees of freedom from 24 to 5, following the example of Kundu (1976). Unfortunately, the record lengths were just too short to achieve the sort of resolution that was hoped for, although much improvement was evident. (It should be appreciated that one of the alternative spectral techniques, such as, MLM or MEM would have been more appropriate for this purpose). At mooring A, where the inertial period is 22.37 hrs, insufficient resolution was obtained from which to separate the inertial and diurnal components. Tidal analysis of long sea level records at Lamberts Bay shows domination by the semi-diurnal constituents (pers comm B. de Cuevas UCT) and, as such, bias from the diurnal tides in the current spectra was considered to be negligible. Winds at Stompneus Point, however, depicted a strong land sea breeze cycle and a transfer of wind energy to the underlying currents would, therefore, be expected. Despite this, the analysis did show a 2 percent increase in the inertial frequency at mooring A. Furthermore, consideration of the asymmetry in the spectral peak also suggested a slight bias towards the diurnal frequency, indicating that the true shift in the inertial frequency may have been slightly greater than observed. At mooring C, control on the bandwidth was less of a problem, since the inertial period (21.82 hrs) lay sufficiently far from the influences of the diurnal cycle to avoid biasing of one by the other. At this site, re-analysis of the upper and lower time series showed a 7 percent increase in the inertial frequency, and was very close to that (8%) observed by Kundu (1976) off the coast of Oregon.

Unlike the internal tides, inertial motions were not evident in the temperature structure at either the upper or lower depths. To examine whether inertial motions could be important to the region in some other way, in particular whether they could contribute significantly to the bottom tubulence, estimations were made of the downward energy flux and compared to the turbulent production rate associated with he quasi-geostrophic flow at the bottom. To obtain this information, the phase speeds were first calculated from the vector phase diagrams presented in Section 4. At mooring A, the phase angle at the near inertial frequency was about -110 degrees, giving a phase delay in the upper layer of approximately 6.5 hours. In turn, this yielded a constant phase speed, taken over the water column separating the upper and lower current meters (75 m), of about 0.32 cm.s . From Kundu (1976), the vertical component of the group velocity was determined from the expression

$$C_g=c[(f/w)^2-1] \quad \text{..............................} \quad 5.4.5$$

where $w=f'$, giving $c=0.014$ cm.s$^{-1}$ .

In estimating the vertical energy flux, it was necessary to first calculate the ratio (R) of the potential plus kinetic energy to the horizontal kinetic energy for internal waves, using the method of Fofonoff (1969). For N>>w this ratio is expressed in the simplified form

$$R=(w^2-f^2)/(w^2+f^2) \quad \text{..............................} \quad 5.4.7$$

(Kundu 1976), giving R=0.011.

Hence, the energy density was determined using the expression

$E=(1+R)p0.5(V)^{2}$ ........................................ 5.4.8

(Kundu 1976). At the bottom current meter (25 m off the sea bed), bursts of inertial currents ranged in speed from about 8 $cm.s^{-1}$ to 12 $cm.s^{-1}$, between days 3 and 14. Therefore, taking V=10 $cm.s^{-1}$as a typical inertial speed, E was found to be approximately $5\times10^{-2}kg.m^{-1}.s^{-2}$. Finally, the downward energy flux, given by

$F=Ec_{g_v}$ ................................................ 5.4.9

was estimated to be about $0.7\times10^{-6}$ $kg.s^{-3}$.

At the bottom, the work done by the quasi-geostropic flow against the the bottom stress was calculated from

$W=V_g\tau$ .................................................. 5.4.10

where $V_g$ was taken to be the mean speed of the sub-inertial flow (V =5 $cm.s^{-1}$). With only the single current meter at 25 m off the bottom, it was only possible to obtain a crude approximation of the bottom stress τ, given by

$\tau=pu_*$ .................................................. 5.4.10

based on an empirical estimate of frictional velocity, $u_*=0.04V_g$ derived for the oceanic case by Weatherly (1972). On substituting typical values into (5.4.10) and (5.4.9), the turbulent production rate, due to the sub-inertial current, was estimated to be about $1.0\times10^{-6}kg.s^{-3}$. Bearing in mind the simplicity of the approach, the above results indicated that inertial motions could play an active role in promoting bottom turbulence, and thus, perhaps, be a contributing factor in enhancing the bottom regeneration of particulate matter in St Helena Bay.

At mooring C, a similar analysis found the downward energy flux to be nearly a quarter of that estimated at A, while the turbulent production rate associated with the quasi-geostrophic flow was found to be greater by a factor of 10. Considering the generally higher bottom current speeds associated with the longshore flow, it was, therefore, inferred that inertial motion in this region would be of mimimal importance in terms of bottom mixing.

Based on observation, the scale of vertical coherence associated with inertial motion is generally considered to be confined to a few tens of metres, (Webster 1968, Halpern 1974, Kundu 1976). Some exceptions have been noted in enclosed seas, however, where vertical coherence of more than a 1 km has been found (Perkins 1972). Vector coherence analysis described in Section 4, indicated coherence at the inertial frequency over a vertical depth of 75 m at mooring A, but not elsewhere along the peninsula, where inertial activity was less pronounced. Webster (1968) and Schott (1971) have shown that horizontal coherence typically extends over a few tens of kilometers. The spacing between moorings during the winter 1982 were thus rather too far apart to look at the this particular aspect, but it might resonably be surmised that good spatial coherence would, in fact, be the case within the sheltered region of St Helena Bay.

Finally, the relationship between inertial currents and local winds was not examined due to the lack of near surface measurements. Studies elsewhere, however, have revealed good agreement between observation and the theoretical account of the surface mixed layer based on the model of Pollard and Millard (1972). Application of this model to the surface layer in St Helena Bay was, therefore, seen as a natural extension to the above work, to be performed when suitable data becomes available.

## 5.5 The 5 to 6 day perturbation.

Thoughout the study period, current meter records at each site revealed the presence of large amplitude, low frequency, longshore perturbations at about 80 m and 150 m. The results of a rotary spectral analysis conducted on the longer time series at moorings A and C (Sections 4.1 and 4.3) showed that:

a) these oscillation had periods of about 5.5 days.

b) stable ellipse axes occurred at each site, with the major ellipse orientation tending to parallel the bathymetry.

c) current ellipse eccentricities all lay close to 1, indicating unidirectional flow, typical of that generally associated with shelf waves.

In addition, cross vector coherence and phase analysis between current measurements at each site (Sections 4.1, 4.2 and 4.3) revealed that

d) the flow was predominantly barotropic, exhibiting exceptional vertical coherence and zero phase.

While a similar analysis between current measurements at the two outer moorings (Section 4.4) found that

e) the perturbations were strongly coherent over a longshore distance of at least 100 km, and that they propagated southwards with a phase velocity of about 5.5 $m.s^{-1}$. Corresponding to the phase and period above, this indicated that the perturbations had a wavelength of about 2600 km.

Consideration of the above points, led to the belief that the 5 to 6 day current fluctuations were due to a form of continental shelf wave, generated north of the study area.

Continental shelf waves have been studied intensively since Hamon (1962) first observed that sea level fluctuations along the east coast of Australia could not be wholly explained in terms of the inverse barometer effect. This discovery quickly led to the shelf wave model of Robinson (1964), and subsequently to the wind-generated theory of Adams and Buchwald (1969). Thereafter, numerous models were developed, each exploring a particular aspect, such as, the effect of topography and stratification. The tremendous progress in this field, made during the 1970's and early 80's, is reflected in the literature reviews by Le Blond and Mysak (1977, 1978), Mysak (1980a,b), Allen (1980), and Beardsley and Boicourt (1981). Since Hamon's first observation, the presence of shelf waves has been established in most of the important upwelling regions of the World, and are particularly well documented for the Pacific coast of the American continent, i.e., off Oregon by Mooers and Smith (1968); Cutchin and Smith (1973); Kundu and Allen (1976); Huyer, Sobey and Smith (1979); and off the coast of Peru by Smith (1978); Brink (1983).

Wang (1976) broadly described shelf waves as falling into one of two categories: the baroclinic Kelvin wave (Charney 1955) and the barotropic shelf wave (Robinson 1964). The former is essentially a coastally trapped gravity wave that propagates in a stratified ocean, with a flat bottom and vertical boundary. In the southern hemisphere, waves in both categories are constrained to travel with shallow water on their left; hence shelf waves propagate polewards along the west coast of southern Africa. For a Kelvin-type wave to propagate at 5.5 $m.s^{-1}$, the shelf depth h (given by $h=c^2/g$) would need to be about 3 m. Consequently, Kelvin waves, such as, those associated with, say, a storm surge, could not be responsible for the wave-like features observed.

The second class of shelf waves are essentially quasi-geostrophic, and propagate in a homogeneous ocean with a sloping bottom. Governing their motion is the conservation of potential vorticity. Where changes in the relative vorticity arise from variations in depth, the waves are often referred to as 'barotropic topographic Rossby waves' (Wang 1976). Unlike the Kelvin-type waves, barotropic waves do not require a coastal boundary in order to propagate (Gill 1982). However, Gill and Schumann (1974) have shown that such a boundary is important for these waves to be initiated by the wind.

In order to see whether the wave-like motion, encountered during the study period, fitted in with the concept of barotropic waves, the observed wave frequency and phase were compared with that produced by the barotropic shelf wave model of Buchwald and

Adams (1968), used locally with some success by Van Foreest et al (1984), to study stationary frontal features in the Benguela Current system.

The model, based on the reduced equations of motion

$$\partial u/\partial t - fv = -g\partial \zeta/\partial x \quad \text{5.5.0}$$

$$\partial v/\partial t + fu = -g\partial \zeta/\partial y \quad \text{5.5.1}$$

and the equation of continuity

$$\partial (hu)/\partial x + \partial (hv)/\partial y + \partial \zeta/\partial t = 0 \quad \text{5.5.2}$$

makes the assumptions that a) the shelf topography is constant in the longshore direction, b) the ocean basin, beyond the shelf is flat bottomed and stretches to infinity, c) the fluid is unstratified and d) f=constant. The greatest initial difficulty in setting up the model was to provide it with a suitable topographic section. This difficulty arose because of the fairly large differences observed between typical shelf profiles along the peninsula, at B and C, and that further north in the vicinity of mooring A. The problem, however, proved to be less severe than originally envisaged. Examination of the dispersion curves, for 6 different topographic sections along the west coast (Van Foreest et al 1984, their Fig 7), showed that, at very long wavelengths, the model exhibits relative insensitivity to variations in the nearshore topography. As a result, the model was evaluated, using the program of Van Foreest (UCT) and Van Ballegooyen (NRIO), for a central topographic section, running off shore from Cape Columbine at 250 degrees to the 5000m contour, a distance of approximately 630 Km.

The truncated dispersion relationships for the first four barotropic modes are shown in Fig(50). In addition, the wave periods and phase speeds corresponding to $\lambda$ =2600 km are tabulated in Table (8).

TABLE 8.

| | Mode 1 | Mode 2 | Mode 3 | Mode 4 |
|---|---|---|---|---|
| Period (days) | 5.0 | 11.9 | 26.0 | 38.9 |
| Phase speed ($m.s^{-1}$) | 6.0 | 2.6 | 1.2 | 0.8 |

As seen, the wave period and phase speed for the first mode were in very close agreement with observation. Values associated with the higher modes, on the other hand, were substantially different and thus, it was felt, could be neglected for the purpose of this study.

Inspection of the first mode non-dimensional sea surface profile (Fig 51), showed a maximum elevation at the coast, with the gradient decreasing to zero at a distance of about 240 km off shore. Beyond, the profile adopted a slight negative gradient, the line tending towards a horizontal asymtote with increasing off shore distance. As expected, the model predicted southward setting currents over the inshore region corresponding to the shoreward rise towards the wave crest, Fig (52). (To obtain a better physical impression of the current structure, the non-dimensional N/S isotachs were scaled assuming an arbitary speed of 15 $cm.s^{-1}$ at the 180 m contour - corresponding to the position of mooring B). Although the position of the current reversal was illustrated to lie well beyond the shelf break, the sea surface slope levelled off fairly rapidly away from the coast, indicating that current measurements would be unlikely to detect southward flow much beyond 60 to 80 km. With only single moorings at each latitude, it was impossible to compare these aspects of the model with observation. However, a clear visual correlation, between longshore flow and the rise and fall of the sea surface elavation at the coast, was evident between the current record at mooring A and the filtered tide gauge measurements at Lamberts Bay (tide gauge records acquired from the Fisheries Development Corporation courtesy of B de Cuevas of UCT), Fig (53). Note the sudden rise in the coastal sea level during the period of strong southward flow centered on day 14, and the fall during peak northward flow on days 29, 39 and 48.

In applying the model to the west coast, it must be remembered that its validity (tentative as it may be) can only be assumed to hold in the inshore waters, away from the baroclinic influence of oceanic front. At the front, perennial northward flow, in the form of a baroclinic jet, would tend to mask the off shore

of the oceanic thermal front. Here, perennial northward flow, in the form of a baroclinic jet (Clowes 1954; Shannon 1966, 1985; Bang and Andrews 1974; Bang 1976), would tend to mask the off shore

influence of the barotropic waves, with complex wave interactions resulting at their confluence. When the frontal jet is taken into consideration, a more realistic off shore current profile, might look like that shown in Fig (54a). This section, drawn from the results of a current profiling experiment, undertaken off Cape Columbine in May 1983, depicts, what the author feels to be, a typical cross section of the longshore currents in that region, during the passage a barotropic shelf wave. At the coast, barotropic flow is observed, with highest current speeds inshore as prescribed by the model. Off shore, in the frontal region (see Fig 54b), baroclinic northward flow occurs, with the interface between the opposing flows rising up towards the coast. Interestingly, the slope of the interface, in this example, is closely approximated by Margules equation for geostrophic flow. In the light of above section, it would appear, therefore, that the width of the southward flow, associated with barotropic shelf waves, would be limited off Cape Columbine to the distance off shore of the front, generally noted to be between 20 and 30 km (Shannon 1985).

In Robinson's (1964) dynamical model of continental shelf waves, fluctuations in sea level were taken to be directly associated with changes in atmospheric pressure. On applying the model to both east and west coasts of Australia, Hamon (1966) found good correlation between sea surface variation and the passage of anticyclones across the coast. Subsequently, however, Adams and Buchwald (1969) showed that, in fact, wind stress formed the principal generating mechanism, and that the apparent correlation between sea level and atmospheric pressure occurred due to the direct correlation between atmospheric pressure and wind stress. Later, Gill and Schumann (1974) showed that a shallow Ekman divergence was, by itself, insufficient to generate shelf waves, since the vertical velocities induced within the deeper lower layer could not create a significant change in relative vorticity - an essential requirement for shelf waves to exist (Longuet Higgins 1968). In the presence of a coastal boundary, however, where the onshore Ekman transport is physically obstructed, an off shore flux is necessary below to maintain continuity. Under this condition, Gill and Schumann (1974) showed that sufficient vorticity could be generated within the lower layers, thus providing one mechanism for shelf wave generation. (shelf waves may also occur where currents move over varying topography). Applied to the west coast of southern Africa, it can, therefore, be expected that shelf waves might occur during sustained periods of northerly winds. Fig(55) summerises the events during winter 1982, presenting a composite picture of the concurrent time series of atmospheric pressure, N'/S' wind speed, sea surface elevation (corrected for the inverse barometer effect) and the upper N/S current speeds at mooring A. (To visually enhance the low frequency components, both wind and current time series were smoothed using the cosine-Lanczos filter described in Appendix XIX).

The weather conditions prevailing thoughout the study period were typical of winter, with northerly winds, associated with the passage of cyclones and frontal systems, disrupting a background pattern of southerly winds in circulation around the South Atlantic High. At the coast, local wind variations were in evidence due to the land/sea breeze cycle and the southward movement of coastal lows spawned off Luderitz, Namibia. The coherence and phase analysis (Section 4.5) clearly depicted a marked functional relationship between the coastally trapped waves and wind stress measured at the Stompneus Point weather station. Furthermore, the method of complex demodulation and inspection of the daily weather bulletins firmly established a real time correlation between the shelf waves and northerly winds occasioned by approaching cold fronts. As such, it is perhaps fair to conclude that shelf waves are probably a perennial feature in the west coast shelf dynamics, reaching maximum expression in winter when frontal systems are most energetic at sub-tropical latitudes. The average period with which the frontal systems brush the continent is frequently quoted, from Preston-whyte and Tyson (1973), to be between 3 and 6 days. Brief observations of weather station data collected by the Sea Fisheries Reseach Institute (unpublished data), however, suggest that 3 to 10 days might be a more general estimate, thus indicating the occurrence of shelf waves within the study area on a similar time scale.

The phase relationship between currents and wind stress (Section 4.5) showed that shelf waves in the study area moved ahead of the winds by about 5 hours. As such, this placed the minimum generation point about 100 km north of mooring A. In considering the spatial scales associated with the frontal systems involved, it is probably more reasonable to expect the source, or sources, of wave generation to lie considerably further north than this. In fact, sea level records collected during October 1983, show southward propagating waves travelling from Walvis Bay on the west coast of Namibia to Gansbaai on the south coast of South

Africa (Brundrit et al 1984). In addition, Hagen (1985) has reported evidence of barotropic shelf waves having a 5 day period at latitude 20.5 S. Consequently, these observations indicate that shelf waves along the west coast are likely to have spatial scales concomitant with that of the driving weather systems.

The close correlation observed between synoptic weather events and coastal currents on sub-inertial time scales provides hope for a future model of a wind driven coastal circulation for the west coast of South Africa. To date, a number of models have been developed and used to describe some of the important current features apparent in the Bengela Current system (Van Foreest and Brundrit, 1982, 1983a, 1983b, 1985). Considering the results of the present work, it would seem resonable to suppose that a more sophisticated model may be evolved in the future to accommodate shelf waves in the near shore region during periods of northerly winds. Before this can be properly considered, however, much work has to be done to improve our understanding of how shelf waves are generated in the region and to what extent they can be described by contemporary modelling techniques.

## 5.6 Fulfilment of research objectives.

The study objectives set out at the beginning of this work were to determine the important time and spatial scales in the coastal currents within the St Helena Bay - Cape Columbine region during winter 1982 and, in addition, to investigate the response of the lower water column to synoptic scale weather events. Using time series analysis techniques, three important time scale were established, these relating to the semi-diurnal tides, inertial motions and the southward propagation of barotropic shelf waves, having a period of about 5 to 6 days. Although the shelf wave properties were fairly well descibed, due to their large vertical and horizontal coherence, insufficient data precluded the separation of the barotropic and baroclinic tidal components, leaving a fuller description of their characteristics for future study. A proper description of the vertical structure of the tides and inertial motions was also negated by the lack of data in the upper water column.

Spatial scales were examined using vector coherence and phase analysis. Good horizontal coherence between the outer mooring was established at the shelf wave frequency, thereby acknowledging a minimum spatial scale of 100 km . Evidence from other sources in the literature, however, indicated that these waves probably have a spatial scale of hundreds to a few thousand km. At the inertial and semi-diurnal tidal frequencies, good vertical coherence occurred at mooring A, but was otherwise less obvious further south at mooring B and C.

In seeking linkages between synopic weather events and currents, the study revealed a statistically significant correlation between currents, asociated with propagating shelf wave, and the northerly winds that precede the passage of cold fronts. Consequently a fairly convincing point to emerge from the study was that shelf waves could be considered to be a consistent feature of the west coast oceanography, with greatest expression in winter, when the procession of atmospheric fronts stretch far into the sub-tropical latitudes (Nelson and Hutchings 1983).

## Future work.

The current meter experiment in 1982 identifed three important time scales in the coastal currents. A detailed description of the individual flow characteristics, however, was restricted due to the inadequacies of the data. Consequently, several areas for further research can be identified to improve our knowledge of the system. Areas on which future work will focus are:

a) The semi-diurnal tides. Further measurement are required to separate the barotropic and baroclinic components, so that the vertical structure of the internal tides can be fully described. To achieve this aim, current measurements will need to be obtained at a large number of depths at selected sites. Inherent in any description of internal tides, of course, is a sound knowledge of the vertical temperature structure. Here, clearly, is an area that will need to be persued in tandum with curent measurements.

b) Inertial motions. Inertial, or more appropriately 'near inertial' motions, are generated within the Ekman surface layer in response to the wind (Gill 1982). Studies elsewhere have shown that good correspondence, between wind and inertial currents, can be achieved using a simple modelling technique. To apply this to the St Helena Bay region, current data are required in the surface mixed layer, thus necessitating the use of instruments with good cosine response in order to eliminate possible contamination from surface wave motion.

During 1982, it was established that near inertial motions were able to propagate downwards and contribute to the turbulent production rate in the bottom boundary layer. This feature needs to be examined in greater detail in order to assess the biological and chemical consequences. Near bottom current measurement within St Helena Bay are, therefore, imperative to this reaseach, as too is the need to employ alternatives to the convensional method of spectral analysis, such as MEM or MLM, in order to better resolve near inertial motions.

c) Shelf waves. The dominant contribution by barotropic shelf waves to the winter 1982 current meter records calls for further examination of these phenomenon to discover their full importance to the dynamics of the region and their consequences for the west coast fishery. Certain immediate questions need to be addressed.

1. What is the variability in the time scale for these waves? Is 5 to 6 Days a typical estimate, or should we think more loosely in terms of a couple of days to a few weeks between events?
2. What are the typical spatial scales in the longshore and off shore currents, and where are these waves generated?
3. Can an working functional relationship be established between the local winds and the southward shelf wave currents in St Helena Bay, thus forming the basis for a simple predictive model for the longshore circulation?

Some headway towards tackling a number of the above issues has already commenced. In December 1982, the Cape Columbine mooring was replaced, and has been continually updated up to the present time. Until March 1983, moorings remained in position for only 3 months. Subsequently, moorings were deployed on a 6 monthly replacement basis, returning data throughout both summer and winter periods. During summer 1984 two accompanying moorings, each carrying two current meters were deployed at shallow positions (110 m isobath) off Elands Bay and Island Point to re-examine the spatial coherence in the longshore flow over an extended northern coastal region. In addition, the siting of the coastal weather station on the Cape Columbine peninsula was moved from Stompneus Point, in the lee of the headland, to Cape Columbine where it is hoped that better representation of the marine wind field will be obtained. Although, so far, this data has yet to be properly analysed, preliminary findings look encouraging, with barotrpic wave-like perturbations having been detected in both summer and winter seasons.

With reference to tidal and inertial motions, a single mooring supporting 4 acoustic current meters was put into service west of Elands Bay in October 1984 to examine the vertical structure of these two important processes. Data from this experiment remains to be analysised.

In conclusion, therefore, data collected during winter 1982 showed the St Helena Bay - Cape Columbine area to be dynamic region, characterised by local and remotely forced physical processes, each playing an important role in determining the environmental habitat for resident and itinerant biological species. In identifying the important processes, the direction of future studies in the area has become much clearer, and a number of subsequent experiments have already begun to look at some of the individual processes in detail. With parallel work ongoing off the Cape Peninsula, and with future current metering studies planned further north at sites extending as far as the Walvis Ridge, a comprehensive description of the coastal currents along the west coast of South Africa is, therefore, envisaged for the not too distant future. Armed with this information, physical and biological oceanographers can look forward to gaining a better insight into some of the complex movements and variations in the pelagic stocks which collectively comprise one of South Africa's most valuable re-newable resources.

## ACKNOWLEDGEMENTS

The work comprising this thesis resulted from the Sea Fisheries' coastal dynamics research programme undertaken in the St Helena Bay - Cape Colunbine region in 1982. I am, therefore, grateful to the Director of the Sea Fisheries Research Institute for permitting the results of this work to be presented to the University of Cape Town for examination. Sincere thanks are also extended to Dr L.V. Shannon for his encouragement and support throughout the entire project and to VISCOR for defraying the costs of the thesis.

Special thanks are expressed to Mr C Wainman and the techincal staff at Ebenezer Road for gathering the data and to Mr G Nelson and A Polito for reading and translating the instrument tapes. I am particularly indebted to Professor G Brundrit for his patience and guidence thoughout the analysis and writing of this work and to Dr Van Foreest (UCT) and Mr Van Ballegooyen (NRIO) for permitting me the use of their computer program to evaluate the dispersion relationships for barotropic shelf waves.

Last, but not least, i would like to thank my immediate colleagues and friends for their support and useful discussions, particularly for their assistance during the writing of the computer softwear for spectral analysis. In this regard, i am equally grateful to those in the Electronic Data Processing section, at Foretrust House (SFRI), for the prompt technical backup that was provided at all times.

## 6. REFERENCES.

ADAMS, J.K. and V.T. BUCKWALD 1969 - The generation of continental shelf waves. J. Fluid Mech., 35, 815-826.

ALLEN, J.S. 1980 - Models of wind-driven currents on the continental shelf. Annu. Rev. Fluid Mech. 12, 389-433.

ALLEN, J.S and R.L. SMITH 1981 - On the dynamics of wind-driven shelf currents. Philosophical Transactions of the Royal Society of London, A 302, 617-634.

BADAN-DANGON, A.R.F. 1980 - On the dynamics of subinertial currents off Northwest Africa. Ph.D. dissertation, Oregon State University, 167 pp.

BAKUN, A and R.H. PARRISH 1980 - Environmental inputs to fisheries population models for eastern boundary current regions. In Proceedings of the Workshop on the Effects of Environmental Variations on the Survival of Larval Pelagic Fishes, Lima, Peru, April-May, 1980. UNESCO Paris; IOC Workshop Report 28, 67-104.

Bang, N.D. 1973 - Characteristics of an intense ocean frontal system in the upwell regime west of Cape Town. Tellus, 25, 256-265.

BANG, N.D. 1976 - CSIR/NRIO, S. Afr., Internal General Report SEA IR 7616, 14 pp plus 4 pp figures

BANG, N.D. and W.R.H. Andrews 1974 - Direct current measurements of a shelf-edge frontal jet in the southern Benguela system. J. Mar. Res. 32, 405-417.

BEARDSLEY, R.C. and W.C. BOICOURT 1981 - On estuarine and continental-shelf circulation in the Middle Atlantic Bight. In "Evolution of Physical Oceanography." (B.A. Warren and C. Wunsch, eds), Chapter 7. MIT Press, Cambridge, Massachusetts.

BLOOMFIELD, P. 1976 - Fourier Analysis of Time Series: An Introduction. New York, Wiley.

BINGHAM, C., M.D. GODFREY and J.W. TUKEY 1967 - Modern techniques of power sectrum estimation. IEEE Trans. Audio Electroacoust. AU-15, 56-66.

BRINK, K.H. 1983 - The near-surface dynamics of coastal upwelling. Prog. Oceanog. 12, 223-257.

BRINK, K.H., D HALPERN and R.L. SMITH 1980 - Circulation in the Peruvian upwelling system near 15 S. J. Geophys. Res., 85, 4036-4048.

BRUNDRIT, G.B. 1980 - Time series analysis of vector current measurements. In Proceedings of the Workshop on digital time series analysis with geophysical applications April 22-24, 1980. CSIR Report S238, 189-199.

BRUNDRIT, G.B., B. de CUEVAS and A.M. SHIPLEY 1984 - Significant sea-level variations along the west coast of southern Africa 1979-83. S. Afr. J. Sci. 80(2), 80-82.

BUCHWALD, V.T., and J.K. ADAMS 1968 - The propagation of continental shelf waves. Proc. Roy. Soc. London, A305, 235-250.

BUYS, M.E.L. 1957 - The South African pilchard (Sardinops ocellata). Temperature variations in the upper 50 metres in the St Helena Bay area, September, 1950-August, 1954. Investl Rep. Div. Fish. S. Afr. 27, 114 pp.

BUYS, M.E.L. 1959 - The south African pilchard (Sardinops ocellata) and maasbanker (Trachurus trachurus). Hydrological environment and the commercial catches, 1950-57. Investl Rep. Div. Fish. S. Afr. 37, 176 pp.

CHARNEY, J.G. 1955 - The generation of ocean currents by wind. J. Mar. Res. 14, 433-498.

CHATFIELD, C. 1980 - The Analysis of Time Series: An Introduction. London: Chapman and Hall.

CLOWES, A.J. 1950 - An introduction to the hydrology of South African waters. Investl Rep. Fish. mar. biol. Surv. Div. S. Afr. 12, 42 pp plus 20 pp. of charts.

CLOWES, A.J. 1954 - The South African Pilchard (Sardinops ocellata). The temperature, salinity and inorganic phosphate content of the surface layer near St Helena Bay, 1950-52. Investl Rep. Div. Fish. S. Afr. 16, 47 pp.

CUTCHIN, D.L. and R.L. SMITH 1973 - Continental shelf waves: Low-frequency variations in the sea level and currents over the Oregon continental shelf. J. Phys. Oceanogr., 3, 73-82.

DAY, C.G. and F. WEBSTER 1965 - Some current measurements in the Sargasso Sea. Deep Sea Res., 12, 805-814.

DE DECKER, A.H.B. 1970 - Notes on an oxygen-depleted subsurface current off the west coast of South Africa. Investl Rep. Div. Fish. S. Afr. 84, 24 pp.

DEFANT, A. 1937 - Die Troposphare des Atlantischen Ozeans. Wiss. Ergebn. Dt. Atlantic. Exp. "Meteor" 1925-1927, VI, 1, 289-411.

DEFANT, A. 1949 - Uber interne Gezeitenwellen und ihre Stabilitatsbedingunggen. Arch. Met. Geophys. Bioklim. A, 1, 39-61.

DUNCAN, C.P. 1964 - Seasonal occurrence of thermoclines off the South-West Cape, 1955-61. Investl Rep. Div. Fish. S. Afr. 50, 15 pp.

DUNCAN, C.P. and J.H. NELL 1969 - Surface currents off the Cape coast. Investl Rep. Div. Fish. S. Afr. 76, 19 pp.

FAHRBACH, E. 1976 - Einige Beobachtungen zur Erzeugung ung Ausbreitung interner Gezeitenwellen am Kontinentalabhang vor Sierra Leone. "Meteor"-Forsch. Ergebn. A, 18, 64-77.

FOFONOFF, N.P. 1969 - Spectral characteristics of internal waves in the ocean. Deep Sea Res., 16, 58-71.

GILL, A.E. 1982 - Atmosphere-Ocean Dynamics. London: Academic Press.
GILL, A.E. and E.H. SCHUMANN 1974 - The generation of long shelf waves by the wind. J. Phys. Oceanogr., 4, 83-90.

GONELLA, J. 1971 - A local study of inertial oscillations in the upper layers of he ocean. Deep Sea Res., 18, 775-788.

GONELLA, J. 1972 - A rotary-component method for analysing meteorological and oceanographic vector time series. Deep Sea Res. 19, 833-846.

GORDON, R.L. 1978 - Internal wave climate near the coast of northwest Africa during Joint-1. Deep Sea Res., 25, 625-643.

HAGEN, E. 1985 - Meso-scale upwelling off Namibian coast. Int. Symp. Upw. W Afr., Inst. Inv. Perq. Barcelona Vol 1, 161-179.

HALPERN, D. 1974 - Observations of the deepening of the wind mixed layer in the Northeast Paccific Ocean. J. Phys. Oceanogr., 4, 454-466.

HALPERN, D. 1976 - Structure of a coastal upwelling event observed off Oregon during JUly 1973. Deep Sea Res., 23, 495-508.

HALPERN, D. 1977 - Description of wind and of upper ocean current and temperature variations on the continental shelf off Northwest Africa during March and April 1974. J. Phys. Oceanogr., 7(3) 422-430.

HAMON, B.V. 1962 - The spectrums of mean sea level at Sydney, Coff's Harbour, and Lord Howe Island. J. Geophys. Res., 67, 5147-5155; correction in 68, 4635.

HAMON, B.V. 1966 - Continental shelf waves and the effects of atmospheric pressure and wind stress on sea level. J. Geophys. Res.,71, 2883-93.

HART, T.J. and R.I. CURRIE 1960 - The Benguela Current. "Discovery" Rep. 31: 123-298.

HAYES, S.P. and D. HALPERN 1976 - Observations of internal waves and coastal upwelling off the Oregon coast. J. Mar. Res., 34, 247-267.

HICKEY, B.M. 1979 - The California Current System - hypothesis and facts. Prog. Oceanog, 8, 191-273.

HOLDEN, C.J. 1985 - Currents in St Helena Bay infered from radio-tracked drifters. in South African Ocean Colour and Upwelling Experiment. Shannon, L.V. (Ed.). Cape Town; Sea Fisheries Research Institute: 97-109.

HOLLOWAY, P.E. 1985 - A comparison of semi-diurnal tides from different bathymetric locations on the Australian north west shelf. J. Phys. Oceanogr. 15, 240-251.

HORN, W. and J. MEINCKE 1976 - Note on the tidal current field in the continental slope area off northwest Africa. Mem. Soc. R. Sci. Liege, 10, 31-42.

HUTHNANCE, J.M. 1978 - On Coastally Trapped Waves: Analysis and Numerical Calculations by Inverse Iteration. J. Phys. Oceanog., 8, 75-92.

HUTHNANCE, J.M. and P.G. BAINES 1982 - Tidal currents in the northwest African upwelling region. Deep Sea Res., 29, 285-306.

HUYER, A., B.M. HICKEY, J.D. SMITH, R.L. SMITH and R.D. PILLSBURY 1975 - Alongshore coherence at low frequencies in currents observed over the continental shelf off Oregon and Washington. J. Geophys. Res., 80, 3495-3505.

HUYER, A., R.L.SMITH and E.J.C. SOBEY 1978 - Seasonal differences in low frequency current fluctuations over the Oregon continental shelf. J. Geophys. Res., 83, 5077-5089.

HUYER, A., SOBEY, E.J.C. and R.L. SMITH 1979 - The spring transition in currents over the Oregon continental shelf. J. Geophys. Res., 84, 6995-7011.

HSIEH, W.W. 1982 - Observations of continental shelf waves off Oregon and Washington. J. Phys. Oceanog., 12, 887-896.

JENKINS, G.M. and D.G. WATTS 1972 - Spectral Analysis and its Application. San Francisco: Holden-Day.

JOHNSON, W.R. 1981 - The propagation of tidal and inertial waves in thge upwelling region off Peru. In: Coastal upwelling, F.D. Richards, editor, American Geophysical Union, Washimgton, D.C., pp79-86.

KNOX, R.A. and M.H. SESSIONS 1979 - Compact current meter moorings: design and preliminary results. Deep Sea Res. **26A**, 109-119.

KUNDU, P.K. 1976 - An analysis of inertial oscillations observed near Oregon coast. J. Phys Oceanogr., **6**, 879-893.

KUNDU, P.K. and J.S. ALLEN 1976 - Some three-dimensional characteristics of low-frequency current fluctuations near the Oregon coast. J. Phys. Oceanogr., **6**, 181-199.

LACOSS, R.T. 1971 - Data adaptive spectral analysis methods. Geophysics, 36, 661-675.

LANCZOS, C. 1961 - Applied Analysis. Englewood Cliffs, N.J.: Prentice-Hall.

LEAMAN, K.D. 1975 - The vertical propagation of internal waves in the ocean. Ph.D thesis, MIT-Woods Hole, 174 pp.

LEAMAN, K.D. 1980 - Some observations of baroclinic diurnal tides over a near-critical bottom slope. J. Phys. Oceanogr., 10, 1540-1551.

Le BLOND, P.H. AND L.A. MYSAK 1977 - Trapped coastal waves and their role in shelf dynamics. In "The Sea." (E.D. Goldberg et al., eds), Vol 6, pp. 459-495. Wiley (Interscience), New York.

Le BLOND, P.H. and L.A. MYSAK 1978 - "Waves in the ocean." Elsevier, Amsterdam.

MOOERS, C.N.K., and R.L. SMITH 1968 - Continental shelf waves off Oregon. J. Geophys. Res., 73, 549-557.

MONIN, A.S., V.M. KAMENKOVICH and V.G. KORT 1977 - In Variability of the oceans. Wiley.

MITTELSTAEDT, E. 1983 -The upwelling area off Northwest Africa - A description of phenomena related to coastal upwelling. Prog. Oceanogr. 12, 307-331.

MYSAK, L.A. 1980a - Topographically trapped waves. Annu. Rev. Fluid Mech., 12, 45-76.

MYSAK, L.A. 1980b - Recent advances in shelf wave dynamics. Rev. Geophys. Space Phys. 18, 211-241.

NELSON, G. 1985 - Notes on the physical oceanography of the Cape Peninsula upwelling System. In South African Ocean Colour and Upwelling Experiment. Shannon, L.V. (Ed.). Cape Town; Sea Fisheries Research Institute, 63-95.

NELSON, G. and L. HUTCHINGS 1983 - The Benguela upwelling area. Prog. Oceanogr. 12(3), 333-356.

NRIO, 1976 - CSIR Report C/SEA 7611, Stellenbosch, s. Afr., 15 pp plus figures and appendix.

PARRISH, R.H., C.S. NELSON and A. BAKUN 1981 - Transport mechanisms and reproductive success of fishes in the California Current. Biol. Oceanogr. 1(2), 175-203.

PARRISH, R.H., A. BAKUN, D.M. HUSKEY and C.S. NELSON 1983 - Comparative climatology of selected environmental processes in relation to eastern boundary current pelagic fish reproduction. in the proceedings of a joint FAO-IOC sponsored "Expert consultation to examine changes in abundance and species composition of neritic fish stocks", San Jose, Costa Rica, 18-29 April 1983.

PERKINS, H. 1970 - Inertial oscillations in the Mediterranean. Deep Sea Res., 19, 289-296.

POLLARD, R.T. and MILLARD 1970 - Comparison between observed and simulated wind-generated internal oscillations. Deep Sea Res., 17, 813-821.

PRESTON-WHYTE, R.A. and P.D. TYSON 1973 - Note on pressure oscillations over South Africa, Mon. Weath. Rev., 101, 650-659.

PRITZLAFF, J.A. and J.P. LANIEWSKI 1964 - Development of a self contained deep mooring buoy system. in the Transactions of the 1964 Buoy Technology Symposium 24,25 March 1964. Washington.

REID, J.L., J.R. RODEN and J.G. WYLLIE 1958 - Studies of the California Current System. Calif. Coop. Oceanic Fish. Invest., Prog. Rep., 1 July 1956 to 1 January 1958, p. 27-57.

ROBINSON, A.R. 1964 - Continental shelf waves and the response of sea level to weather systems. J. Geophys. Res., 69, 367-368

ROMEA, R.D. and R.L. SMITH 1983 - Further evidence for coastal trapped waves along the Peru coast. J. Phys. Oceanogr., (in press).

SCHICK, G.B. 1964 - Design of a deep moored oceanographic station. in the Transactions of the 1964 Buoy Technology Symposium, 24,25 March 1964. Washington.

SCHOTT, F. 1971 - Spatial structure of the internal-period motions in a two-layered sea, based on observations. J. Mar. Res., 29, 85-102.

SCHUMANN, E.H. 1976 - The routine processing and analysis of Aanderaa meter data. NRIO Internal General Report, SEA IR 7624.

SCHUMANN, E.H. and L-A. PERRINS 1982 - Tidal and inertial currents around South Africa. Proceedings of the Eighteenth Coastal Engineering Conference ASCE/Capetown, South Africa/Nov. 14-19, 1982.

SHANNON, L.V. 1966 - Hydrology of the south and west coasts of South Africa. Investl Rep. Div. Sea Fish. S. Afr. 58, 22 pp. plus 30 pp. plates.

SHANNON, L.V. 1985 - The Benguela Ecosystem part 1. volution of the Benguela, physical features and processes. Oceanogr. Mar. Biol. Ann. Rev., 1985, 23, 105-182.

SMITH, R.L. 1974 - A description of current, wind, and sea level variations during coastal upwelling off the Oregon coast, July-August 1972. Geophys. Res. 79, 435-443.

SMITH, R.L. 1978 - Poleward propagating disturbances in currents and sea levels along the Peru coast. J. Geophys. Res. 83, 6083-6092.

TORGRIMSON, G.M. and B.M. HICKEY 1979 - Barotropic and baroclinic tides over the comtinental slope and shelf off Oregon. J. Phys. Oceanogr., 9, 945-961.

VAN FOREEST, D. and G.B. BRUNDRIT 1982 - A two-mode numerical model with applications to coastal upwelling. Prog. Oceanogr. 11, 329-392.

VAN FOREEST, D. and G.B. BRUNDRIT 1983a - A two-mode numerical model with surface mixed layer. 1. The vertical struture. Benguela Ecology Programme. Internal Report, University of Cape Town., 14 pp.

VAN FOREEST, D. and G.B. BRUNDRIT 1983b - A two-layer numerical model with surface mixed layer. 2. The Galerkin procedure. Benguela Ecology Programme. Internal Report, University of Cape Town., 31 pp.

VAN FOREEST, D. and G.B. BRUNDRIT 1985 - Numerical modelling of the southern Benguela system. In South African Ocean Colour and Upwelling Experiment. Shannon, L.V. (Ed.). Cape Town; Sea Fisheries Research Institute., 111-123.

VAN FOREEST, D., F.A. SHILLINGTON and R. LEGECKIS 1984 - Large scale, stationary, frontal features in the Benguela Current system. Continent. Shelf Res. 3(4), 465-474.

WANG D-P. 1976 - Coastal water response to the variable wind theory and coastal upwelling experiment. Technical Rep. TR76-2, University of Miami.

WEATHERLY, G.L. 1972 - A study of the bottom boundary layer of the Florida Current. J. Phys. Oceanogr., 2, 54-72.

WEBSTER, F 1968 - Observations of inertial-period motions in the deep sea. Rev. Geophys., 6, 473-490.

WOOSTER, W.S. and J.L. REID 1963 - Eastern boundary currents. In: The Sea, M.N. Hill (ed.)., Interscience Publ., New York, 2:253-280.

WUNSCH, C. 1969 - Progressive internal waves on slopes. J. Fluid mech., 35, 131-144.

WYLLIE, J.G. 1966 - Geostrophic flow of the California Current at the surface and at 200 m. Calif. Coop. Oceanic Fish. Invest., Atlas No. 4, xxii p, 288 charts.

## APPENDICES.

A small suite of computer programs, written in Fortran 5, were produced to apply filtering and spectral analysis techniques to wind and current measurements. These programs and their operations are charted below.

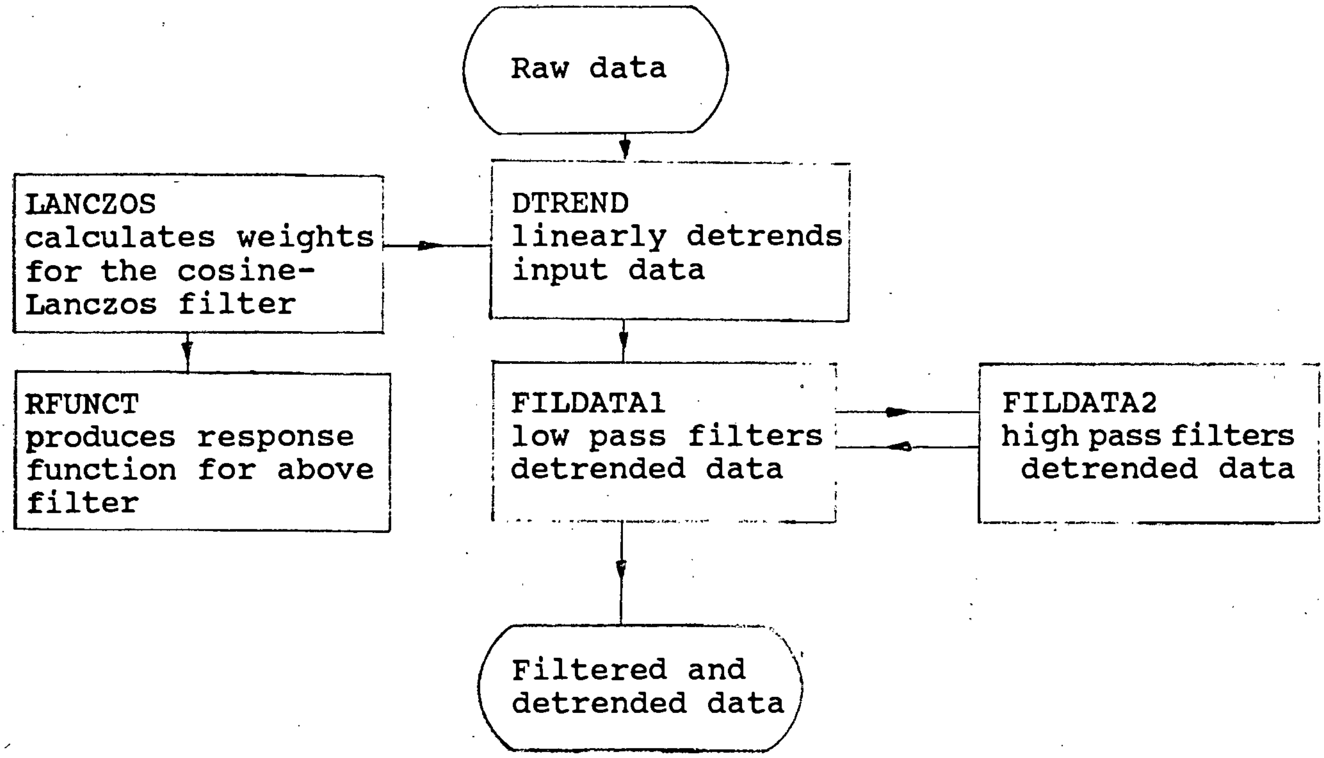

Programs listed above are presented in Appendices I to V .

## Appendix I

```
C         ****************************************************
C                              LFILTR
C         This program determines the weights of the symmetric
C         cosine-Lanczos filter.
C         ****************************************************
          OPEN 1,"LFILTR"
          N=0
          J=0
          TK=0
          UK=0
          VU=0
          SUM=0
C         Number of weights in one wing plus one entered.
          ACCEPT "NUMBER OF WEIGHTS = ",M
C         Frequency of the 1/4 power point entered in Nyquists.
          ACCEPT "QUARTER POWER POINT = ",F
C         This routine calculates the sum of the UI's for I=1 to M-1.
          N=M-1
          DO 50 K=1,N
          TK=0.5*(1+COS(3.14159*K/M))
          UK=TK*(SIN(3.14159*F*K))/(3.14159*F*K)
          SUM=SUM+UK
 50       CONTINUE
C         This routine completes the algorithm by computing V(K) for
C         K=0 to M-1.
          DO 300 K=0,N
          TK=0.5*(1+COS(3.14159*K/M))
          IF (K.GT.0) GO TO 200
          UK=1
          GOTO 220
 200      UK=TK*(SIN(3.14159*F*K))/(3.14159*F*K)
 220      VK=UK/(1+2*SUM)
          A(K)=VK
          WRITE(1,250) A(K)
 250      FORMAT (F11.8)
 300      CONTINUE
          STOP
          END
```

# Appendix II

```
C        *********************************************************

C                              [illegible]

C        This program evaluates the frequency response function
C        for the cosine-Lanczos filter stored in file LFILTR.

C        *********************************************************

C        The response function is defined over the frequency range
C        0 to PI/N, where N is an integer value.
         ACCEPT"Frequency range - 0 to PI/N, enter N",L

         OPEN 1,"LFILTR"
         OPEN 2,"RESPONSE"
         DIMENSION A(0:500)
         REAL M

C        The filter weights generated by program LANCZOS are read
         ACCEPT "NUMBER OF WEIGHTS IN ONE WING = ",N
         DO 50 I=0,N-1
         READ (1,40)W
         A(I)=W
 40      FORMAT (F11.8)
 50      CONTINUE

         M=3.14159
         K=1

C        Filter response is calculated over the requested range.
         DO 100 I=0,20
         SUM=0
         AB=(I*M)/(20*L)
         DO 80 J=1,N-1
         BC=J*AB
         BD=BC/(2*M)
         IBD=BD
         BB=BC-IBD*2*M
         AA=A(J)*COS(BB)*2
         SUM=SUM+AA
 80      CONTINUE
         CC=SUM+A(0)
         ICOUNT=I
         WRITE (2,90) ICOUNT,CC
 90      FORMAT (I5,2X,F8.5)
         K=K+1
 100     CONTINUE
         STOP
         END
```

## Appendix III

```
C     [illegible]
C
C                         [illegible]
C
C        THIS PROGRAM REMOVES LINEAR TREND FROM DATA STORED IN FILE
C        "DATA" BY THE METHOD OF LEAST SQUARES.
C
C        **************************************************************
         OPEN1,"DATA"
         OPEN2,"TRDATA"
         DIMENSION RDATA(4000),DDATA(4000),PAR(7)
         SUM=0
         AA=0
 10      TYPE"SELECT ONE OF THE DATA SETS BELOW."
         TYPE"(1) COUNTER........BE SERIOUS"
         TYPE"(2) TEMPERATURE"
         TYPE"(3) NORTHWARD SPEED COMPONENT"
         TYPE"(4) EASTWARD SPEED COMPONENT"
         TYPE"(5) SPEED"
         TYPE"(6) DIRECTION"
         TYPE"(7) PRESSURE ANOMALY"
         ACCEPT"YOUR CHOICE IS ?",K
         TYPE"  "
         N=100
         IF (K.EQ.7) N=10
         ACCEPT"NUMBER OF RECORDS TO BE READ?",LR
         PR=REAL(LR)
         DO 20 I=1,LR
         READ FREE (1,END=25) (PAR(J),J=1,7)
         RDATA(I)=PAR(K)/N
 20      CONTINUE
 25      DO 150 I=1,LR
         SUM=SUM+RDATA(I)
 150     CONTINUE
         AMEANX=SUM/LR
         AMEANT=REAL((LR+1)/2.)
         DO 200 I=1,LR
         AA=I*RDATA(I)+AA
 200     CONTINUE
         BB=AA-(LR*AMEANT*AMEANX)
         AED=(PR*(PR*PR-1.)/12.)
         GRAD=BB/AED
         CONST=AMEANX-GRAD*AMEANT
         DO 250 I=1,LR
         CC=RDATA(I)-(GRAD*I+CONST)
         COUNT=I
         WRITE(2,70) COUNT,CC
 70      FORMAT(I5,2X,F6.2)
 250     CONTINUE
         STOP
         END
```

## Appendix IV

```
C     *************************************************************
C                              FILDATA
C     FILDATA: filters the detrended data in file TRDATA, using
C     the cosine-Lanczos filter weights produced stored in
C     file LFILTR.
C     *************************************************************

      OPEN 1,"TRDATA"
      OPEN 2,"LFILTR"
      OPEN 3,"FDATA"
      DIMENSION ADATA(1:4000)
      DIMENSION AFILTR(1:1000)
      IM=0

C     Input information from screen
      ACCEPT "Number of filter weights in one wing=",IW
      ACCEPT "Length of record=",LR

C     Data and filter weights are read into arrays.
      DO 60 I=1,LR
      READ (1,50) NUMB,PAR
 50   FORMAT(I5,2X,F6.2)
      ADATA(I)=PAR
 60   CONTINUE

C     Input data is now smoothed and written to file FDATA.
 70   DO 200 I=1,IW
      READ (2,100) AF
      AFILTR (I)=AF
 100  FORMAT (F11.8)
 200  CONTINUE
      IMW=2*IW
      DO 500 M=0,(LR-IMW+1)
      IM=IM+1
      SUM=ADD=0
      DO 250 J=(1+M),(IW+M)
      MC=(IW+1-J+M)
      AA=ADATA(J)*AFILTR(MC)
      SUM=SUM+AA
 250  CONTINUE
      DO 280 J=(IW+1+M),(2*IW-1+M)
      MD=(J-IW+1-M)
      BB=ADATA(J)*AFILTR(MD)
      ADD=ADD+BB
 280  CONTINUE
      TOTAL=SUM+ADD
      ICOUNT=IM
      WRITE(3,80) ICOUNT,TOTAL
 80   FORMAT(I5,2X,F6.2)
 500  CONTINUE
      STOP
      END
```

# Appendix V

```
C       ************************************************************

C                                  FILDATA2

C       FILDATA2 subtracts the filtered data produced by FILDATA1
C       from the original detrended time series. This has the effect
C       of high pass filtering the data.

C       ************************************************************

        DIMENSION RDATA(1:5000)
        DIMENSION DDATA(1:5000)
        OPEN 1,"TRDATA"
        OPEN 2,"FDATA"

        ACCEPT"NUMBER OF RECORDS IN ORIGINAL TIME SERIES= ",IN
        ACCEPT"How many filter weights used in FILDATA1?",IW
        DO 50 I=1,IN
        READ (1,40) INUM,PAR
 40     FORMAT(I5,2X,F6.2)
        RDATA(I)=PAR
 50     CONTINUE
        REWIND 1
        IP=IN-(2*IW)+2
        TYPE IP
 100    DO 200 I=1,IP
        READ(2,80) JNUM,ANN
 80     FORMAT(I5,2X,F6.2)
        DDATA(I)=ANN
 200    CONTINUE
        DO 300 J=1,IP
        SUM(J)=RDATA(J+IW-1)-DDATA(J)
        ICOUNT=J
        WRITE(1,90) ICOUNT,SUM(J)
 90     FORMAT(I5,2X,F6.2)
 300    CONTINUE
        STOP
        END
```

# Appendix VI

The 95% confidence limit for phase spectra taken from Jenkins and Watts (1972), page 381.

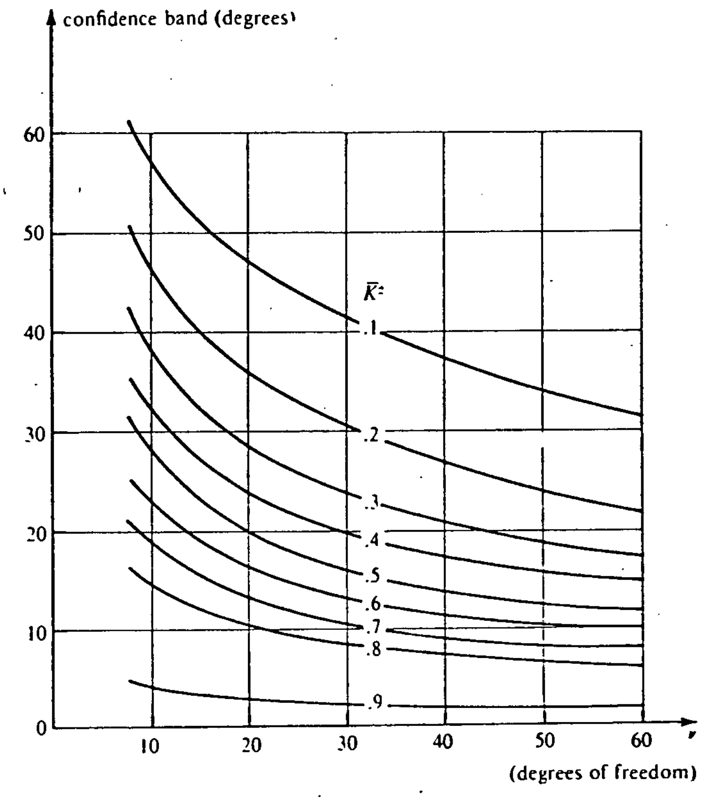

95% confidence limits for the phase spectrum

The following Fortran programs form the basis elements in the production of uni- and bi-variate spectral analysis.

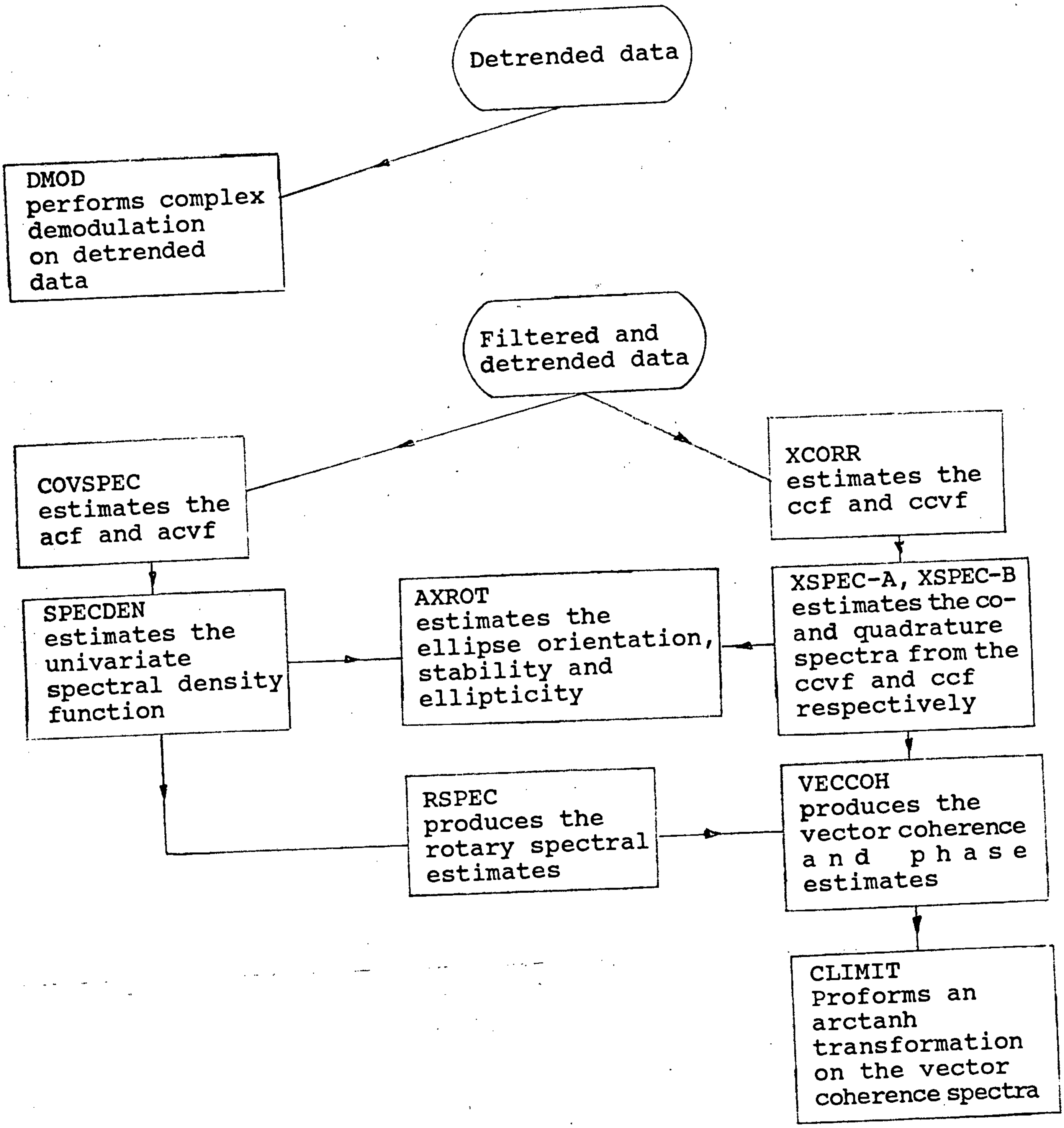

# Appendix VII

```
C        ******************************************************************
C        DMOD demodulates a time series in file TRDATA at frequency
C        f by the method of COMPLEX DEMODULATION described by
C        Bloomfield (1976).
C        ******************************************************************
         DIMENSION AR(1:4000)
         OPEN 1,"TRDATA"
         OPEN 2,"REAL"
         OPEN 3,"PHASE"
         PI=3.1415926
         PPI=2*PI
C        DATA IN FILE TRDATA IS READ INTO ARRAY AR
         ACCEPT"ENTER NUMBER OF RECORDS TO BE READ",LR
         DO 100 I=1,LR
         READ (1,10) ICNT,AA
         AR(I)=AA
 100     CONTINUE
C        Input data is demodulated
         ACCEPT"INPUT DEMODULATION FREQUENCY (cph)",FREQ
         FREQ=2*PI*FREQ
         DO 200 I=1,LR
         F=FREQ*I
         IF (F.LT.PPI) GOTO 120
         F=INT(F/(2*PI))*2*PI
 120     BR=AR(I)*COS(F)
         CR=-AR(I)*SIN(F)
         Z=2*SQRT(BR**2+CR**2)
         SA=-SIN(F)
         CA=COS(F)
         FAYZ=ATAN2(SA,CA)
         WRITE (2,10) I,Z
 10      FORMAT (I5,2X,F6.2)
         WRITE (3,10) I,FAYZ

 200     CONTINUE
         STOP
         END
```

## Appendix VIII

```
C       **********************************************
C                               COVSPEC
C       COVSPEC estimates the covariance and auto correlation
C       functions, writing the output to files COVAR and AUTO.
C       **********************************************
        DIMENSION DDATA(4000),SSUM(0:1000)
        OPEN1,"FDATA"
        OPEN2,"COVAR"
        OPEN3,"AUTO"
        ADD=0
        SUM=0
C       Number of records to be read input from screen. Input data
C       written to array DDATA
        ACCEPT"NUMBER OF RECORDS =",LR
        DO 50 I=1,LR
        READ(1,10) COUNT,FA
 10     FORMAT(I5,2X,F6.2)
        DDATA(I)=FA
 50     CONTINUE
C       The mean is estimated
        DO 75 J=1,LR
        ADD=ADD+DDATA(J)
 75     CONTINUE
        AMN=ADD/LR
C       The window lag is entered from screen.
        ACCEPT"LAG=",L
        DO 200 I=0,L
        DO 100 J=1,LR-I
        SUM=SUM+(DDATA(J)-AMN)*(DDATA(J+I)-AMN)
 100    CONTINUE
        SSUM(I)=SUM/(LR)
        SUM=0
 200    CONTINUE
C       The auto correlation is estimated
        DO 300 K=0,L
        ABC=SSUM(K)/SSUM(0)
        ICOUNT=K
        WRITE(2,70)ICOUNT,SSUM(K)
 70     FORMAT(I5,2X,F11.3)
        WRITE(3,70) ICOUNT,ABC
        SUM=0
 300    CONTINUE
        END
```

# Appendix IX

```
      ***************************************************************

                              SPECTRN

      SPECTRN produces the arithmetic (POWR1) and logarithmic
      (POWR2) spectral estimates by transforming the covarience
      or the auto correlation function, as requested. Either the
      Tukey or Parzen lag window may be selected.

      In the present version, spectral estimates are calculated
      over the frequency range 0 to 0.3 cph.

      ***************************************************************

      DIMENSION ARAY(0:1000),COV(1000)
      SSUM=0
      OPEN1,"AUTO"
      OPEN2,"COVAR"
      OPEN3,"POWR1"
      OPEN4,"POWR2"
      PI=3.14159

      The lag window is selected.
10    TYPE"For the Tukey window type 1 "
      TYPE"For the Parzen window type 2"
      ACCEPT IZ
      TYPE"    "
      TYPE"Enter an even number for the lag window"
      ACCEPT"M=",M
      IF (IZ-1) 10,20,30
20    DO 50 I=0,M
      ARAY(I)=(1+COS((I*PI)/M))/2
50    CONTINUE
      GOTO 100
30    DO 70 I=0,M/2
      AA=(I*1.0)/M
      AB=1-6*(AA**2)+6*(AA**3)
      ARAY(I)=AB
70    CONTINUE
      DO 90 I=(M/2+1),M
      AC=1-(I*1.0)/M
      AD=(AC**3)*2
      ARAY(I)=AD
90    CONTINUE

C     The number of evaluations (Q) in the interval 0 to 0.6PI/Q
C     are written to screen
 100  TYPE"The spectral ordinates are calculated over the range"
      TYPE"0 to 0.6PI at Q intervals"
      ACCEPT"ENTER A VALUE FOR Q",LQ
C     The appropriate lag window is selected
      TYPE"To transform the covariance function type 1"
      TYPE"To transform the auto correlation function type 2"
      ACCEPT"TYPE 1 OR 2  ",LNN
      IF (LNN-1) 100,32,122

C     The smoothed spectral estimates are now produced.
 32   DO 120 K=0,M
      READ(2,40) INUM,PP
 40   FORMAT(I5,2X,F11.3)
      COV(K)= PP
 120  CONTINUE
      GOTO 124
```

```
122     DO 123 K=0,M
        READ(1,40)  JNUM,PP
        COV(K)=PP
123     CONTINUE
124     TPI=2*PI
        DO 300 I=0,LQ
        DO 200 J=1,M
        FUN=(PI*I*J*0.6)/LQ
125     IF (FUN.LE.TPI) GOTO 134
        FUN=FUN-INT(FUN/TPI)*TPI
134     ANG=FUN
        ENDTM=ARAY(J)*COV(J)*COS(ANG)
        SSUM=SSUM+ENDTM
200     CONTINUE
        SSUM=2*SSUM
        TOTAL=(ARAY(0)*COV(0)+SSUM)*2
        TTAL=TOTAL
        TOTAL=ABS(TOTAL)
        IF (TOTAL.LE.1) TOTAL=1
        TOTAL=ALOG10(TOTAL)
        ICOUNT=I
        WRITE(3,150)  ICOUNT,TOTAL
150     FORMAT(I5,2X,F11.3)
        WRITE(4,150)   ICOUNT,TTAL
        SSUM=0
300     CONTINUE
        STOP
        END
```

## Appendix X

```
C      ************************************************************
C
C                           AXROT
C
C      AXROT determines the axis through which the N/S - E/W
C      coordinate system should be rotated to best display
C      the time series component with frequency f. The ellipticity
C      and ellipse stability are also determined.
C
C      For correct axis orientation, with theta rotating
C      clockwise about the Oy axis, SPECA equals the autospectra
C      in the Oy direction and SPECB equals the autospectra in the
C      Ox direction.
C
C      ************************************************************

       OPEN1,"CO"
       OPEN2,"SPECA"
       OPEN3,"SPECB"
       OPEN4,"ANGLE"
       OPEN5,"ELLIPS"
       OPEN6,"STBIL"
       OPEN7,"QUAD"

       ACCEPT"Number of records to read=   ",LR
       PI=3.1415926

       DO 100 I=0,LR
       READ(1,10) IA,CSPEC
       READ(2,10) IB,SPA
       READ(3,10) IC,SPB
       READ(7,10) ID,QU

C      The ellipse orientation is now estimated.
       TOP=2*CSPEC
       BOTTOM=SPB-SPA
       QUOT=ABS(TOP/BOTTOM)
       THETA(I)=0.5*ATAN(QUOT)
       DEG=THETA(I)*180/PI
       IF (TOP.GT.0..AND.BOTTOM.GT.0.) DEG=90-DEG
       IF (TOP.GT.0..AND.BOTTOM.LT.0.) DEG=DEG
       IF (TOP.LT.0..AND.BOTTOM.LT.0.) DEG=180-DEG
       IF (TOP.LT.0..AND.BOTTOM.GT.0.) DEG=90+DEG

C      The ellipticity is now estimated.
 5     ELIPS=1-ABS(-2*QU/(SPA+SPB))

C      The ellipse stability is now estimated.
       STB=(SPA+SPB)**2-4*(SPA*SPB-CSPEC**2)
       STB=STB/((SPA+SPB)**2-4*(QU**2))
       STB=SQRT(ABS(STB))

       ICOUNT=I
       WRITE(4,10) ICOUNT,DEG
       WRITE(5,10) ICOUNT,ELIPS
       WRITE(6,10) ICOUNT,STB
10     FORMAT(I5,2X,F11.3)
100    CONTINUE
       STOP
       END
```

# Appendix XI

```
C       **********************************************************

C                                  RSPEC

C       RSPEC computes rotary spectral estimates for wind and
C       current vector time series. Input data are the auto
C       spectral estimates written to files TRANS3 and TRANS4
C       and the quadrature spectral estimates stored in file QUAD.
C       Rotary spectra are evaluated in the frequency range
C       0<f<0.3 cph.

C       **********************************************************

        OPEN 1,"TRANS3"
        OPEN 2,"TRANS4"
        OPEN 3,"QUAD"
        OPEN 4,"ANTI"
        OPEN 5,"CLOCK"
        OPEN 7,"TOTAL"
        OPEN 8,"ARTHA"
        OPEN 9,"ARTHC"
        DIMENSION ASER(0:1000),BSER(0:1000),QU(0:1000)

        Accept"Enter number of evaluations in the range 0<f<0.3",LR
        DO 100 I=0,LR
        READ (1,50) ICONT1,AA
        ASER(I)=AA
        READ (2,50) ICONT2.AB
        BSER(I)=AB
        READ (3,50) ICONT3,AC
        QU(I)=AC
 100    CONTINUE

C       The anticlockwise and clockwise rotary components are
C       now computed.
        DO 200 I=0,LR
        SUM=(ASER(I)+BSER(I))
        AN=(SUM+(2*QU(I)))*0.5
        CL=(SUM-(2*QU(I)))*0.5
        WRITE(8,50) I,AN
        WRITE(9,50) I,CL
        IF (AN.LE.1) AN=1
        IF (CL.LE.1) CL=1
        TL=AN+CL
        TOTAL=ALOG10(TL)
        ANN=ALOG10(AN)
        CLL=ALOG10(CL)
        ICOUNT=I
        WRITE(7,50) ICOUNT,TOTAL
        WRITE(4,50) ICOUNT,ANN
        WRITE(5,50) ICOUNT,CLL
 50     FORMAT(I5,2X,F11.3)
 200    CONTINUE
        STOP
        END
```

## Appendix XII

```
C       ************************************************

C                             XCORR

C       XCORR calculates the covariance and cross correlation
C       functions for time series stored in files TRANS1 and
C       TRANS2.

C       ************************************************

        DIMENSION ASER(1:4000),BSER(1:4000)
        OPEN 1,"TRANS1"
        OPEN 2,"TRANS2"
        OPEN 3,"PLUS"
        OPEN 4,"MINUS"
        OPEN 5,"COVPLUS"
        OPEN 6,"COVMINUS"
        SUM=TTL=0

C       Data in files TRANS1 and TRANS2 are read into arrays
C       ASER and BSER.
        ACCEPT"Enter the record length",LR
        DO 50 I= 1,LR
        READ (1,10) JCOUNT,AA
        READ (2,10) JCOUNT,BB
 10     FORMAT(I5,2X,F6.2)
        ASER(I)=AA
        BSER(I)=BB
 50     CONTINUE

C       The LAG L for the cvf and ccf is entered from screen.
        ACCEPT"ENTER LAG L",L

C       The means of the two series are now computed.
        DO 150 I=1,LR
        SUM=SUM+ASER(I)
        TTL=TTL+BSER(I)
 150    CONTINUE
        AMN1=SUM/LR
        AMN2=TTL/LR
        SUM=TTL=0

C       The variances of the two series are now computed.
        DO 170 I=1,LR
        AVR=ASER(I)-AMN1
        BVR=BSER(I)-AMN2
        AVR=AVR**2
        BVR=BVR**2
        SUM=SUM+AVR
        TTL=TTL+BVR
 170    CONTINUE
        VAR1=SUM/LR
        VAR2=TTL/LR
        SUM=TTL=0
        ROOT=VAR1*VAR2
        ROOT=SQRT(ROOT)

C       The ccvf is now computed.
        DO 300 I=0,L
        DO 200 J=1,LR-I
        SUM=SUM+(ASER(J)-AMN1)*(BSER(J+I)-AMN2)
        TTL=TTL+(ASER(J+I)-AMN1)*(BSER(J)-AMN2)
 200    CONTINUE
```

```
      ICOUNT=1
      SUM=SUM/LR
      TTL=TTL/LR
      WRITE(5,22) ICOUNT,SUM
      WRITE(6,22) ICOUNT,TTL

C     The ccvf is divided by the square root of the product of
C     the variances to give the ccf.
      SUM=SUM/ROOT
      TTL=TTL/ROOT
      WRITE(3,22) ICOUNT,SUM
      WRITE(4,22) ICOUNT,TTL
  22  FORMAT(I5,2X,F11.3)
      SUM=TTL=0
 300  CONTINUE
      STOP
      END
```

## Appendix XIII

```
C         *********************************************************

C                                     YSPEC-A

C         YSPEC-A computes the co-spectrum and the quadrature
C         spectrum using the ccvf determined by YCORR. Spectra
C         are produced over the frequency range 0<f<0.3 cph.

C         *******************************************************

          DIMENSION PARZ(0:1000),PL(0:1000),AMI(0:1000)
          OPEN 1,"COVPLUS"
          OPEN 2,"COVMINUS"
          OPEN 3,"CO"
          OPEN 4,"QUAD"
          PI=3.14159
          SUM=SSUM=0

C         Input files are read into arrays PL and AMI.
          ACCEPT"Enter maximum lag of the ccf",LR
          DO 10 I=0,LR
          READ (1,15) ICOUNT,PLL
  15      FORMAT(I5,2X,F11.3)
          PL(I)=PLL
  10      CONTINUE
          DO 20 I=0,LR
          READ (2,25) JCOUNT,AII
  25      FORMAT(I5,2X,F11.3)
          AMI(I)=AII
  20      CONTINUE

C         Weights for the Parzen window are now computed.
          M=LR
          DO 50 I=0,M/2
          AA=(I*1.0)/M
          AB=1-6*(AA**2)+6*(AA**3)
          PARZ(I)=AB
  50      CONTINUE
          DO 100 I=(M/2+1),M
          AC=1-(I*1.0)/M
          AD=(AC**3)*2
          PARZ(I)=AD
 100      CONTINUE

C         The summation term for the co-spectrum is now evaluated
C         in the frequency range 0<f<0.3 cph.
          ACCEPT"Enter number of evaluations between 0 and 0.3 cph",LQ
          TPI=2*PI
          DO 310 I=0,LQ
          DO 210 J=1,M
          FUN=(PI*I*J*.6)/LQ
 126      IF (FUN.LE.TPI) GOTO 151
          FUN=FUN-INT(FUN/TPI)*TPI
          GOTO 126
 151      ANG=FUN
          ENDTM=PARZ(J)*(PL(J)+AMI(J))*COS(ANG)
          SUM=SUM+ENDTM
 210      CONTINUE
          TOTAL=2*(PARZ(0)*PL(0)+SUM)
          JCOUNT=I
          WRITE(3,24) JCOUNT,TOTAL
  24      FORMAT(I5,2X,F11.3)
          SUM=0
```

```
 310    CONTINUE
        FUN=ENDTM=TOTAL=ICOUNT=0

C       The summation term for the quadrature spectrum is now
C       computed.
        DUMMY=ZERO=0
        WRITE(4,132) DUMMY,ZERO
 132    FORMAT(I5,2X,F11.3)
        DO 510 I=1,LQ-1
        DO 410 J=1,M
        FUN=(PI*I*J*0.6)/LQ
 164    IF (FUN.LE.TPI) GOTO 174
        FUN=FUN-INT(FUN/TPI)*TPI
        GOTO 164
 174    ANG=FUN
        ENDTM=PARZ(J)*(PL(J)-AMI(J))*SIN(ANG)
        SUM=SUM+ENDTM
 410    CONTINUE
        TOTAL=2*SUM
        ICOUNT=I
        WRITE (4,38) ICOUNT,TOTAL
 38     FORMAT(I5,2X,F11.3)
        SUM=0
 510    CONTINUE
        WRITE(4,48)LR,ZERO
 48     FORMAT(I5,2X,F11.3)
        STOP
        END
```

# Appendix XIV

```
****************************************************

                        XSPEC-P

XSPEC-P computes the co-spectrum and the quadrature
spectrum using the ccf determined by XCORR. Spectra
are produced over the frequency range 0<f<0.3 cph.

****************************************************

      DIMENSION PARZ(0:1000),COVR(-1000:1000)
      OPEN 1,"PLUS"
      OPEN 2,"MINUS"
      OPEN 3,"CO"
      OPEN 4,"QUAD"
      PI=3.14159
      SUM=SSUM=0

       Input files are read into arrays PL and AMI.
       ACCEPT"Enter window lag and alignment operator",LR,N
       MR=LR+ABS(N)
       DO 10 I=0,MR
       READ (1,15) ICOUNT,PLL
5      FORMAT(I5,2X,F11.3)
       COVR(I)=PLL
0      CONTINUE
       DO 20 I=0,-LR,-1
       READ (2,25) JCOUNT,AII
5      FORMAT(I5,2X,F11.3)
       COVR(I)=AII
0      CONTINUE

       Weights for the Parzen window are now computed.
       M=LR
       DO 50 I=0,M/2
       AA=(I*1.0)/M
       AB=1-6*(AA**2)+6*(AA**3)
       PARZ(I)=AB
50     CONTINUE
       DO 100 I=(M/2+1),M
       AC=1-(I*1.0)/M
       AD=(AC**3)*2
       PARZ(I)=AD
100    CONTINUE

       The summation term for the co-spectrum is now evaluated
       in the frequency range 0<f<0.3 cph.
       ACCEPT"Enter number of evaluations between 0 and 0.3 cph",LQ
       TPI=2*PI
       DO 310 I=0,LQ
       DO 210 J=1,M
       FUN=(PI*I*J*.6)/LQ
126    IF (FUN.LE.TPI) GOTO 151
       FUN=FUN-INT(FUN/TPI)*TPI
       GOTO 126
151    ANG=FUN
       ENDTM=PARZ(J)*(COVR(J+N)+COVR(-J+N))*COS(ANG)
       SUM=SUM+ENDTM
210    CONTINUE
       TOTAL=2*(PARZ(0)*COVR(0)+SUM)
       JCOUNT=I
       WRITE(3,24) JCOUNT,TOTAL
24     FORMAT(I5,2X,F11.3)
```

```
      SUM=0
0     CONTINUE
      FUN=ENDTM=TOTAL=ICOUNT=0

      The summation for the quadrature spectrum is now
      computed.
      DUMMY=ZERO=0
      WRITE(4,132) DUMMY,ZERO
32    FORMAT(I5,2X,F11.3)
      DO 510 I=1,LQ-1
      DO 410 J=1,M
      FUN=(PI*I*J*0.6)/LQ
64    IF (FUN.LE.TPI) GOTO 174
      FUN=FUN-INT(FUN/TPI)*TPI
      GOTO 164
74    ANG=FUN
      ENDTM=PARZ(J)*(COVR(J+N)-COVR(-J+N))*SIN(ANG)
      SUM=SUM+ENDTM
410   CONTINUE
      TOTAL=2*SUM
      ICOUNT=I
      WRITE (4,39) ICOUNT,TOTAL
38    FORMAT(I5,2X,F11.3)
      SUM=0
510   CONTINUE
      WRITE(4,48)LR,ZERO
48    FORMAT(I5,2X,F11.3)
      STOP
      END
```

# Appendix XV

```
C       **********************************************
C                          VECCOH
C       This program estimates the vector coherence and phase
C.      relationship between to vector quanties. The algorithms
C       used are those presented by Brundrit at the 'Workshop
C       on digital time series analysis with geophysical
C       applications April 22 - 24, 1980'.
C       **********************************************

        DIMENSION FRWRD(0:1000),BKWRD(0:1000),FDEG(0:1000),BDEG(0:1000)

C       Input FILES
        OPEN 31,"CO1"
        OPEN 32,"CO2"
        OPEN 33,"CO3"
        OPEN 34,"CO4"
        OPEN 35,"QUAD1"
        OPEN 36,"QUAD2"
        OPEN 37,"QUAD3"
        OPEN 38,"QUAD4"
        OPEN 39,"ARTHA1"
        OPEN 40,"ARTHC1"
        OPEN 41,"ARTHA2"
        OPEN 42,"ARTHC2"

C       Output FILES
        OPEN 43,"CHNCY"

        PI=3.1415926
        ACCEPT"Number of records=?",LR
        DO 100 J=0,LR
        READ(31,10) I,ANUM1
        READ(32,10) I,ANUM2
        READ(37,10) I,ANUM7
        READ(38,10) I,ANUM8
        READ(35,10) I,ANUM5
        READ(36,10) I,ANUM6
        READ(33,10) I,ANUM3
        READ(34,10) I,ANUM4
        READ(39,10) I,ANUM9
        READ(40,10) I,ANUM10
        READ(41,10) I,ANUM11
        READ(42,10) I,ANUM12

C       Coherence and phase are now estimated.
        BOT1=4*(ANUM9*ANUM11)
        BOT2=4*(ANUM10*ANUM12)

        SUM=(ANUM1+ANUM2-ANUM7+ANUM8)
        SSUM=(ANUM5+ANUM6+ANUM3-ANUM4)
        SW=(SUM**2+SSUM**2)/BOT1
        FRWRD(J)=SQRT(SW)
        TOP=-SSUM
        FANG=ATAN2(TOP,SUM)
        FDEG(J)=FANG*180/PI

        SUM=(ANUM1+ANUM2-ANUM7-ANUM8)
        SSUM=(-ANUM5-ANUM6+ANUM3-ANUM4)
        SW=(SUM**2+SSUM**2)/BOT2
        BKWRD(J)=SQRT(SW)
```

```
      TOP=-SSUM
      BANG=ATAN2(TOP,SUM)
      BDEG(J)=BANG*180/PI
  100 CONTINUE

      DO 200 J=0,LR
      WRITE(43,20)  J,FRWRD(J),BKWRD(J),FDEG(J),BDEG(J)
  200 CONTINUE

   10 FORMAT(I5,2X,F11.3)
   20 FORMAT(I5,4F11.3)
      STOP
      END
```

## <u>**Appendix XVI**</u>

```
C       **************************************************
C                              CLIMIT
C       This program performs an arctanh transformation on the
C       coherence estimates derived obtained by program VECCOH.
C       **************************************************

        OPEN 1,"TMP"
        OPEN 2,"TRMS"

        ACCEPT"Number of records to read?",LR
        DO 100 I=1,LR
        ACCEPT"Input next record",A
        B=0.5*ALOG((1+ABS(A))/(1-ABS(A)))
        WRITE(2,5) I,A,B
 100    CONTINUE
 5      FORMAT(I5,2X,F5.3,2X,F5.3)
        STOP
        END
```

## Appendix XVII

The response function for the cosine-Lanczos filter. Number of weights in one wing: 5. Quarter power point: 0.75 Nyquists.

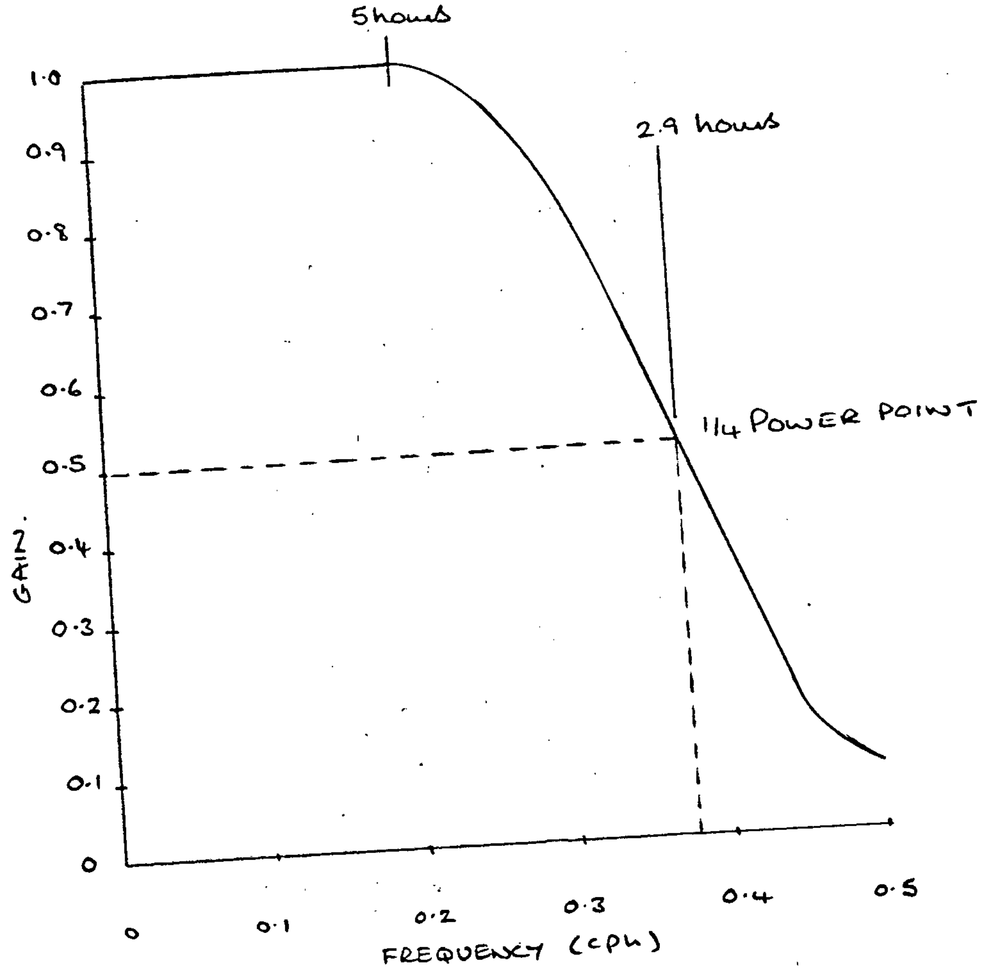

## Appendix XVIII

```
C       ***************************************************************
C                                 NEWCOMP
C       NEWCOMP rotates the N/S - E/W coordinate axes clockwise
C       through an angle theta and determines the appropriate
C       time series components.
C       ***************************************************************
        OPEN 1,"DATA"
        OPEN 2,"NEWDATA"
C       Input variables to screen.
        ACCEPT"RECORD LENGTH =   ",LR

        ACCEPT"AXES ROTATION IN DEGREES =   ",THETA
        PI=3.1416926
        THETA=THETA*PI/180
        ZERO=0
C       Input data is now read and transformed.
        DO 100 I=0,LR
        READ(1,5)IC,TEMP,ANCOMP,ECOMP,SPEED,DIREC,PRESS
        VCOMP=((-ECOMP)*SIN(THETA))+((ANCOMP)*COS(THETA))
        UCOMP=((ECOMP)*COS(THETA))+((ANCOMP)*SIN(THETA))
        ICOUNT=I
        WRITE(2,5) ICOUNT,ZERO,VCOMP,UCOMP,ZERO,ZERO,ZERO
  5     FORMAT(I5,6I6)
  100   CONTINUE
        STOP
  25    END
```

## Appendix XIX

The response function for the cosine-Lanczos filter. Number of weights in one wing: 30. Quarter power point 0.025 Nyquist

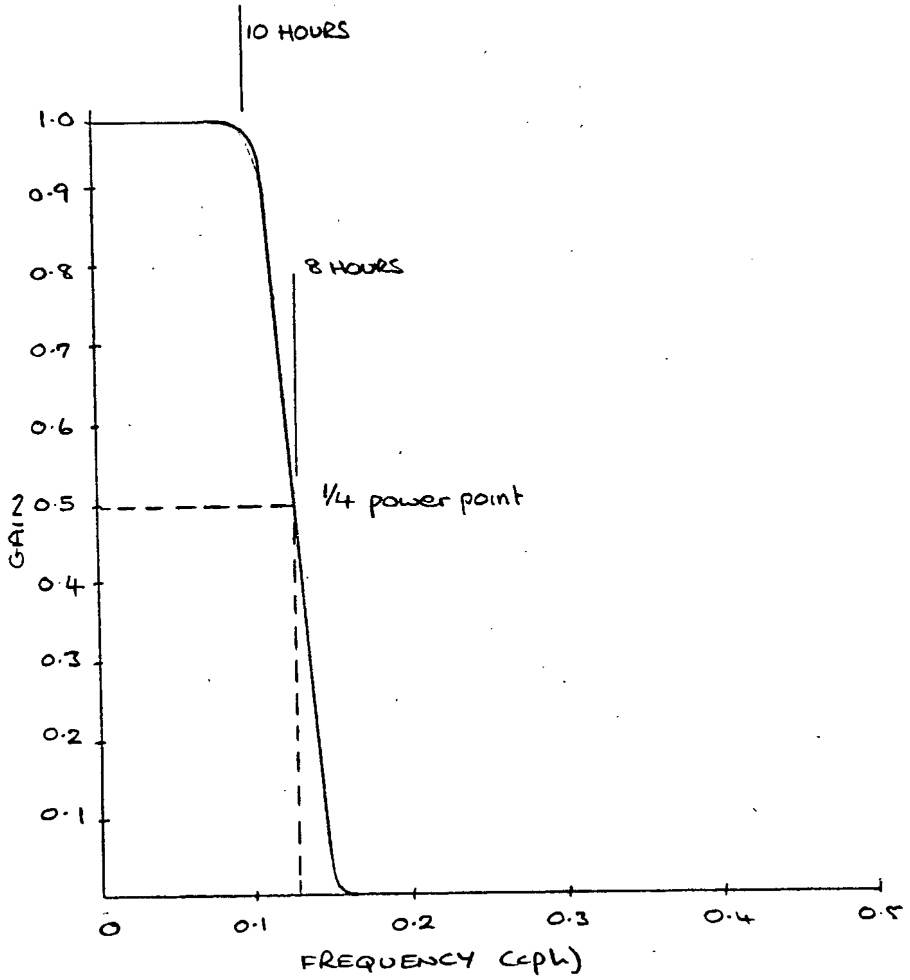

## Appendix XX

The response function for the cosine-Lanczos band pass filter. Low pass response - number of weights in one wing: 5. Quarter power point: 0.75 Nyquists. High pass response - number of weights in one wing: 151. Quarter power point 0.0002 Nyquists.

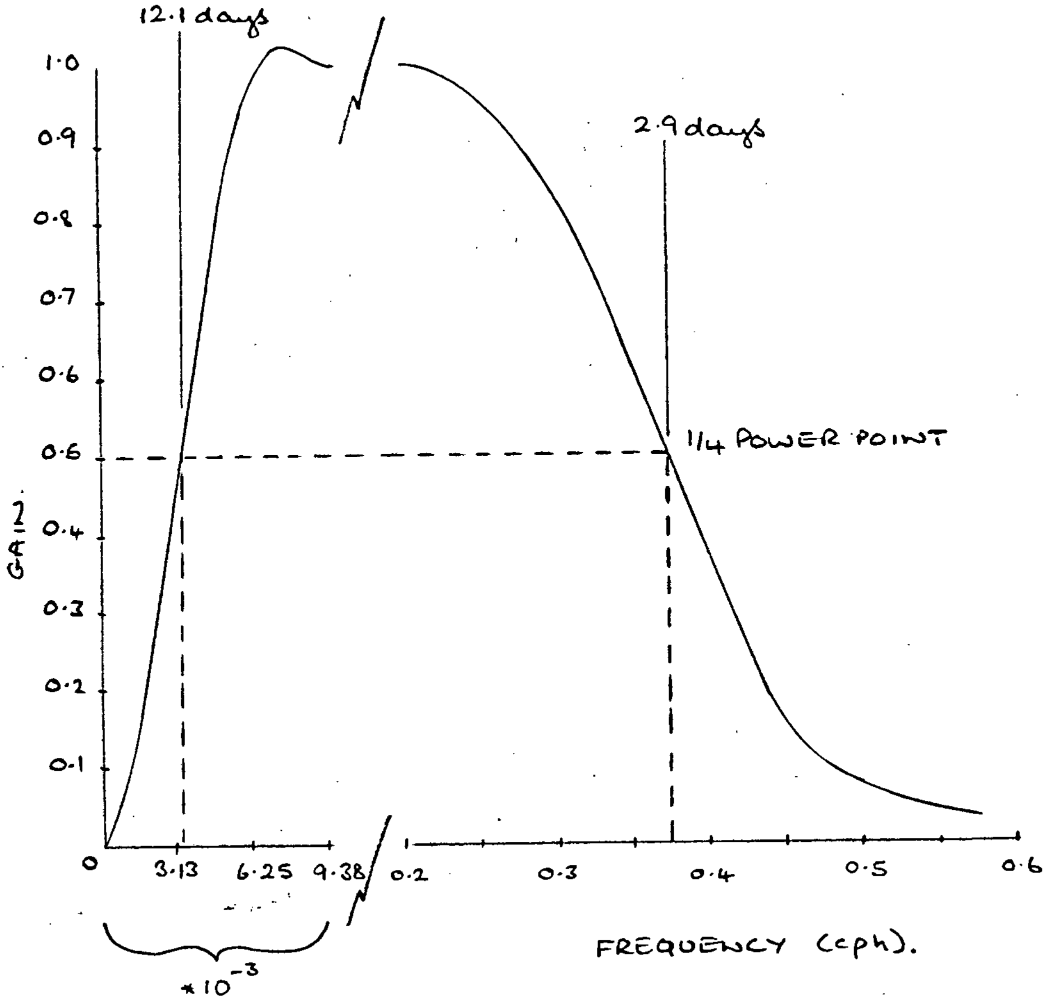

## Appendix XXI

The response function for the cosine-Lanczos filter. Number of weights in one wing: 175. Quarter power point 0.025 Nyquists.

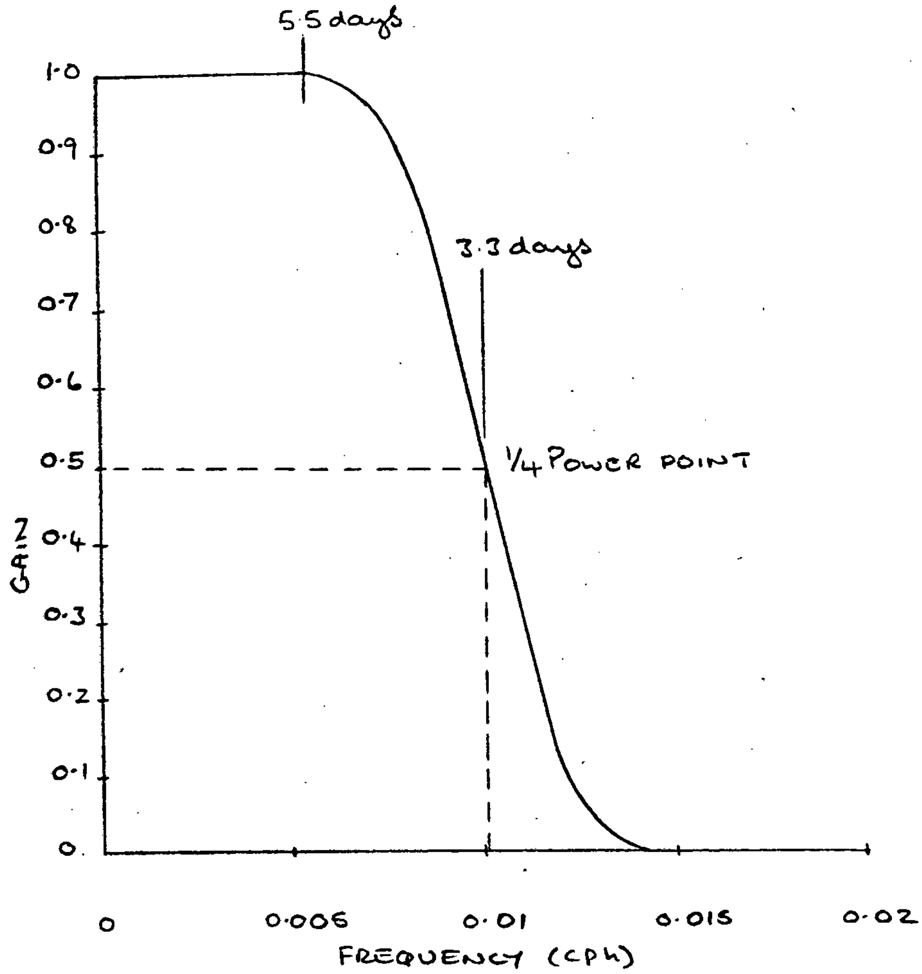

## Appendix XXII

The response function for the cosine-Lanczos band pass filter. Low pass response - number of weights in one wing: 5. Quarter power point: 0.75 Nyquists. High pass response - number of filter weights: 60. Quarter power point: 0.125 Nyquists.

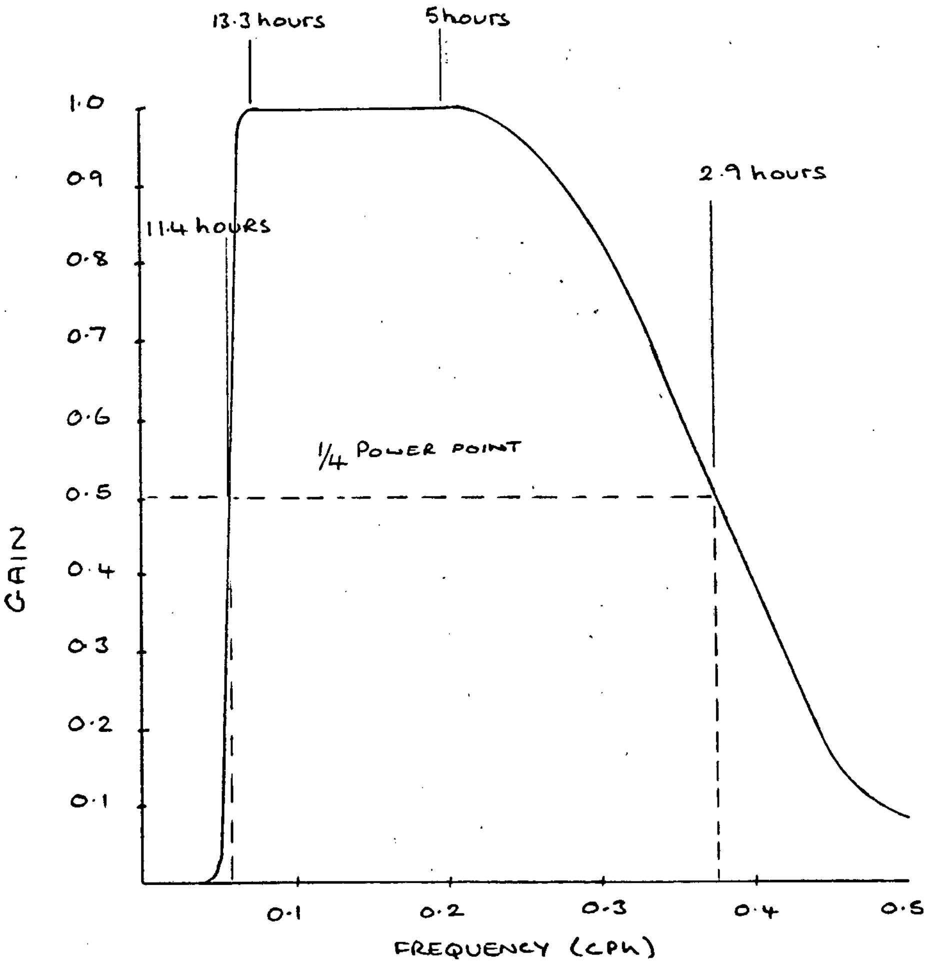

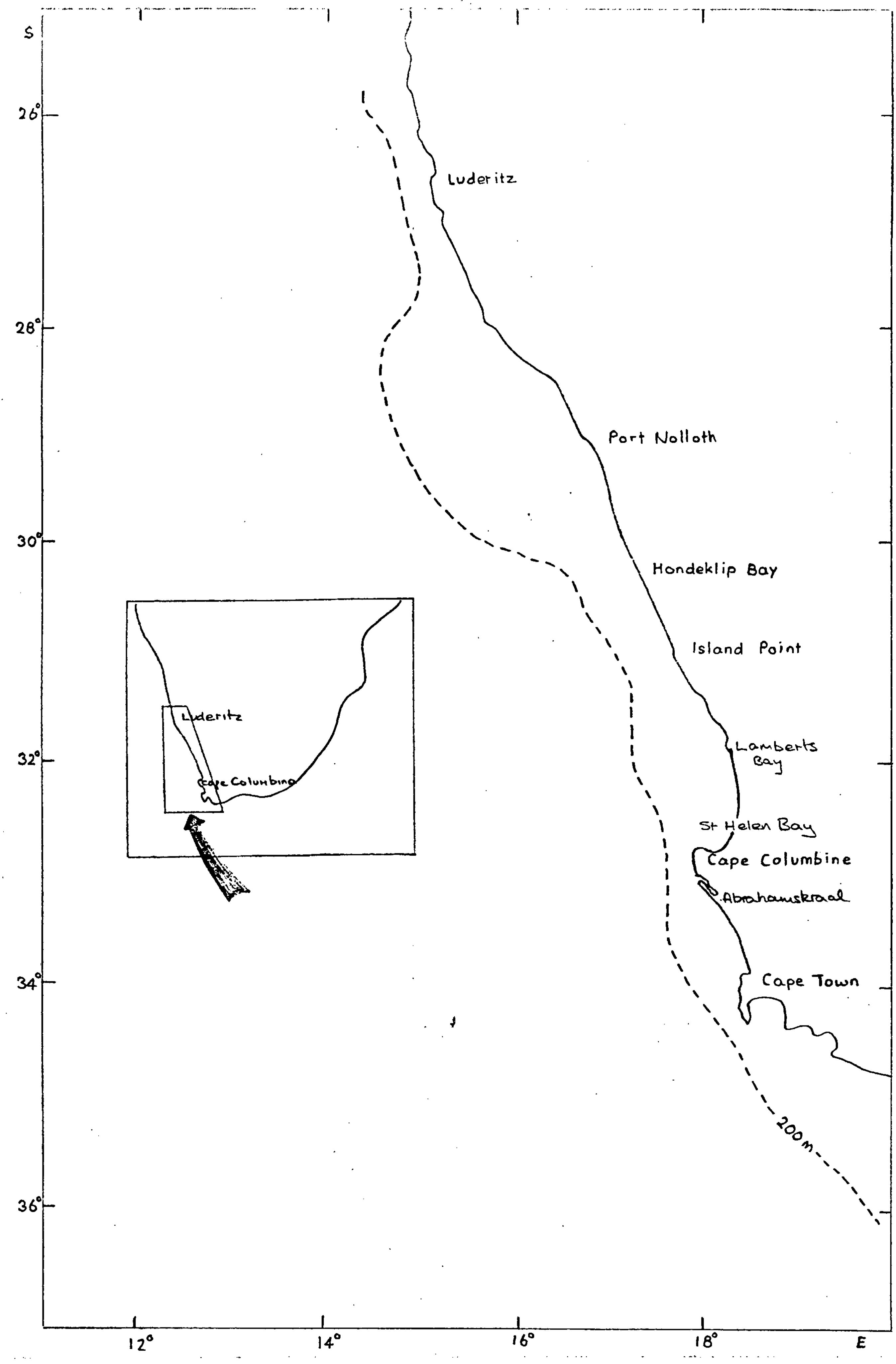

Fig 1: The west coast of South Africa showing the location of the St Helena Bay - Cape Columbine region.

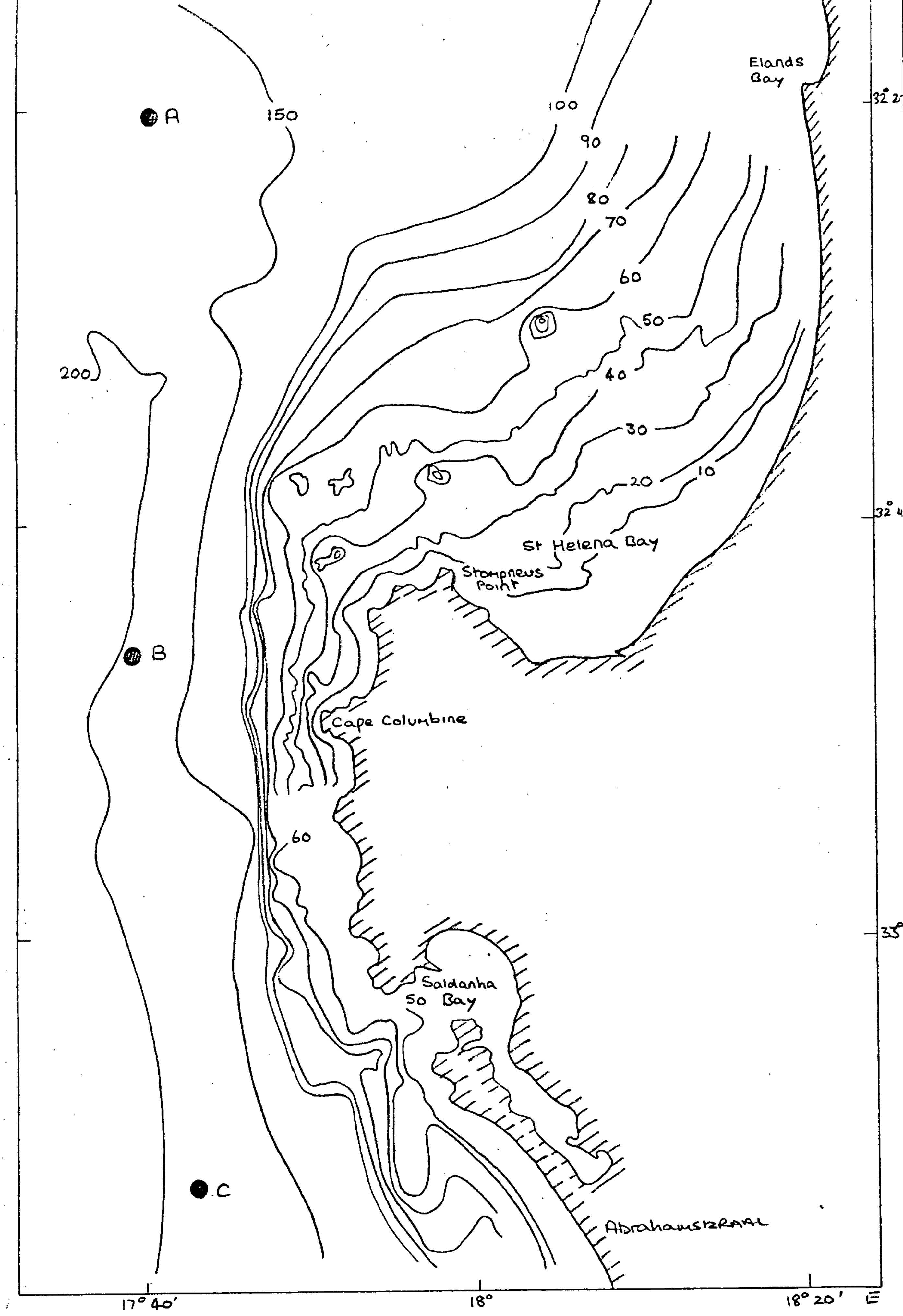

Fig 2: The St Helena Bay region showing the positions of the three current meter moorings deployed approximately on the 180 m isobath during the austral winter of 1982.

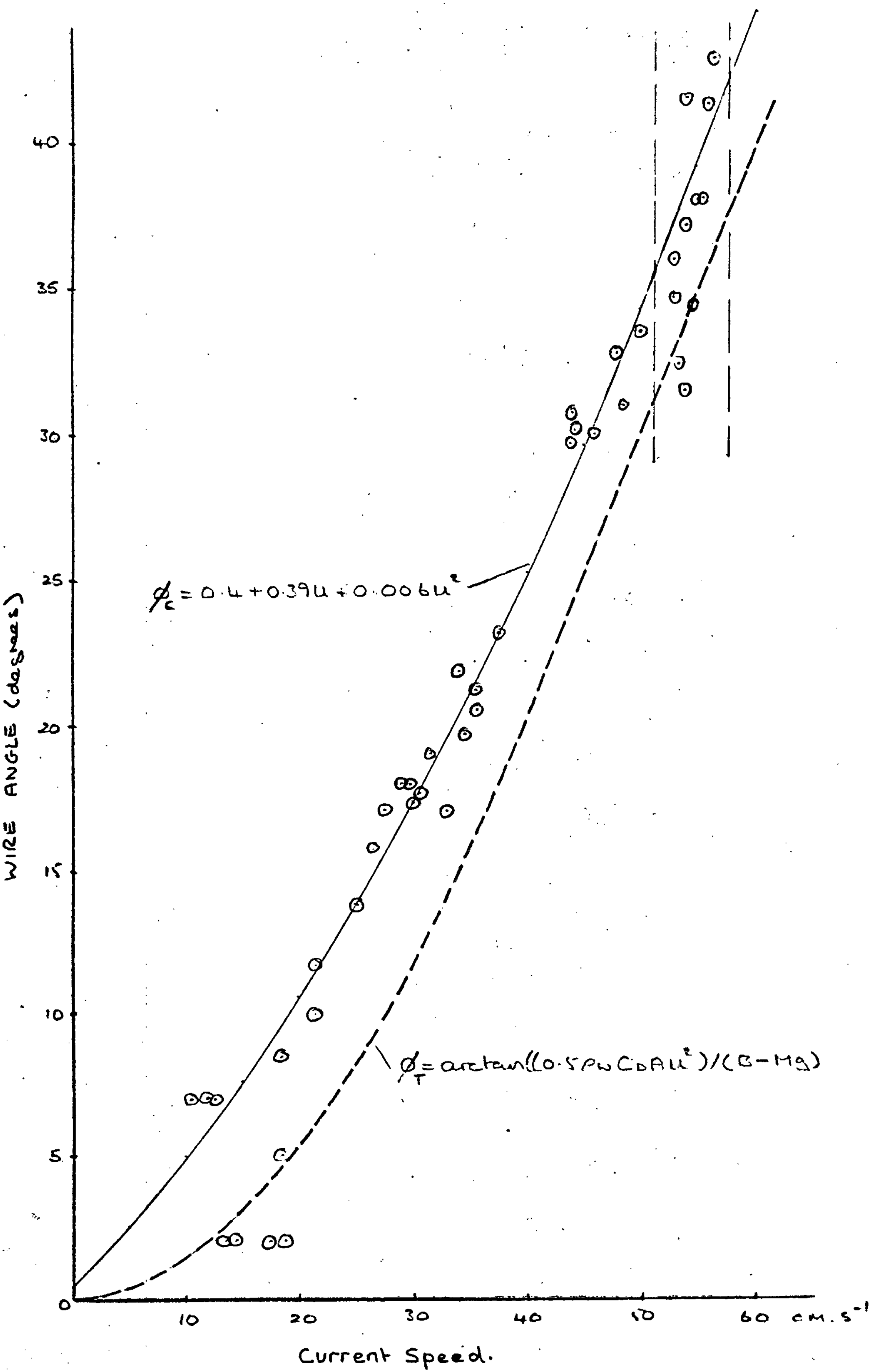

Fig 3: The theoretical and empirical relationships between the wire angle and current speed for mooring B.

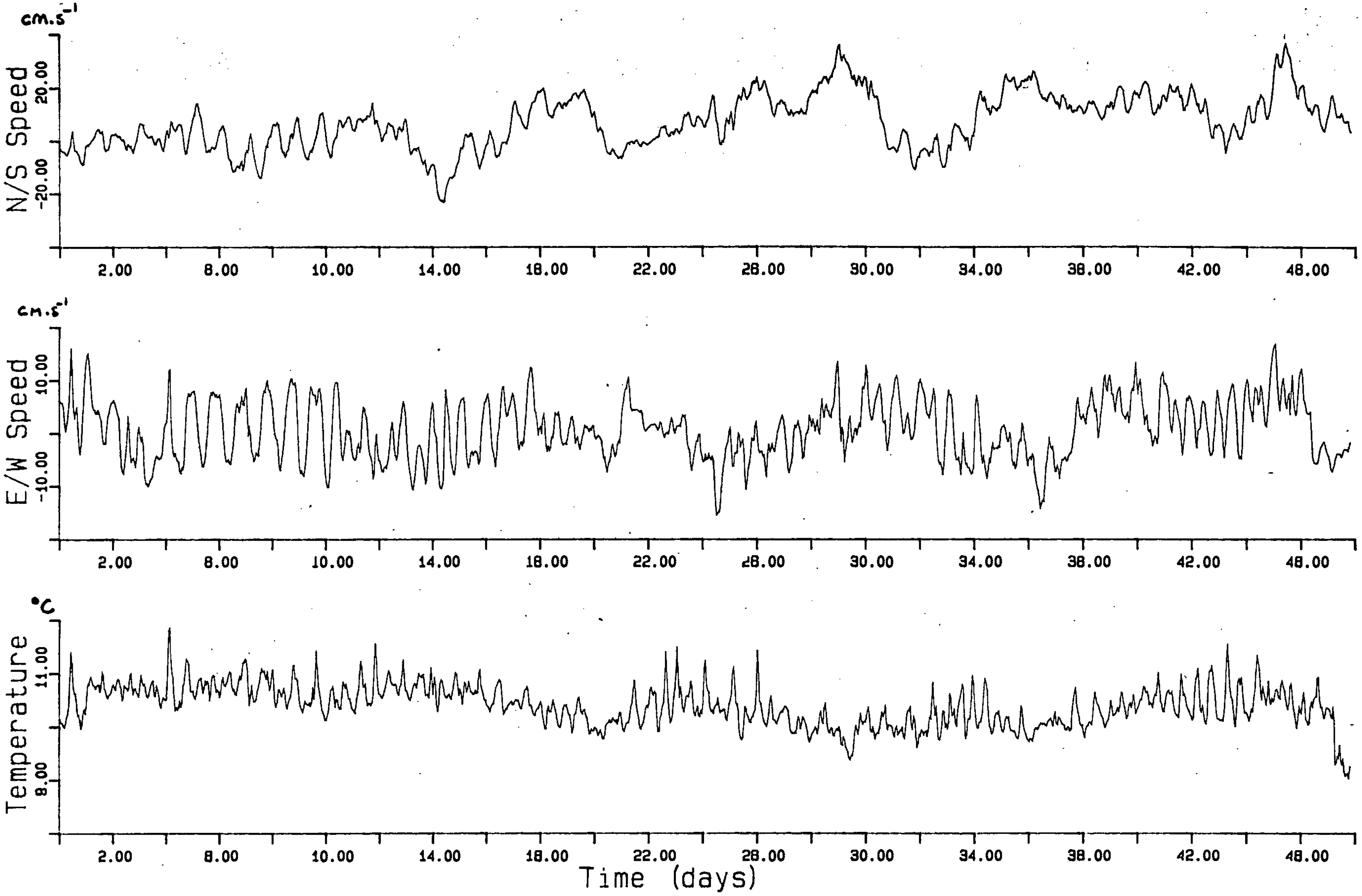

Fig 4: Upper current meter measurements at mooring A. Top - North/South current speed. Middle - East/West current speed. Bottom - water temperature.

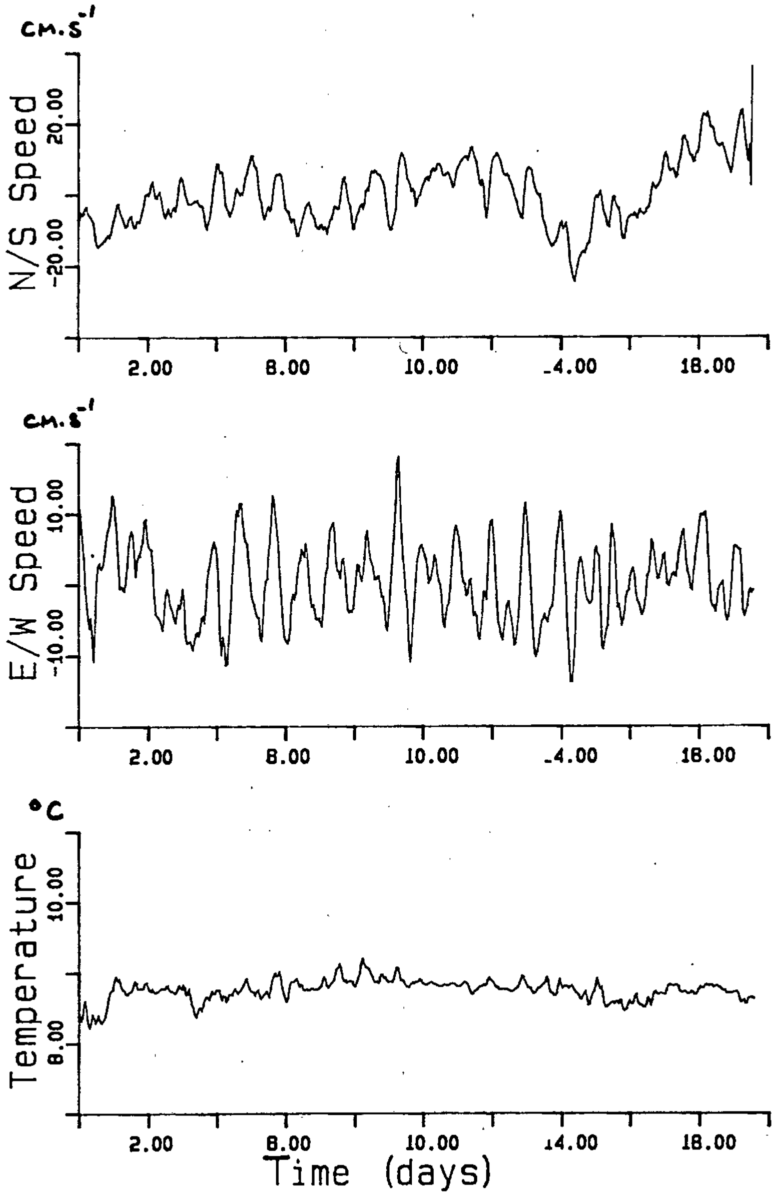

Fig 5: Lower current meter measurements at mooring A. Top - North/South current speed. Middle - East/West current speed. Bottom - water temperature.

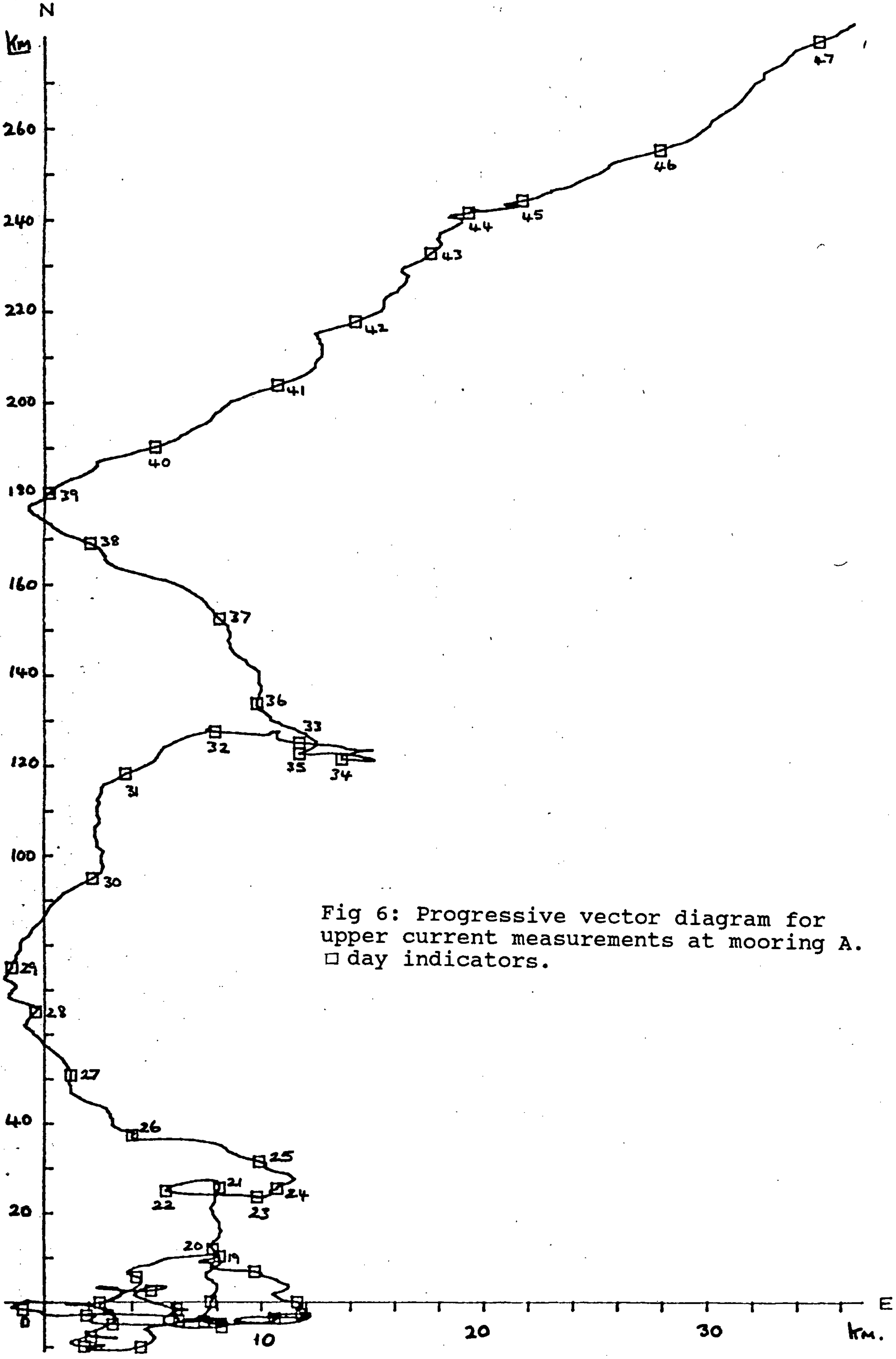

Fig 6: Progressive vector diagram for upper current measurements at mooring A. □ day indicators.

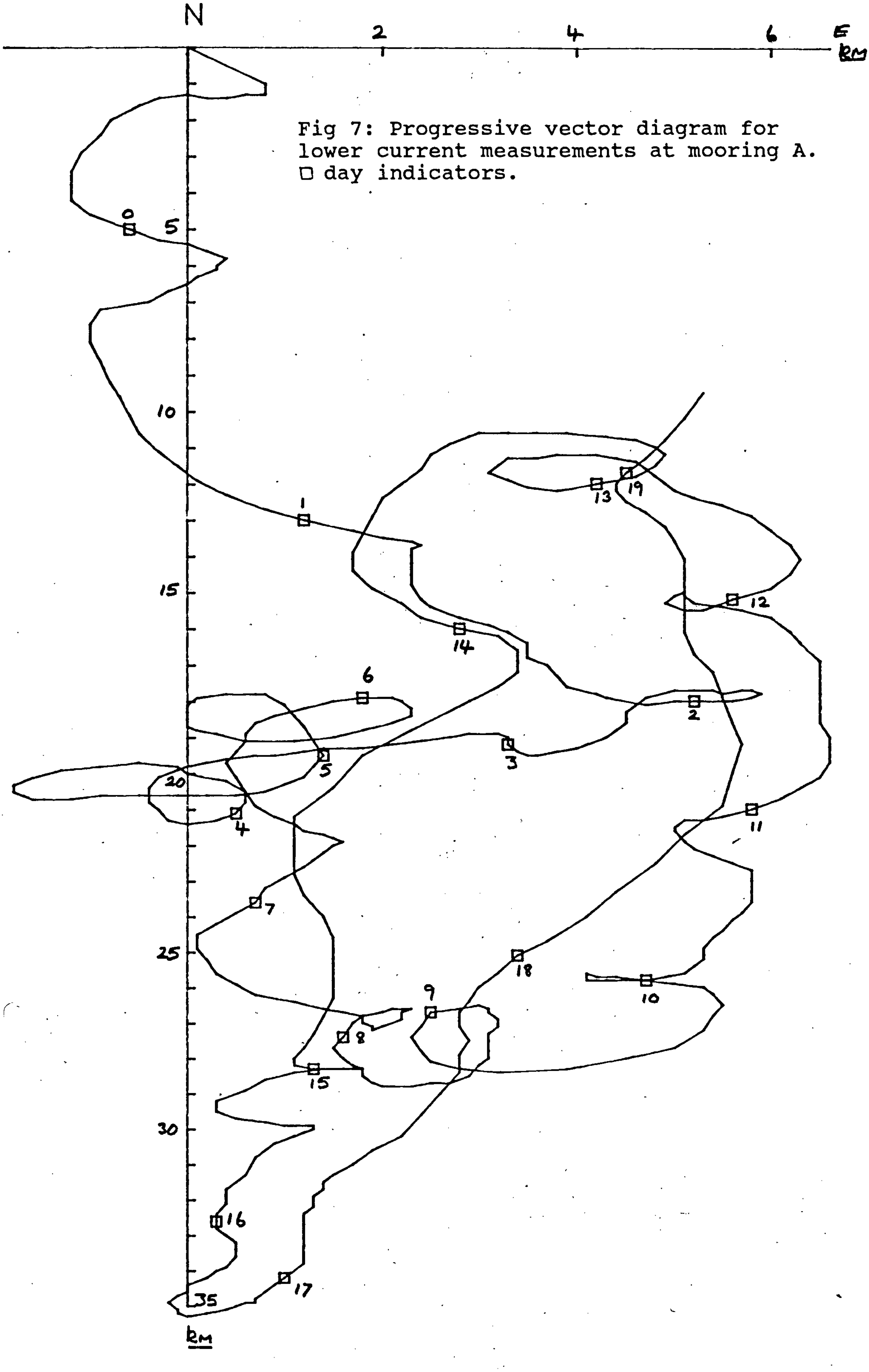

Fig 7: Progressive vector diagram for lower current measurements at mooring A. □ day indicators.

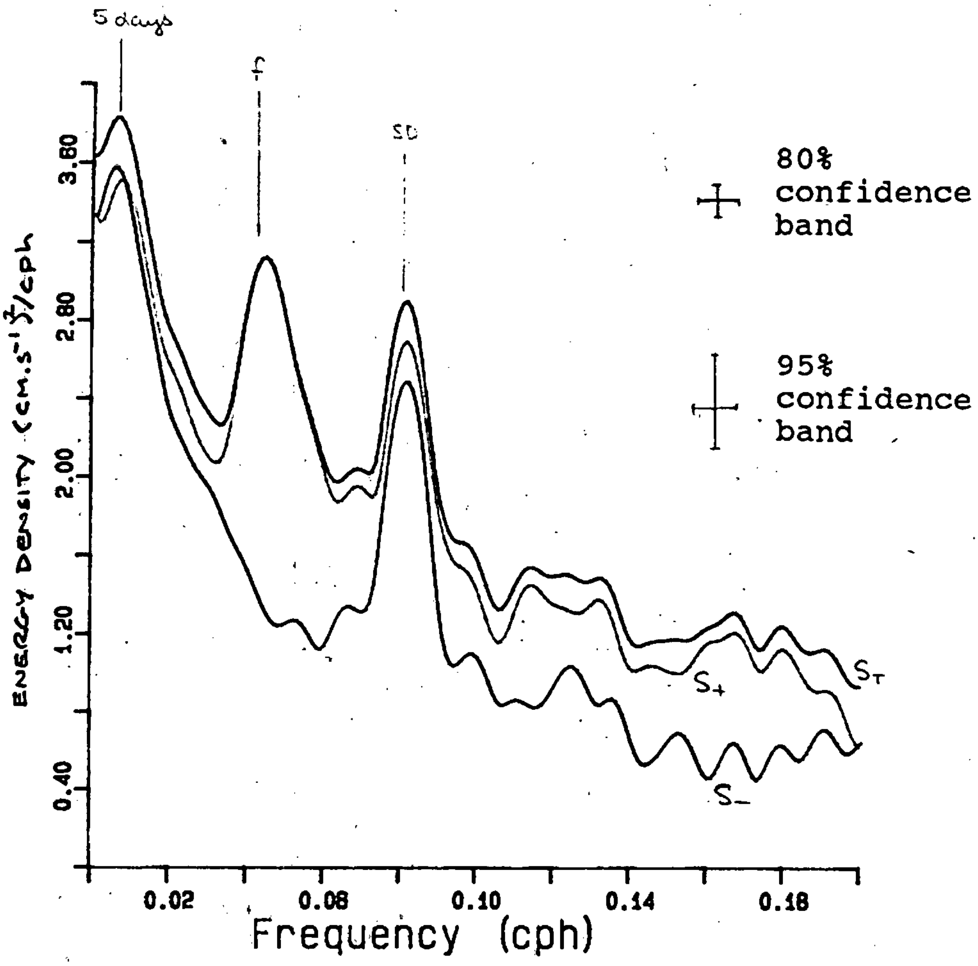

Fig 8: Rotary spectral estimates for upper currents at mooring A. $S_T$ total spectra. $S_-$ clockwise spectra. $S_+$ anticlocvkwise spectra.

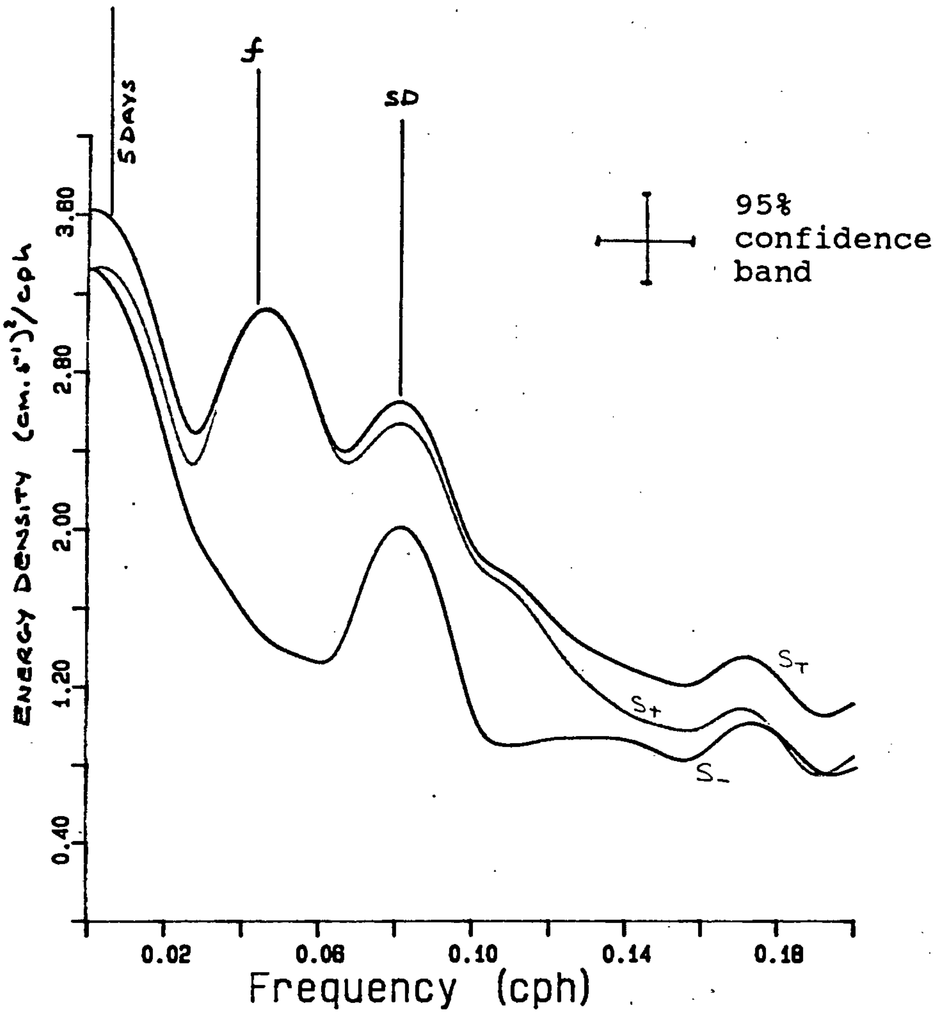

Fig 10: Rotary spectral estimates for lower currents at mooring A. $S_T$ total spectra. $S_-$ clockwise spectra. $S_+$ anticlockwise spectra.

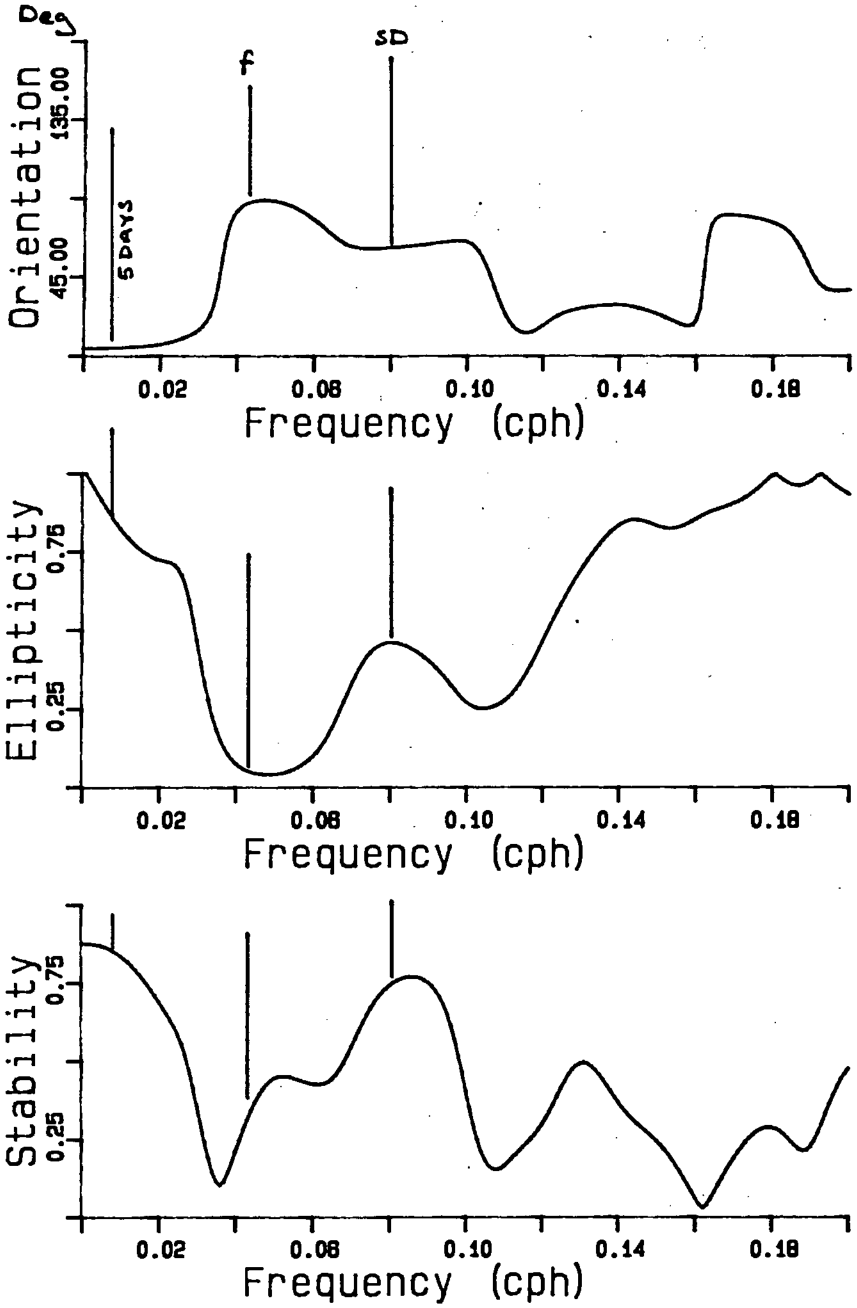

Fig 11: Elliptic properties for lower currents at mooring A. Top - ellipse orientation, with angles taken clockwise about true north. Middle - ellipse eccentricity. Bottom - ellipse stability.

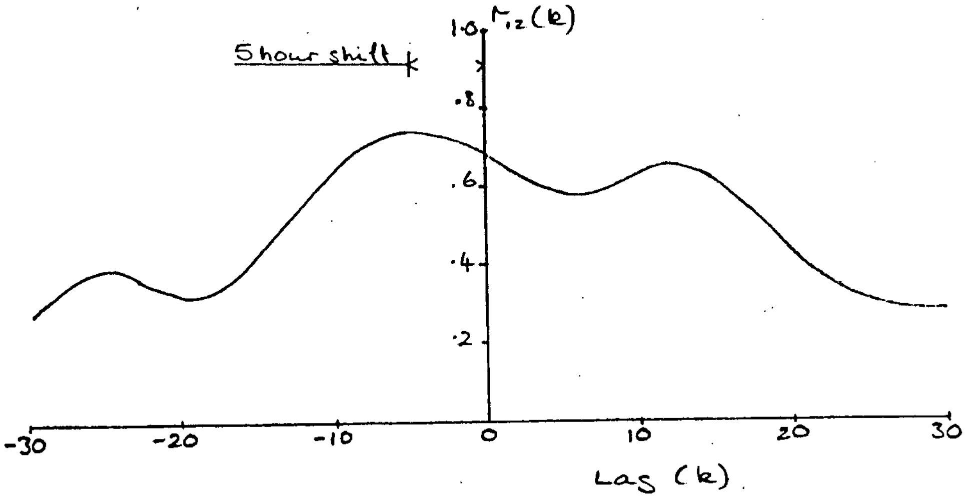

Fig 12: Cross correlation function (ccf) for upper and lower N/S current components at mooring A. Peak at k=-5 indicates a 5 hour lead by currents in the lower layer.

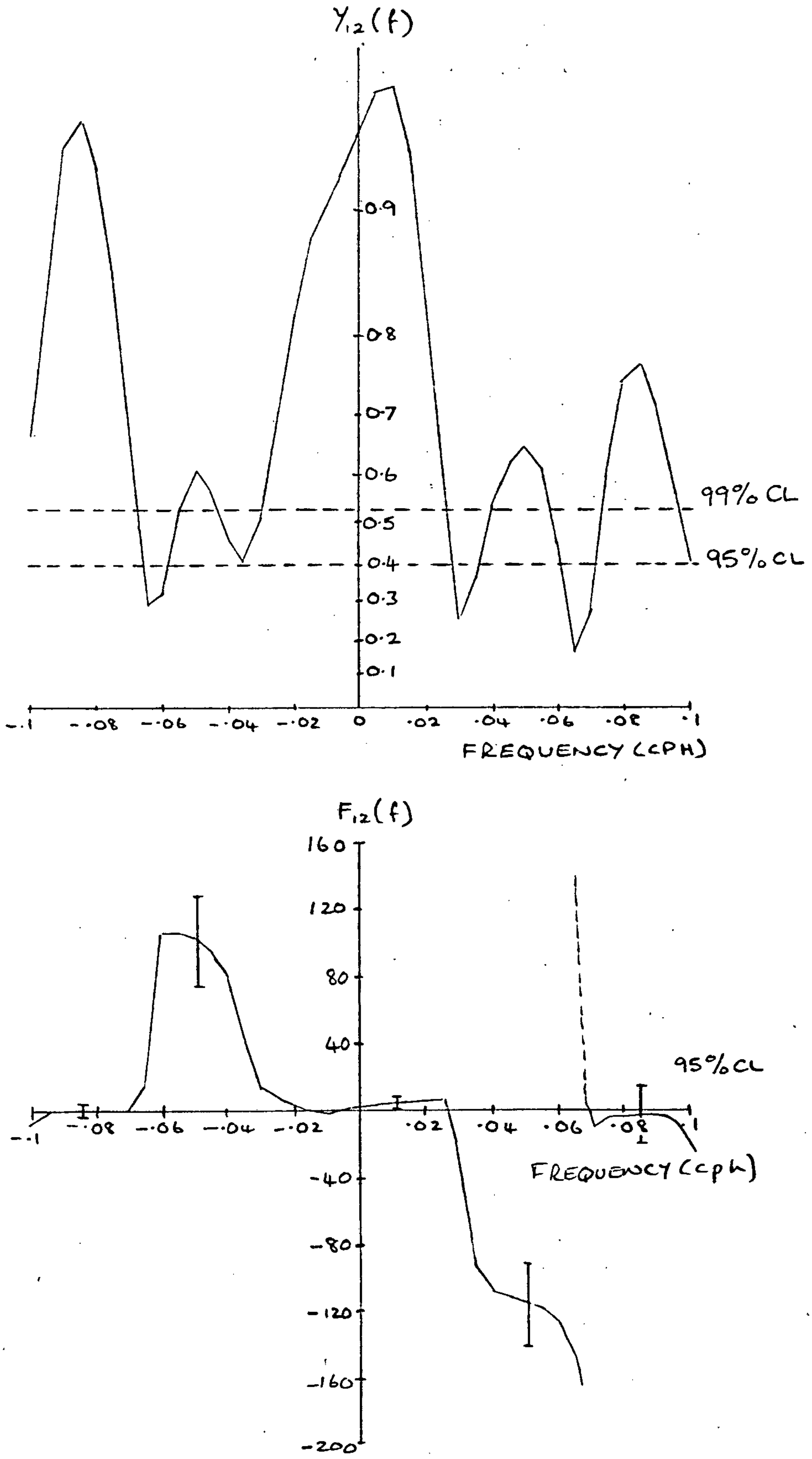

Fig 13: Vector coherence and phase for currents at mooring A.

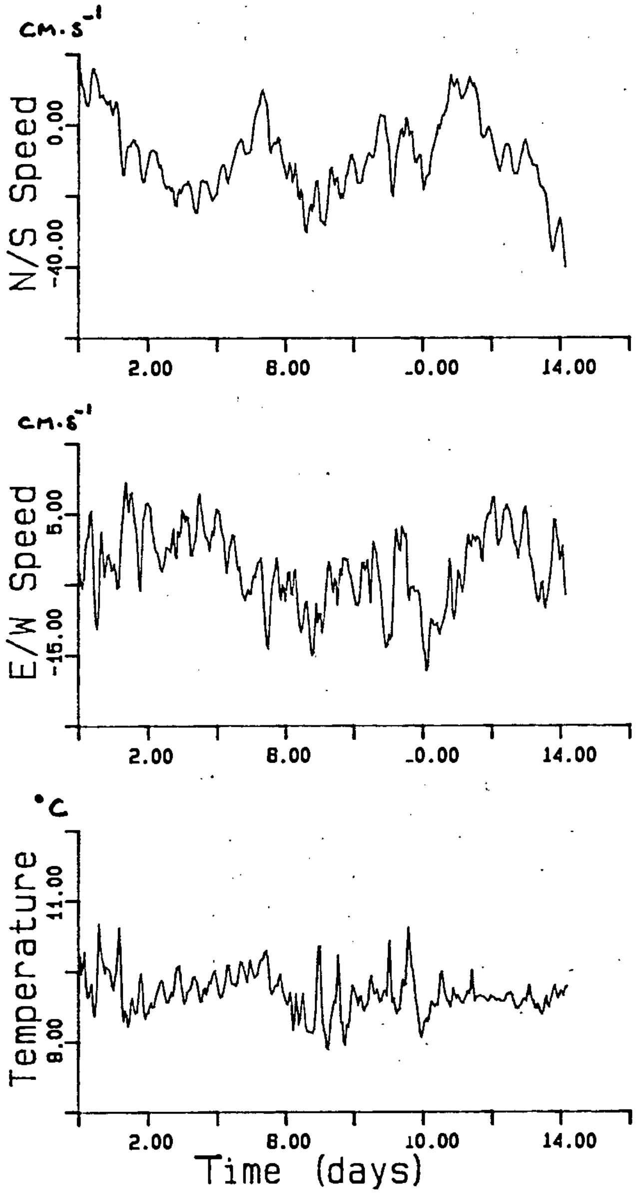

Fig 14: Upper current meter measurements at mooring B. Top - North/South current speed. Middle - East/West current speed. Bottom - water temperature.

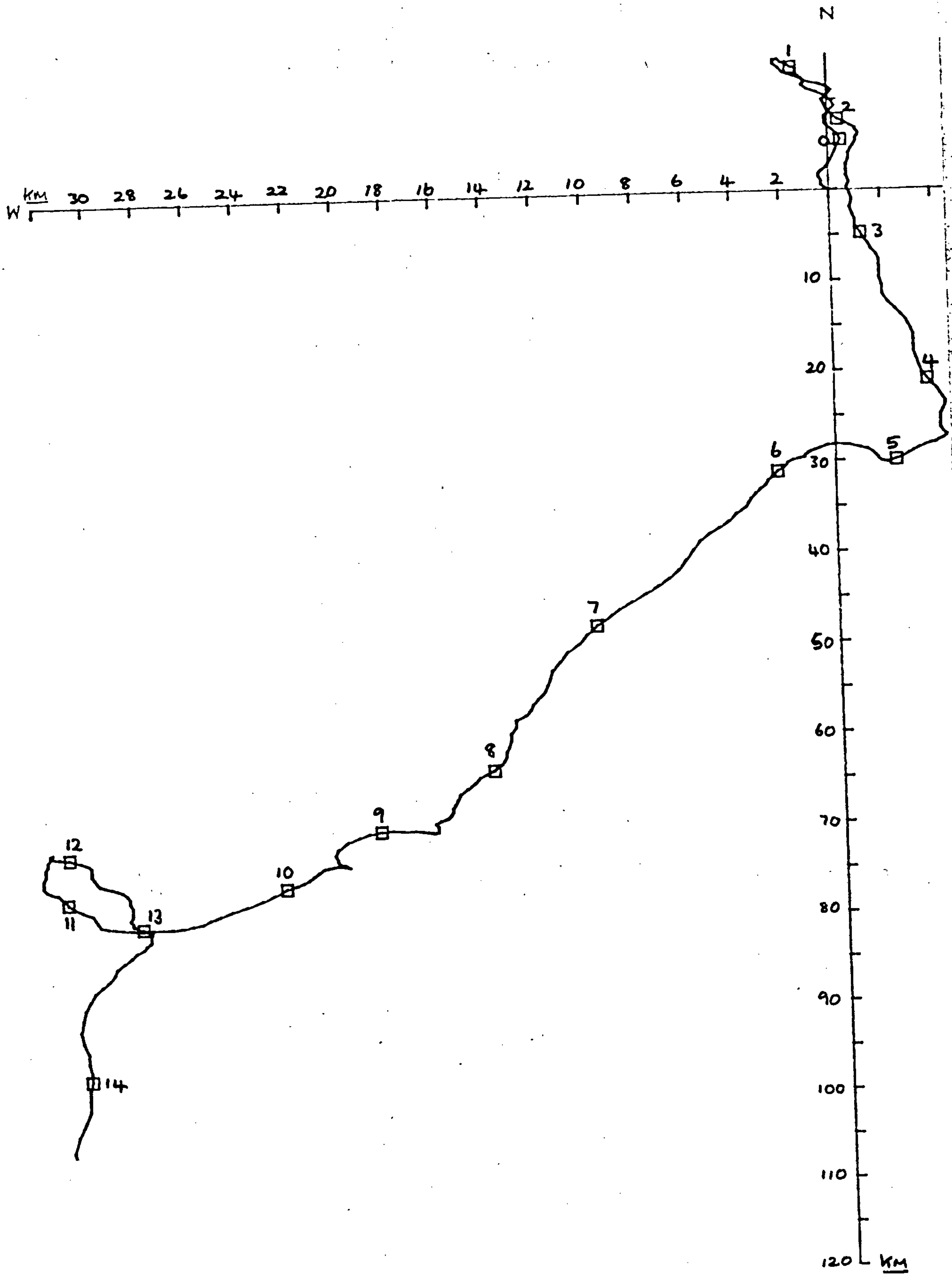

Fig 15: Progressive vector diagram for upper current measurements at mooring B. □ day indicators.

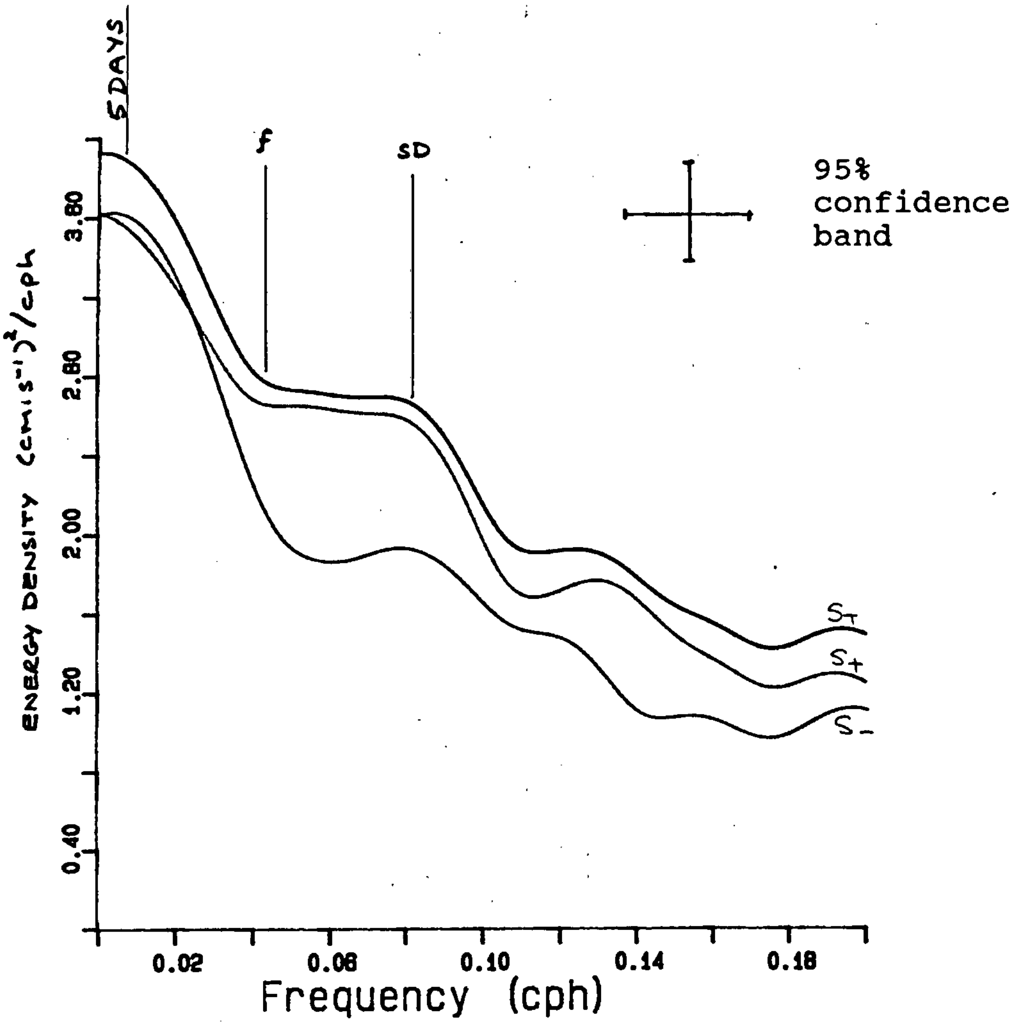

Fig 16: Rotary spectral estimates for upper currents at mooring B. $S_T$ total spectra. $S_-$ clockwise spectra. $S_+$ anticlockwise spectra.

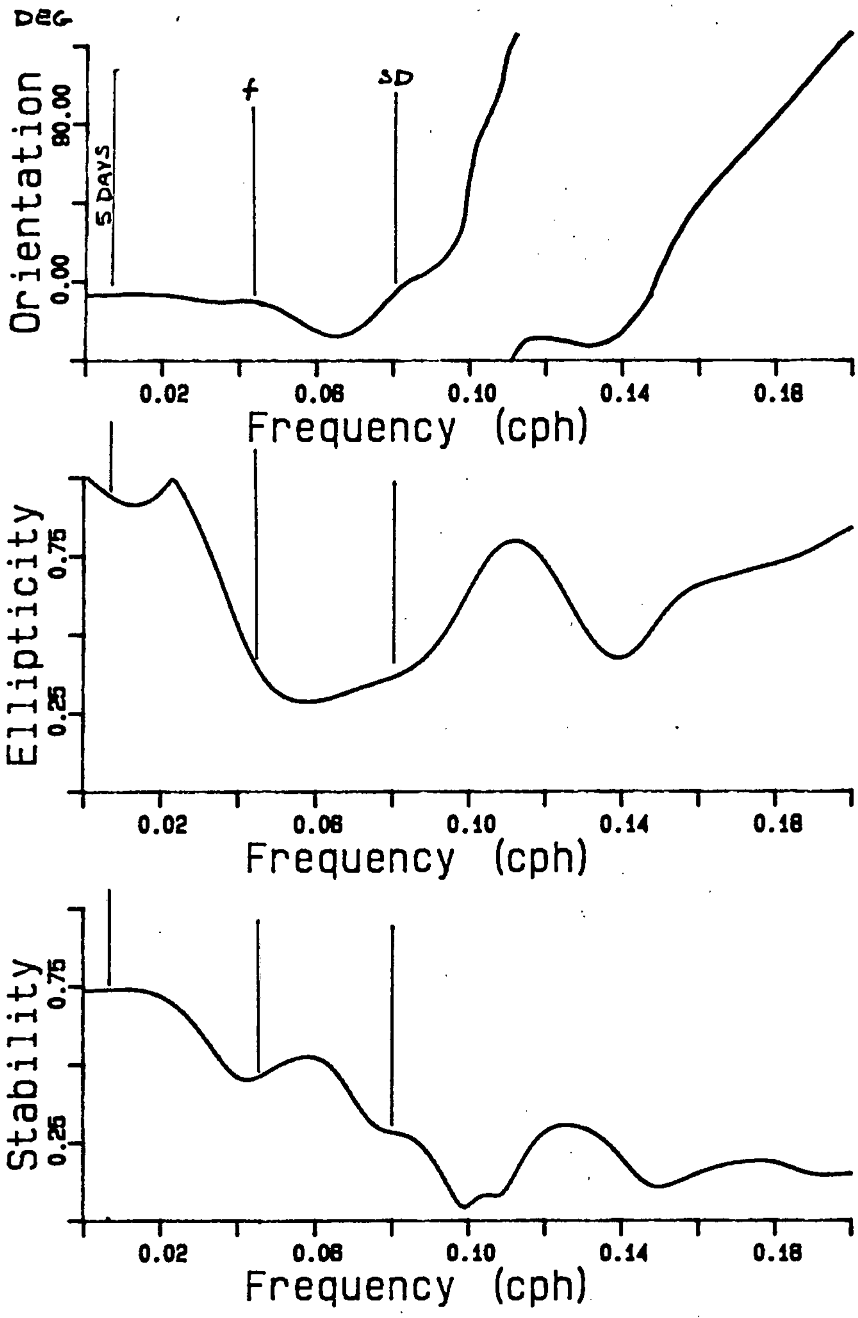

Fig 17: Elliptic properties for upper currents at mooring B. Top - ellipse orientation, with angles taken clockwise about true north. Middle - ellipse eccentricity. Bottom - ellipse stability.

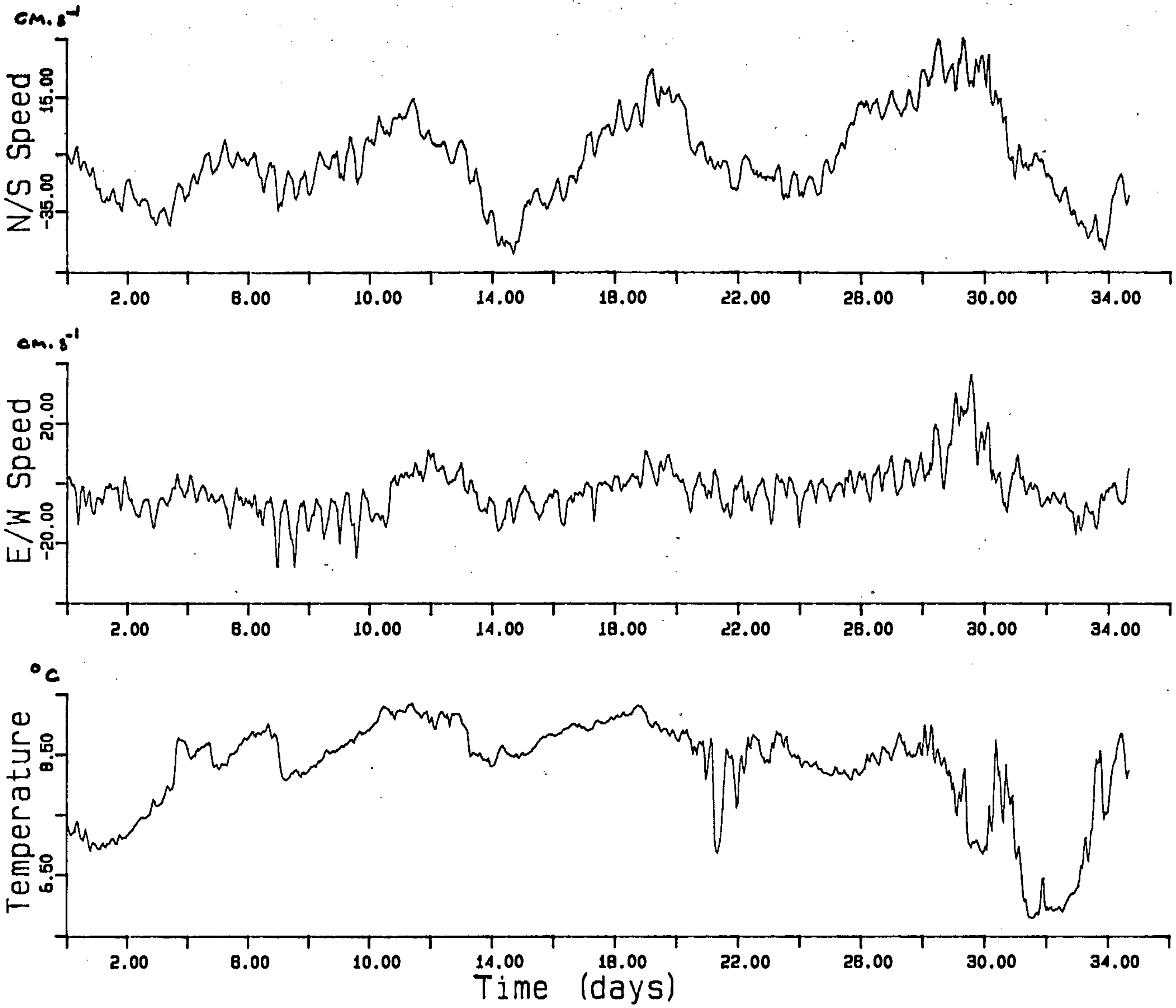

Fig 18: Lower current meter measurements at mooring B. Top - North/South current speed. Middle - East/West current speed. Bottom - water temperature.

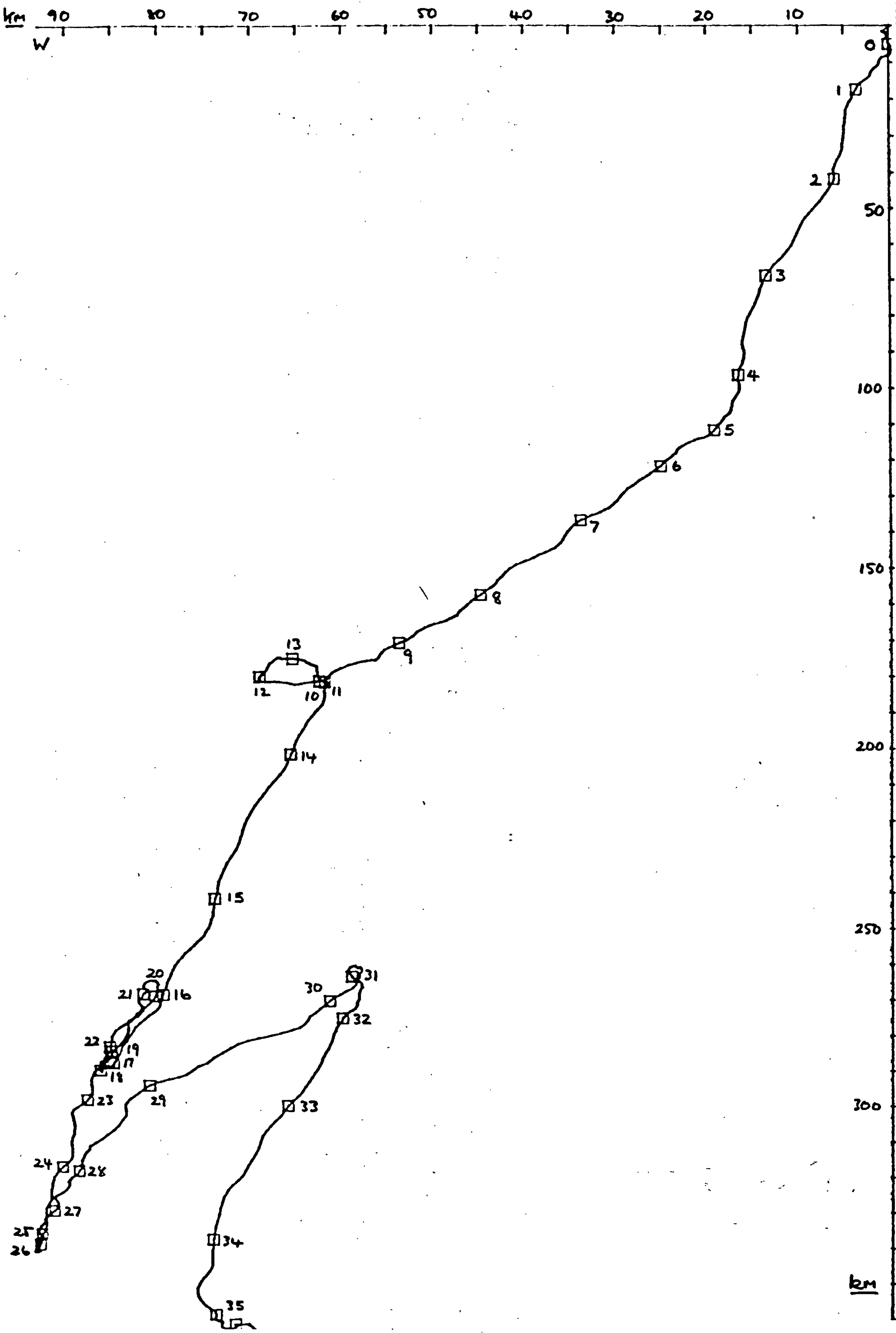

Fig 19: Progressive vector diagram for lower current measurments at mooring B. □ day indicators.

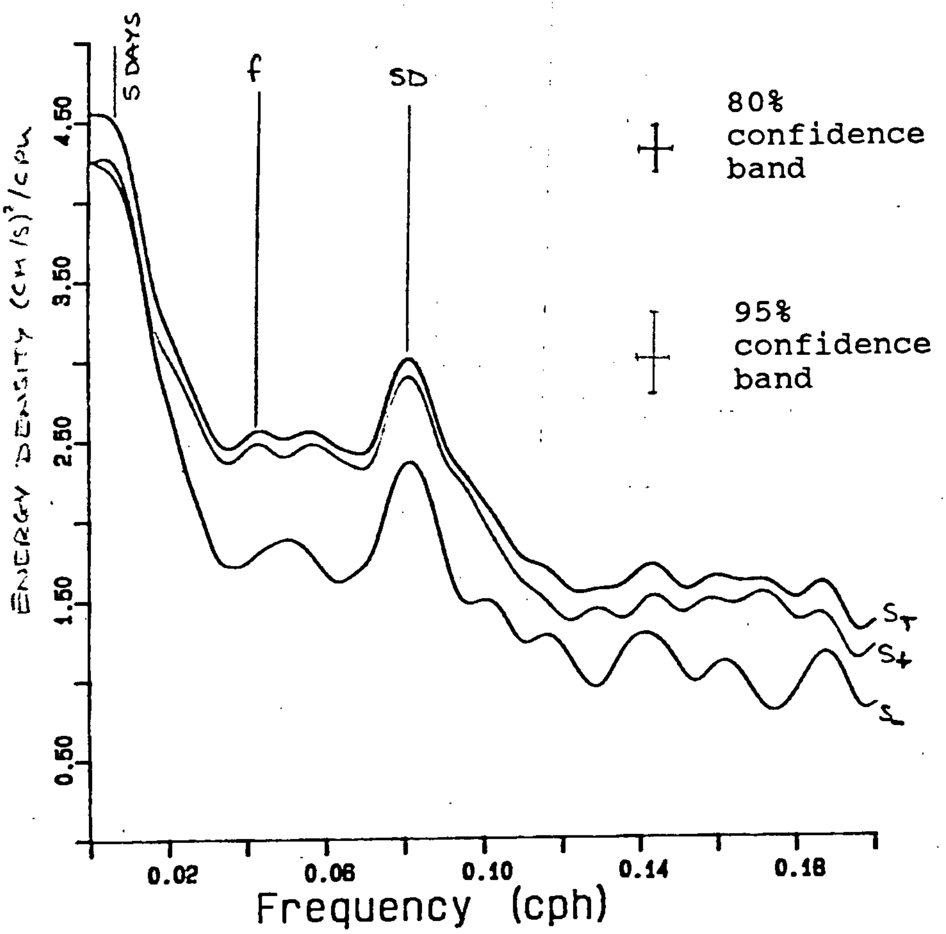

Fig 20: Rotary spectral estimates for lower currents at mooring B. $S_T$ total spectra. $S_-$ clockwise spectra. $S_+$ anticlockwise spectra.

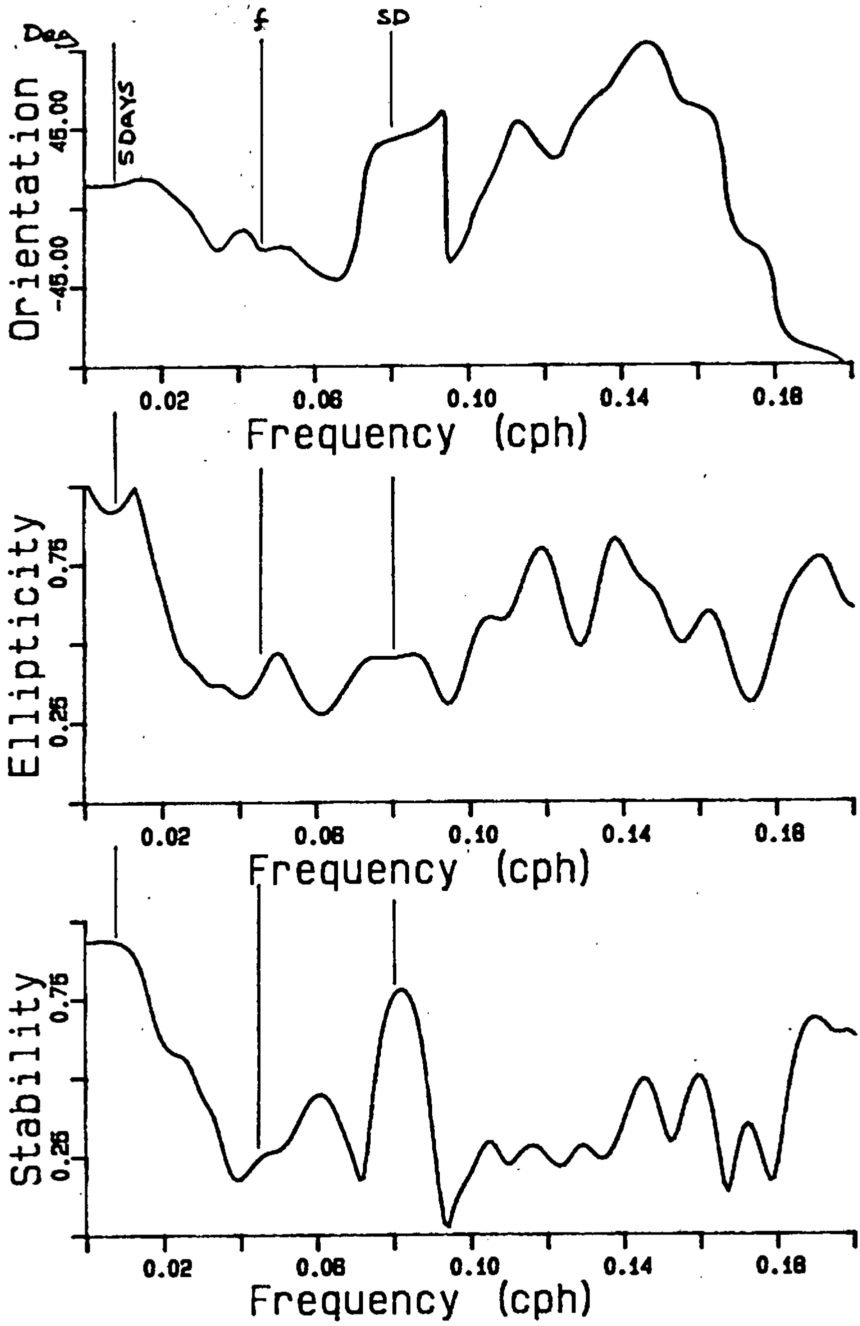

Fig 21: Elliptic properties for lower currents at mooring B. Top - ellipse orientation, with angles taken clockwise about true north. Middle - ellipse eccentricity. Bottom - ellipse stability.

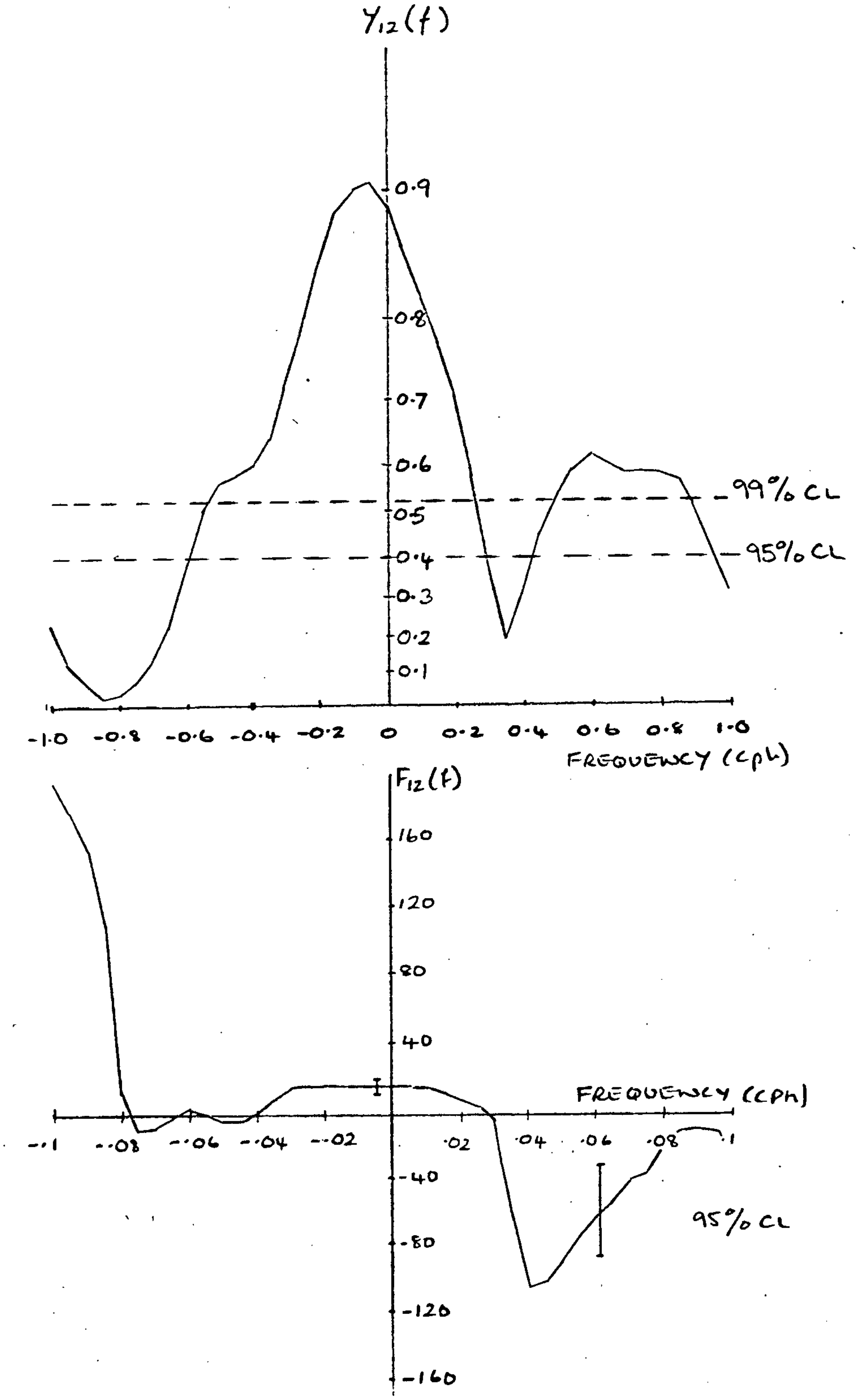

Fig 22: Vector coherence and phase for currents at mooring B.

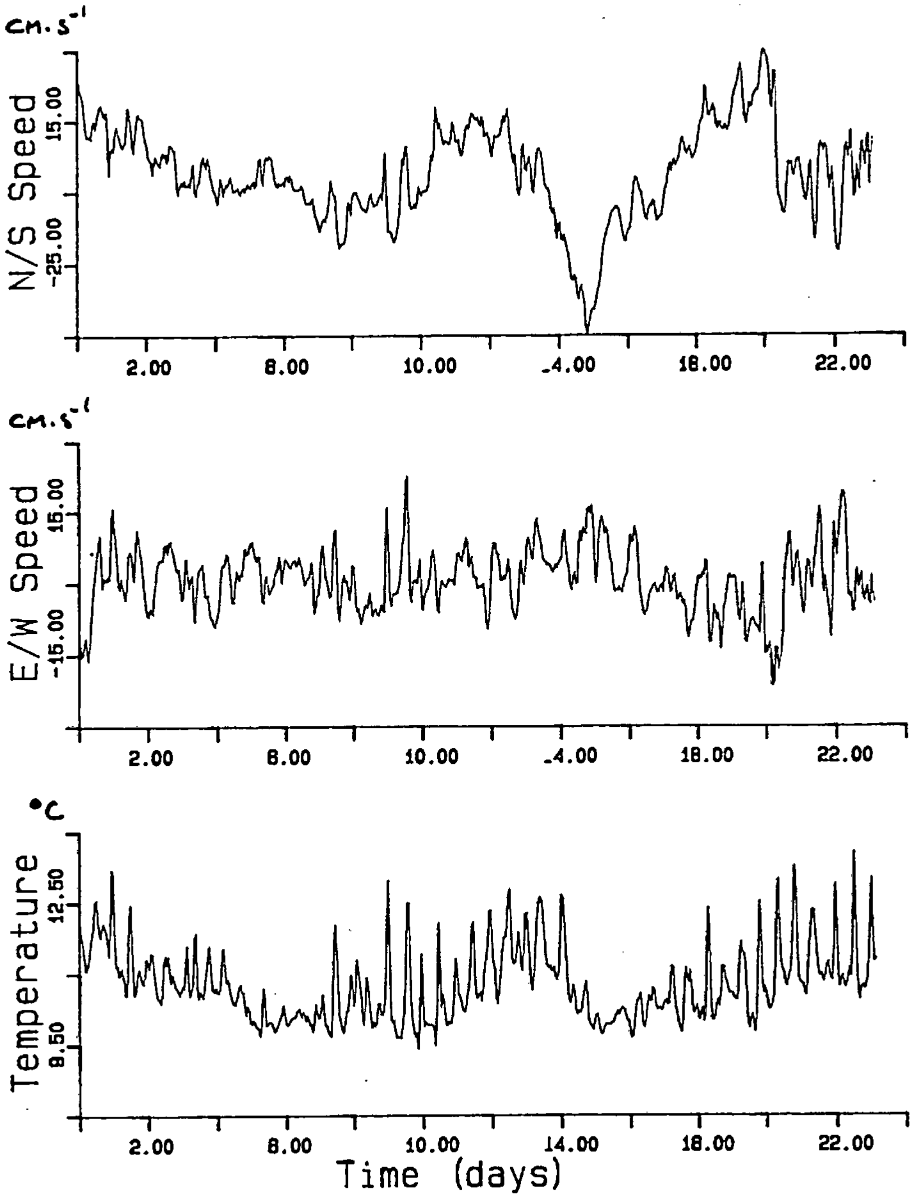

Fig 23: Upper current meter measurements at mooring C. Top - North/South current speed. Middle - East/West current speed. Bottom - water temperature.

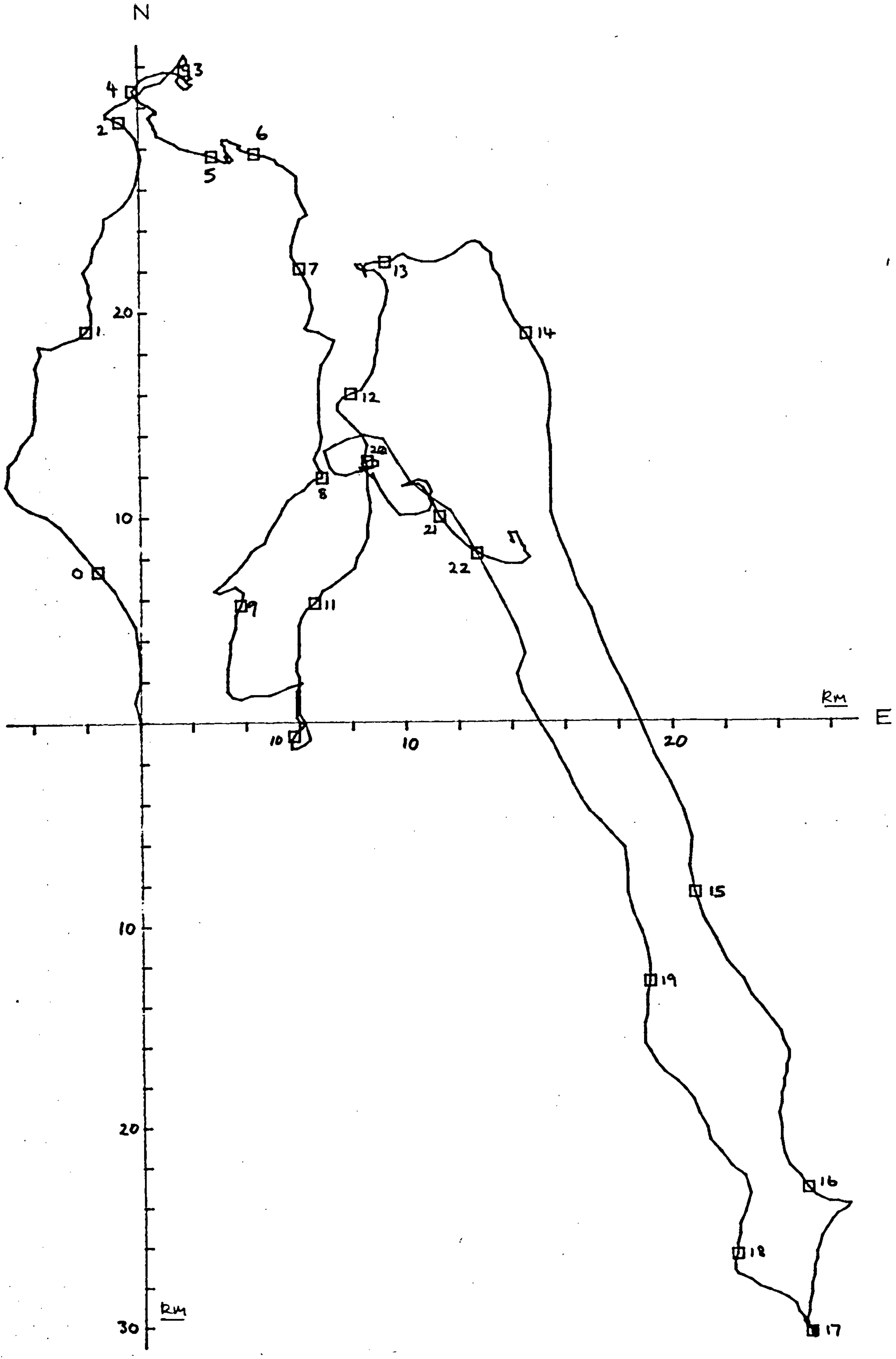

Fig 24: Progressive vector diagram for upper current measurements at mooring C. □ day indicators.

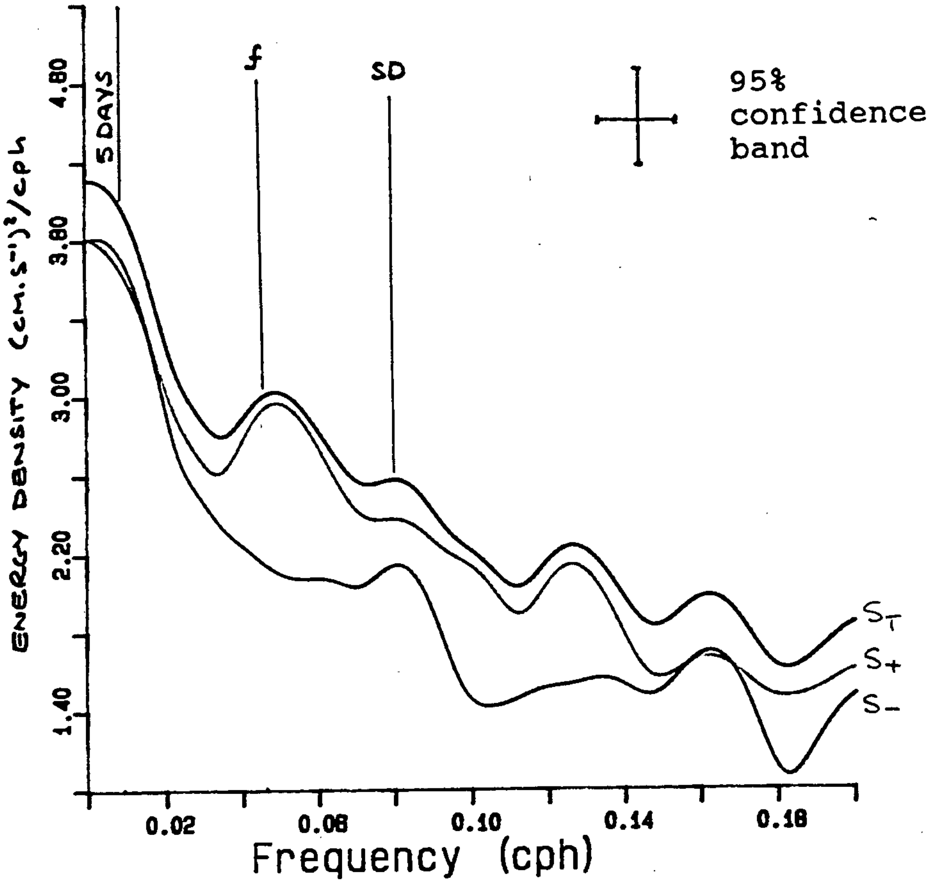

Fig 25: Rotary spectral estimates for upper currents at mooring C. $S_T$ total spectra. $S_-$ clockwise spectra. $S_+$ anticlockwise spectra.

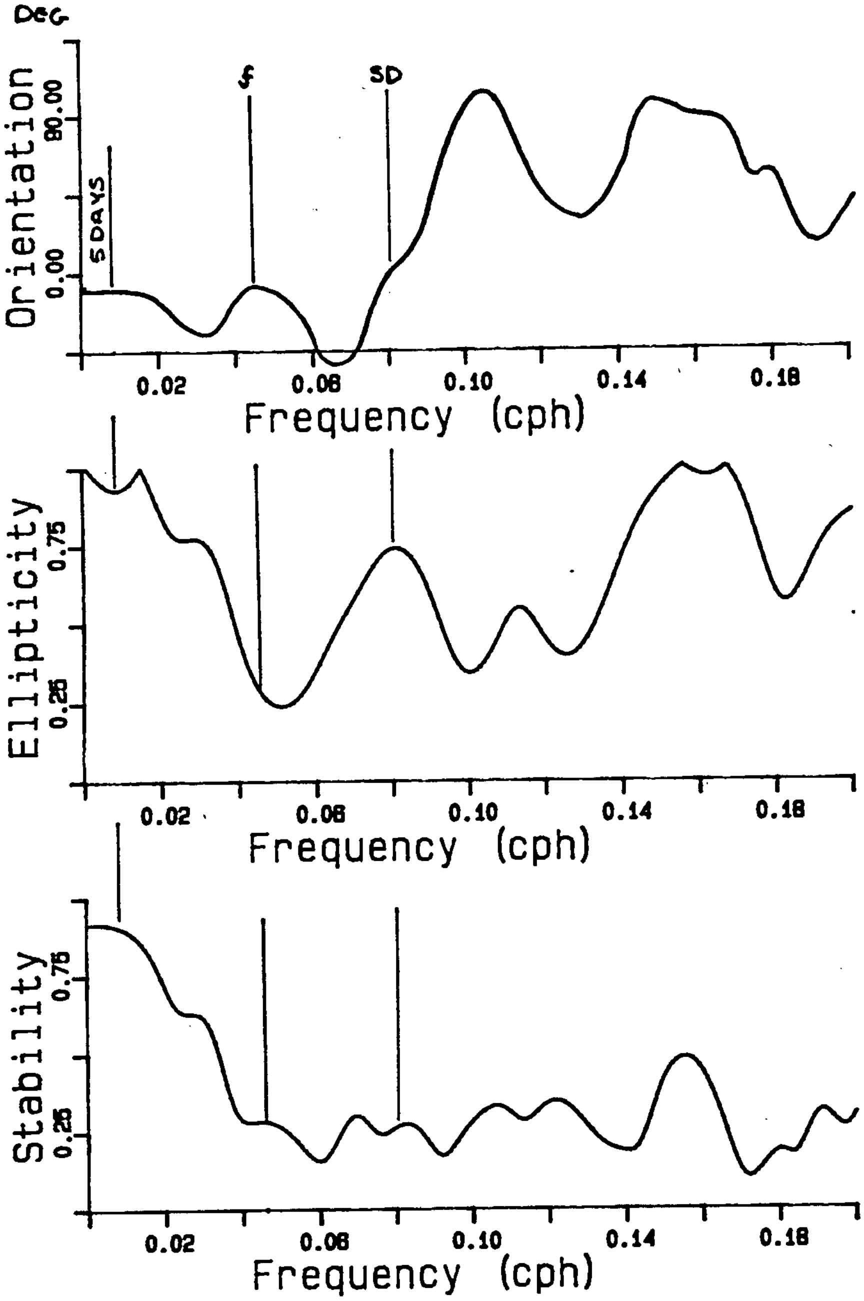

Fig 26: Ellipse properties for upper currents at mooring C. Top - ellipse orientation, with angles taken about true north. Middle - ellipse eccentricity. Bottom - ellipse stability.

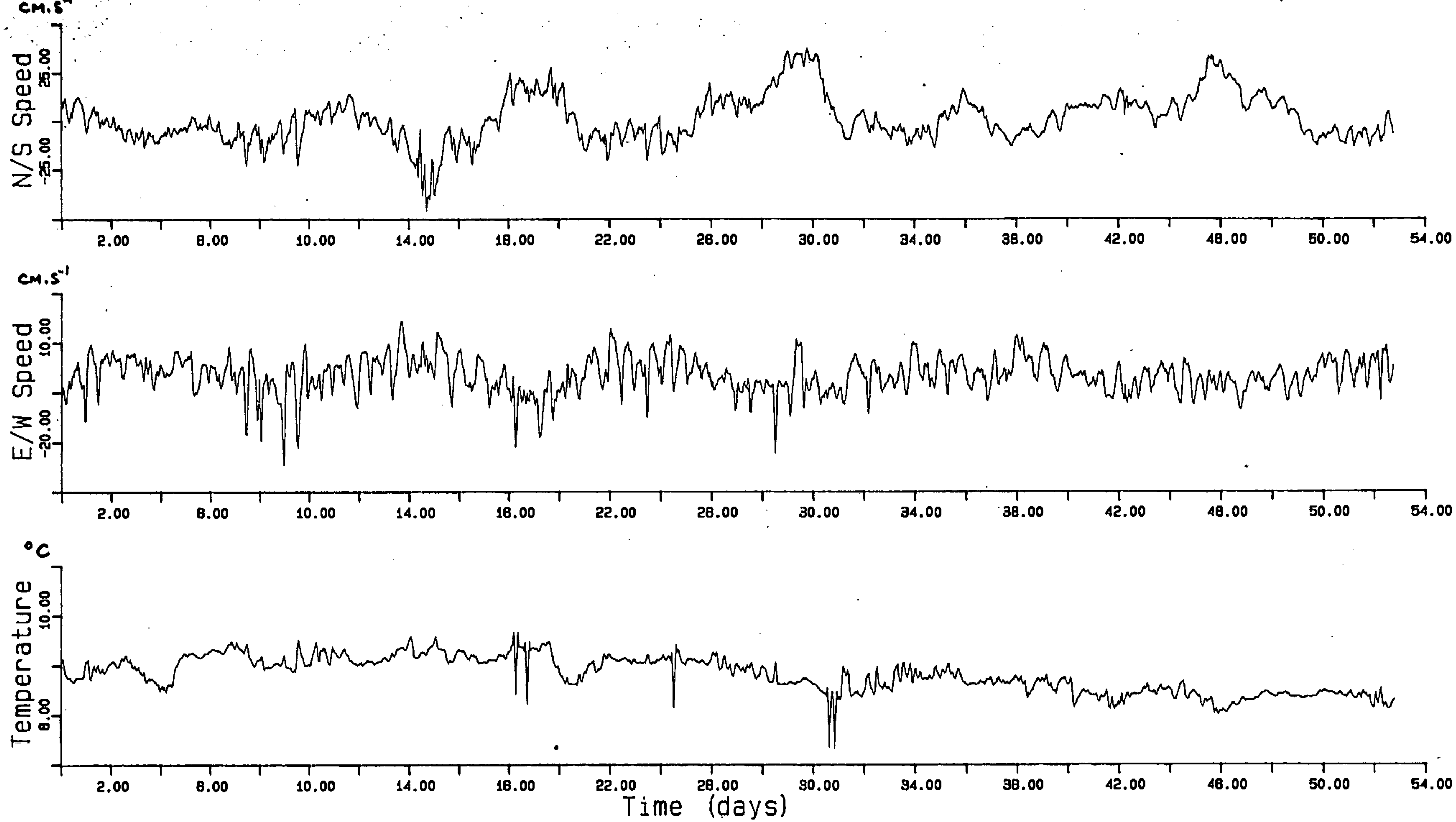

Fig 27: Lower current meter measurements at mooring C. Top - North/South current speed. Middle - East/West current speed. Bottom - water temperature.

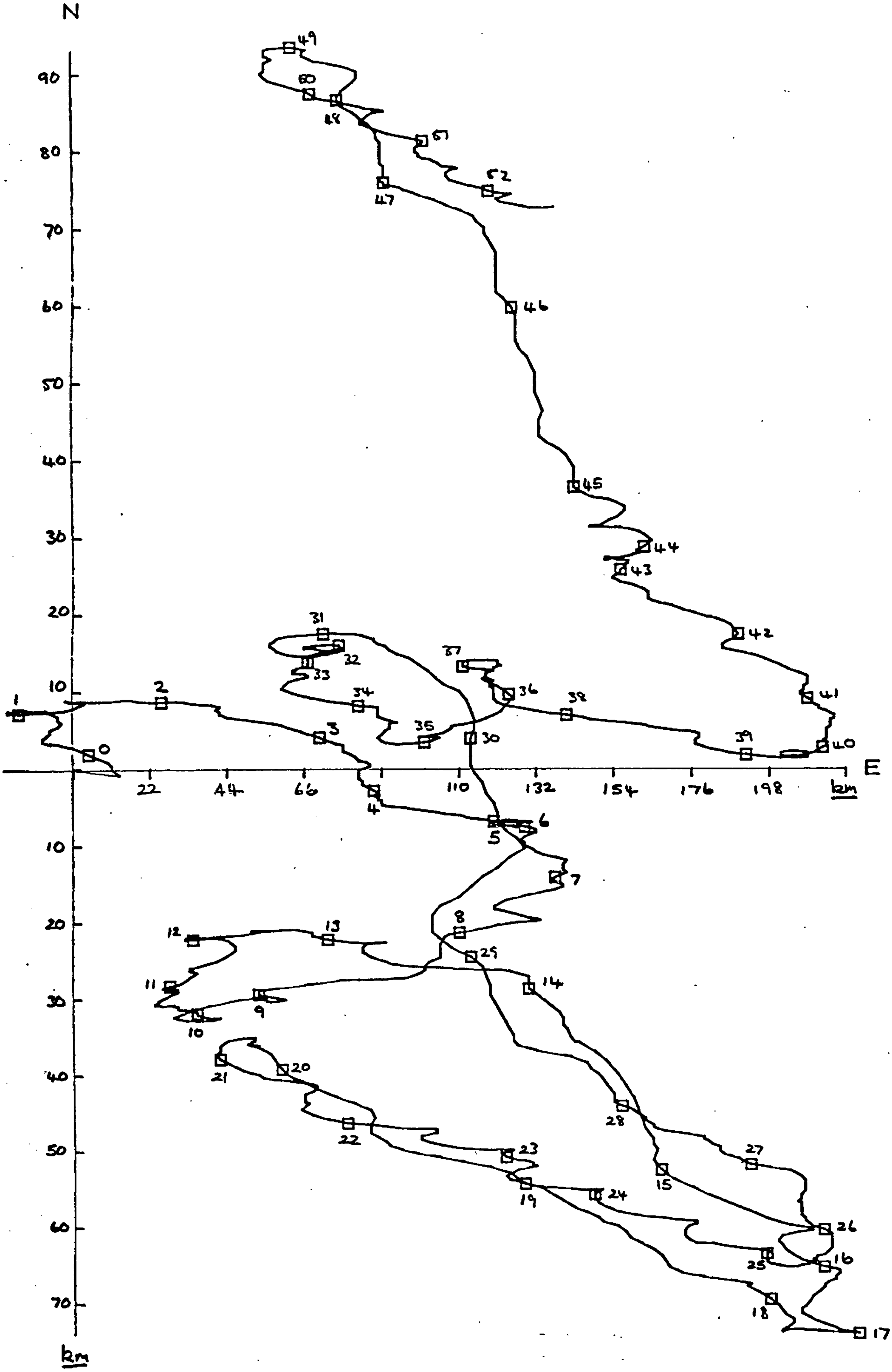

Fig 28: Progressive vector diagram for lower current meter measurements at mooring C. ☐ day indicators.

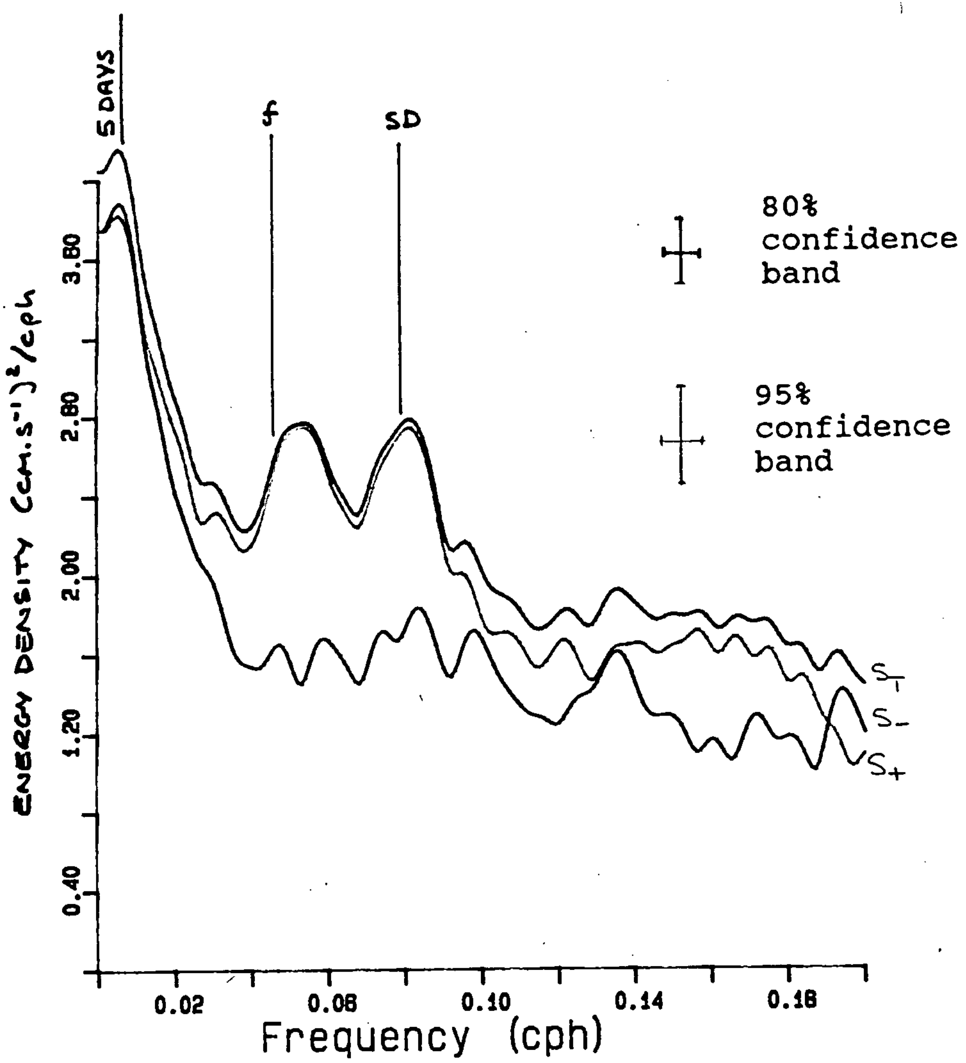

Fig 29: Rotary spectral estimates for lower currents at mooring C. $S_T$ total spectra. $S_-$ clockwise spectra. $S_+$ anticlockwise spectra.

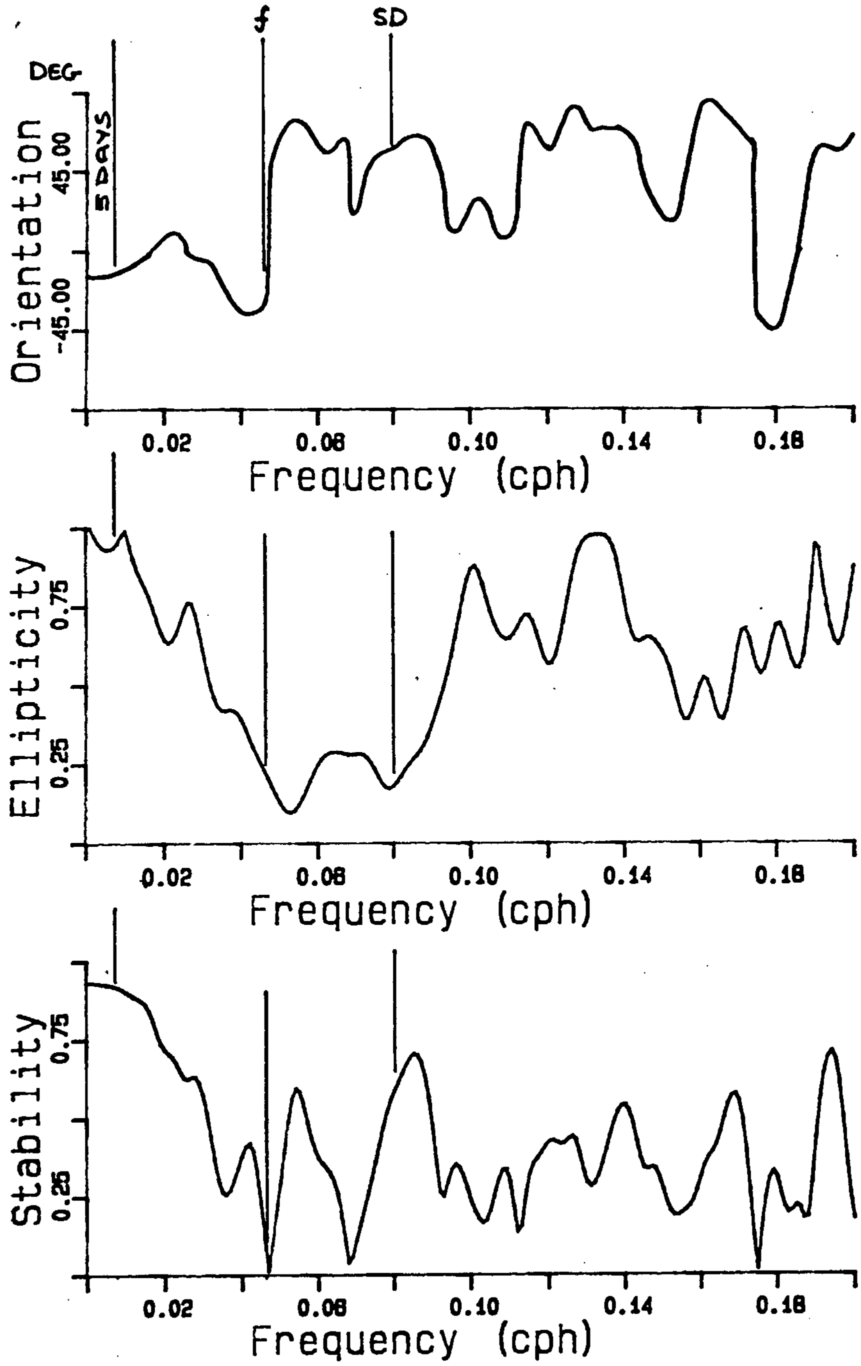

Fig 30: Ellipse properties for lower currents at mooring C. Top - ellipse orientation, with angles taken about true north. Middle - ellipse eccentricity. Bottom - ellipse stability.

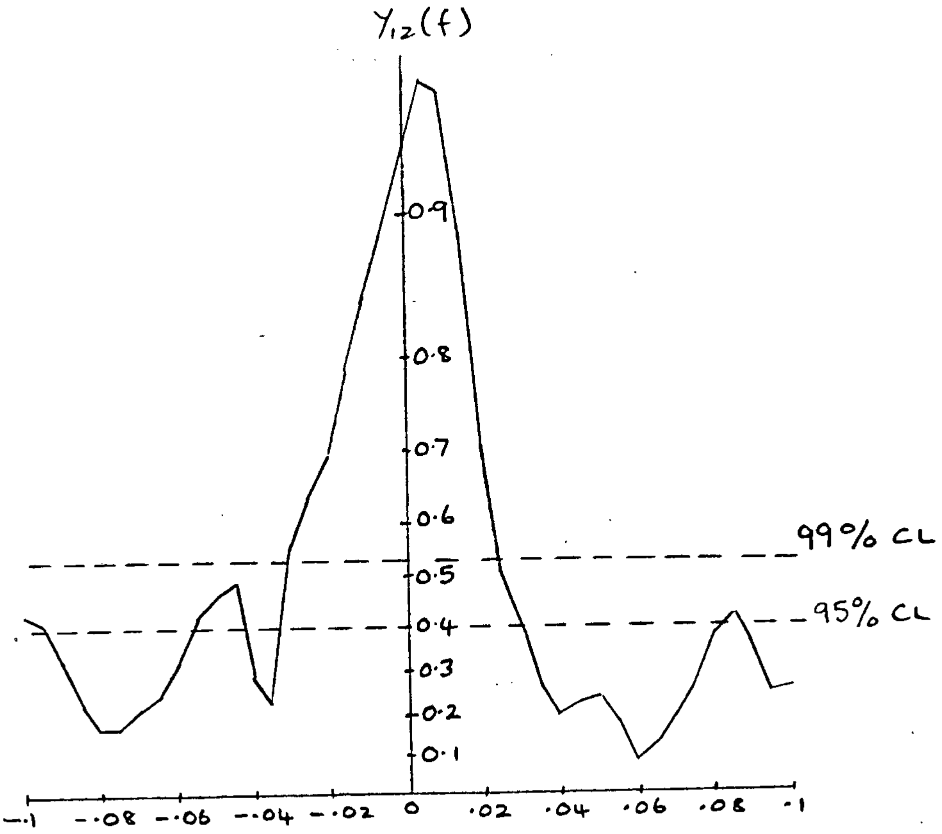

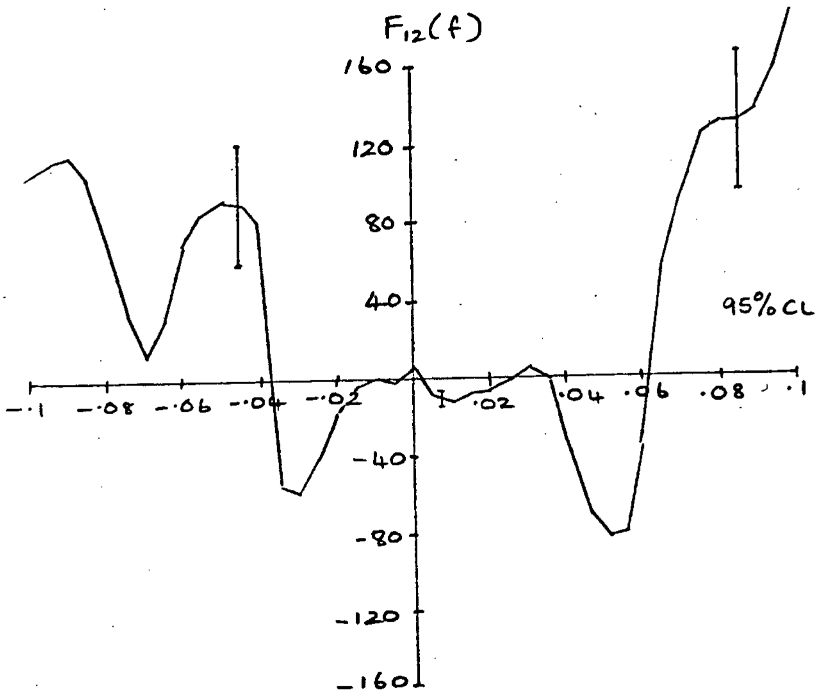

Fig 31: Vector coherence and phase for mooring C.

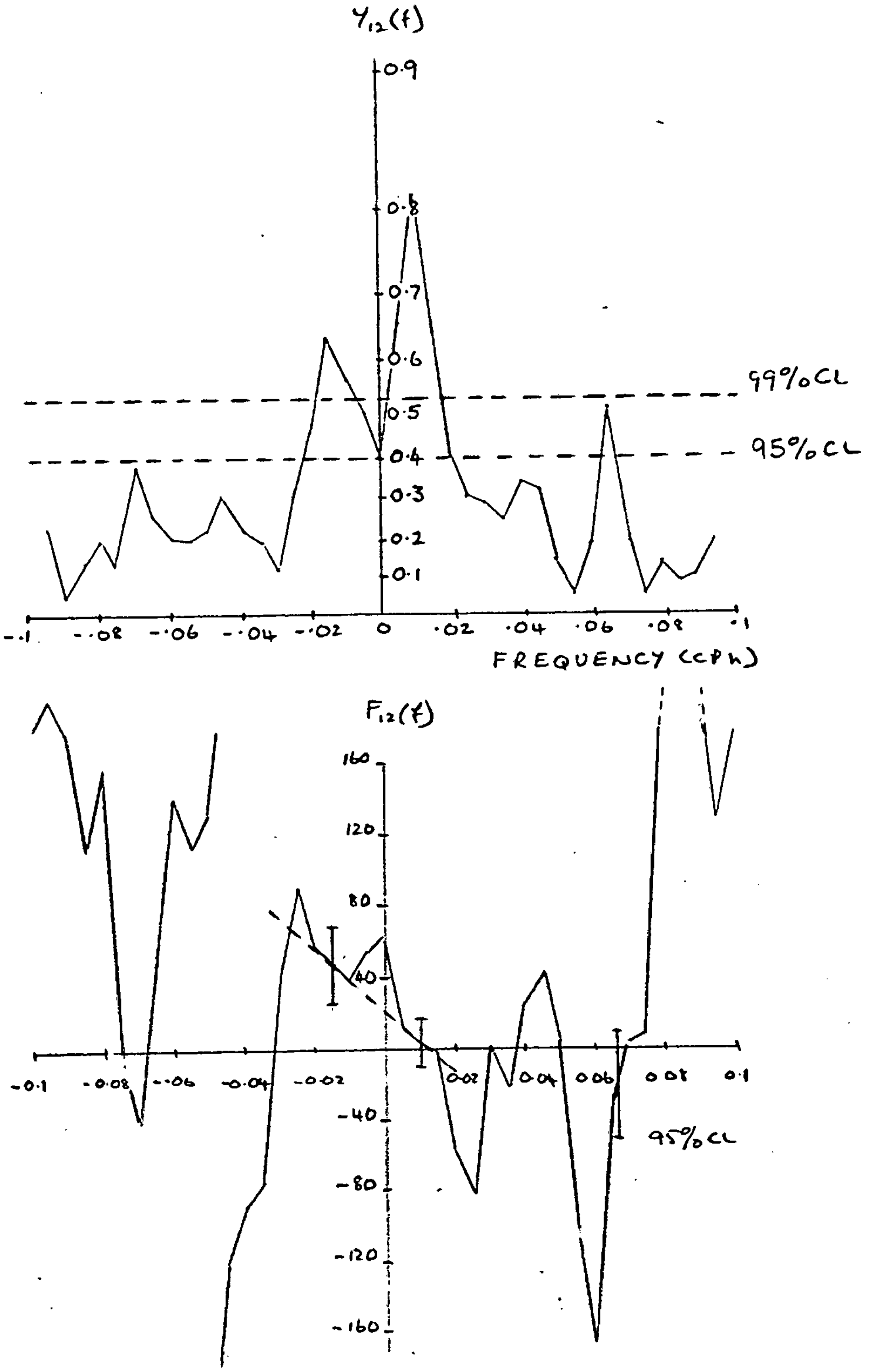

Fig 32: Vector coherence and phase for upper currents at A and lower currents at C.

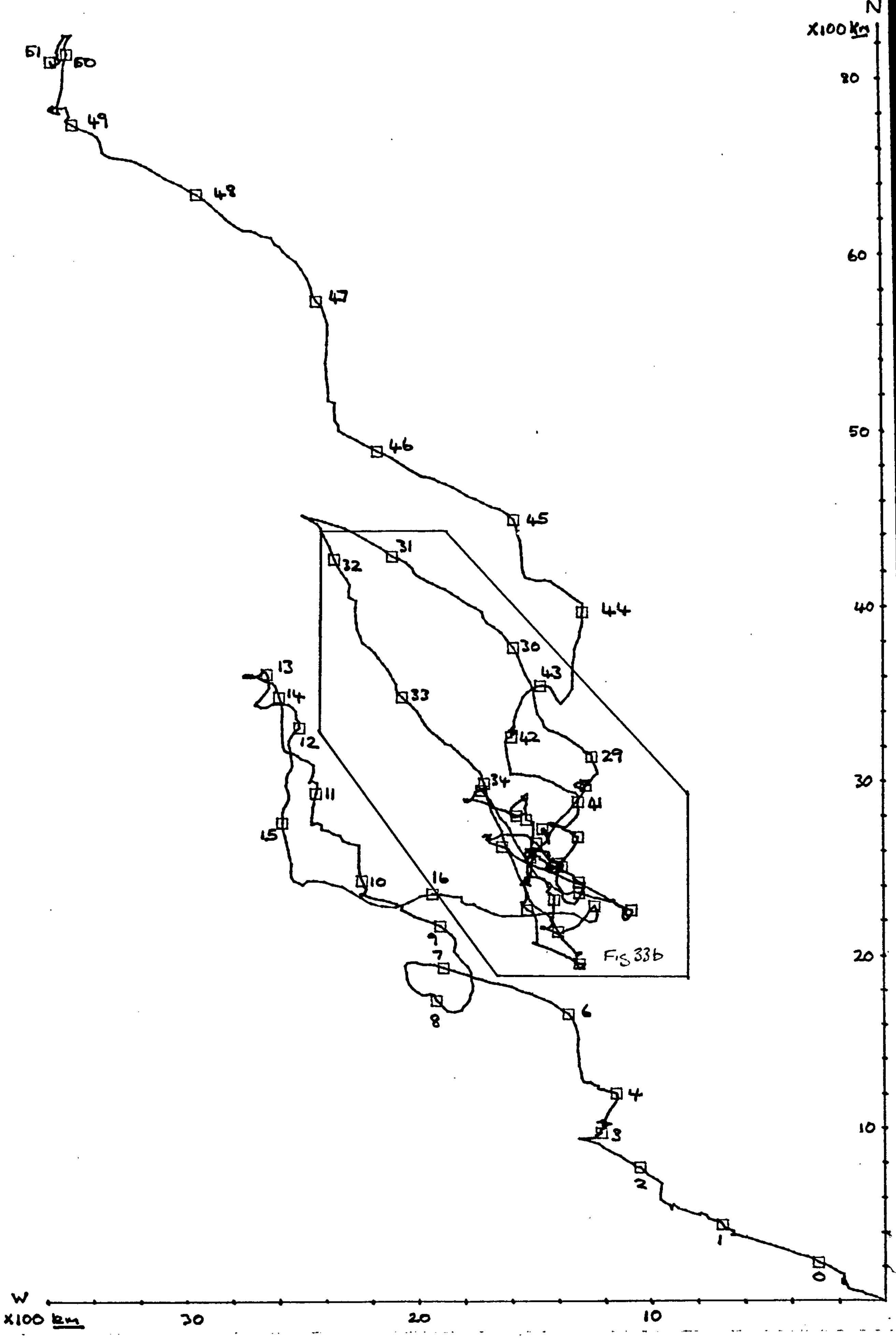

Fig 33a: Progressive vector diagram of wind at Stompneus Point weather station. ◻ day indicators.

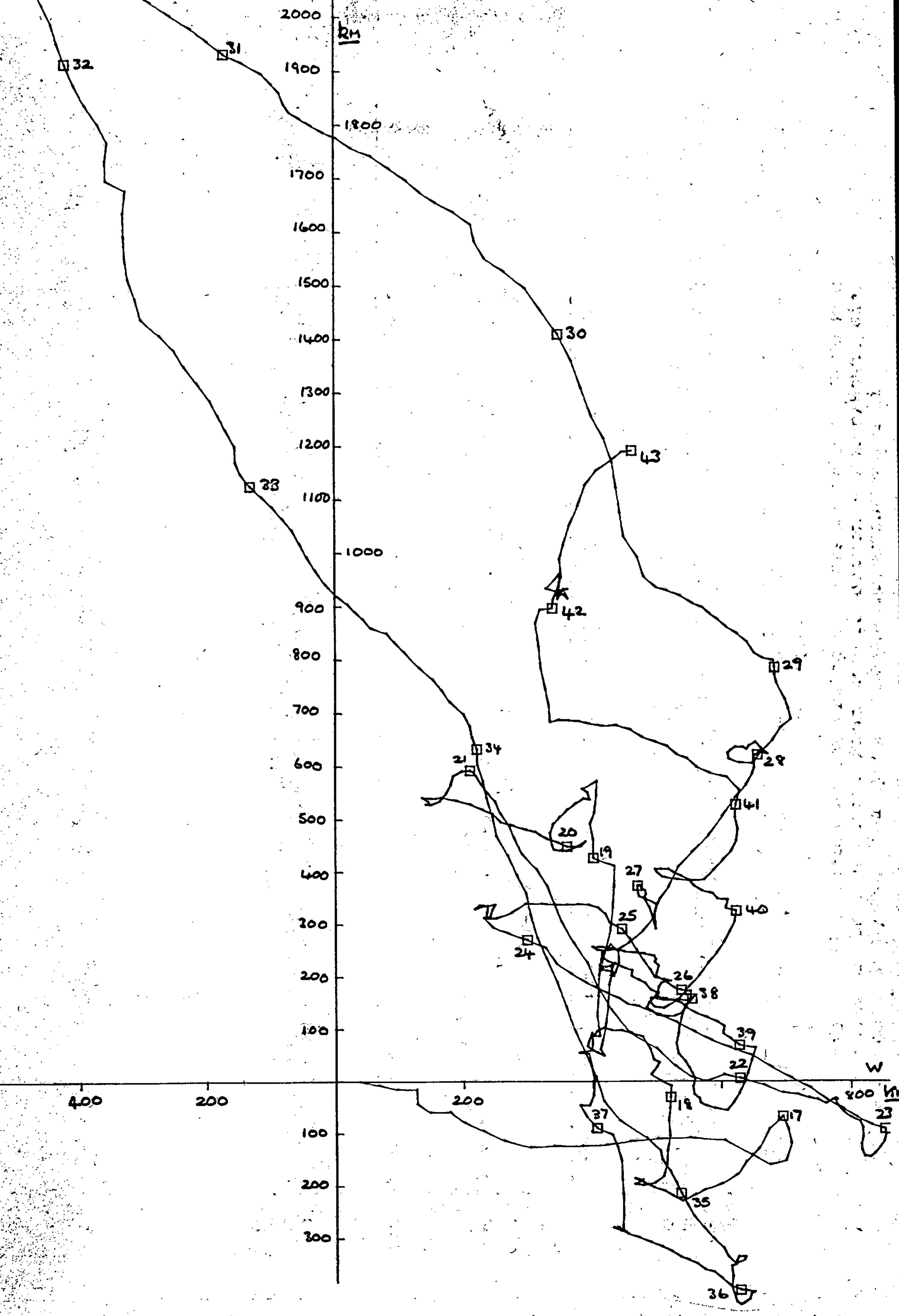

Fig 33b: Enlargement of the progressive vector diagram of wind for days 16 to 43. □ day indicators.

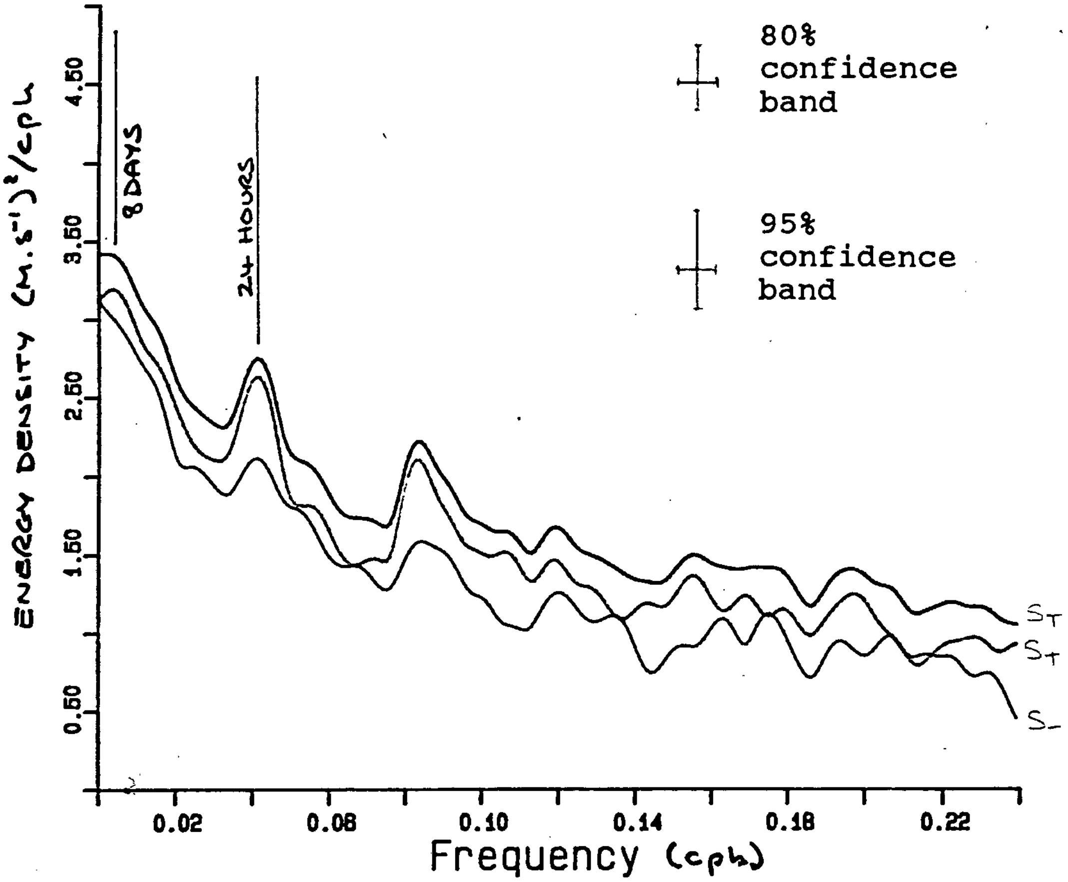

Fig 35: Rotary spectral estimates for winds at Stompneus Point weather station. $S_T$ total spectra. $S_-$ clockwise spectra. $S_+$ anticlockwise spectra.

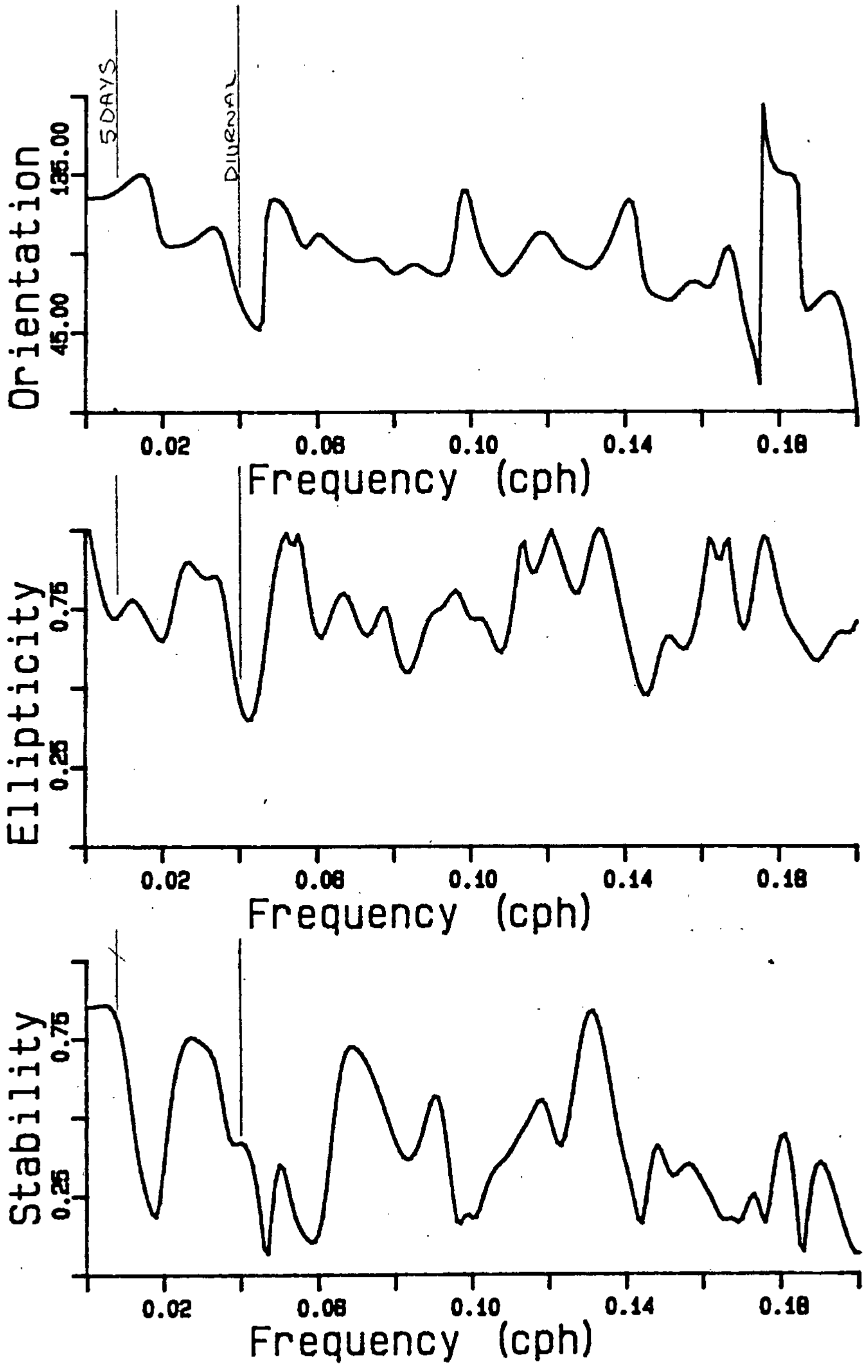

Fig 36: Elliptic properties for winds at Stompneus Point weather station. Top - ellipse orientation, with angles taken clockwise about true north. Middle - ellipse eccentricity. Bottom - ellipse stability.

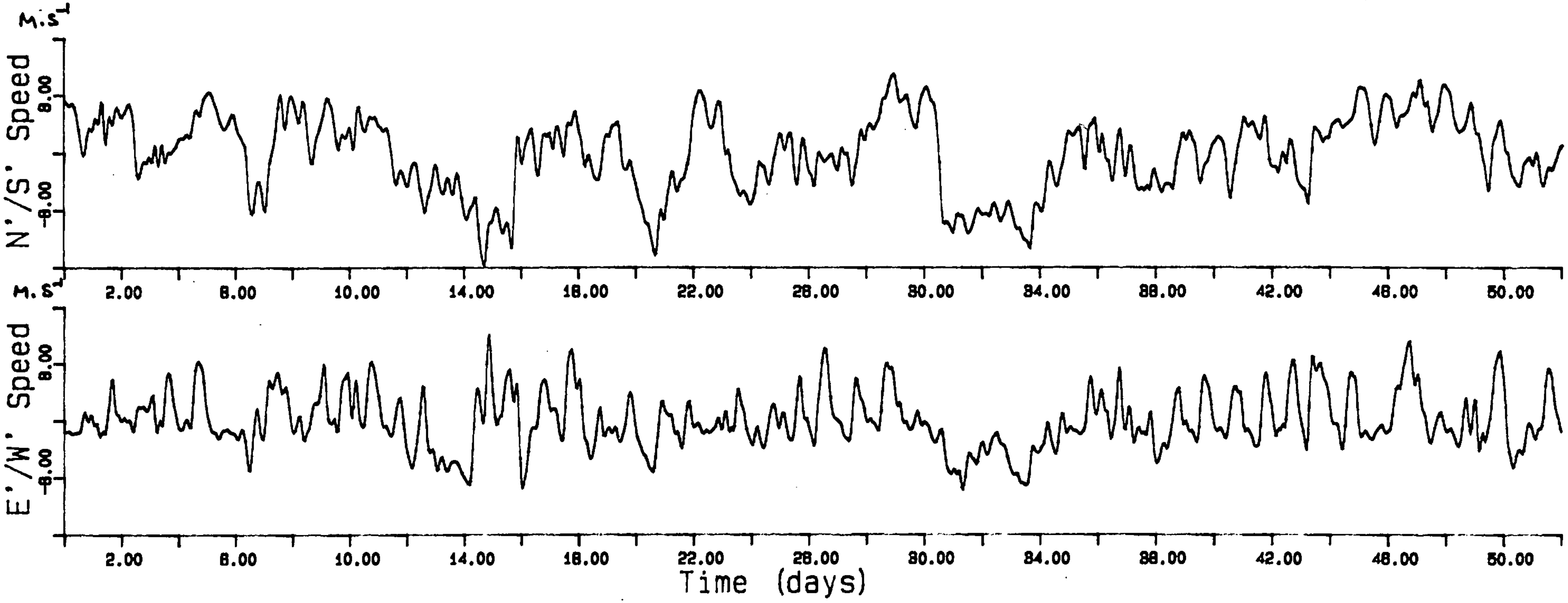

Fig 37: North/South and East/West wind components rotated anticlockwise through 55 degrees.

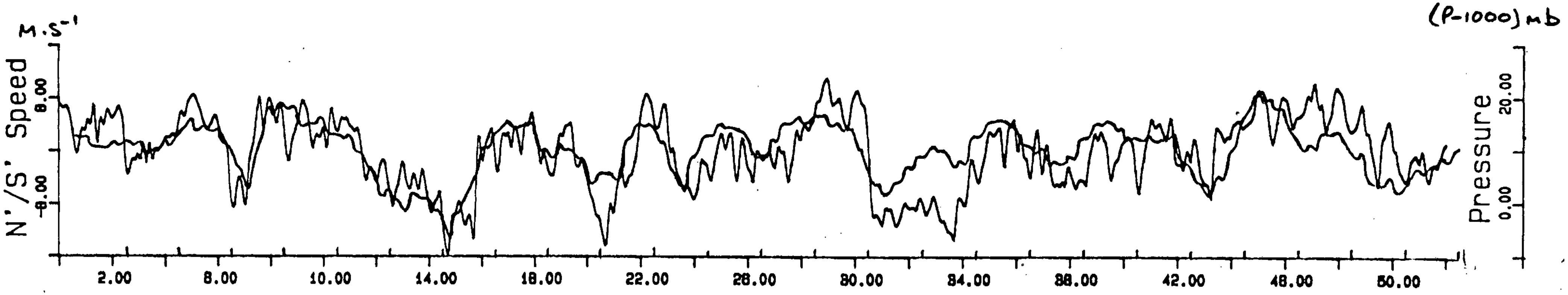

Fig 38: N'/S' wind component, with overlaid atmospheric pressure shifted by 12 hours.

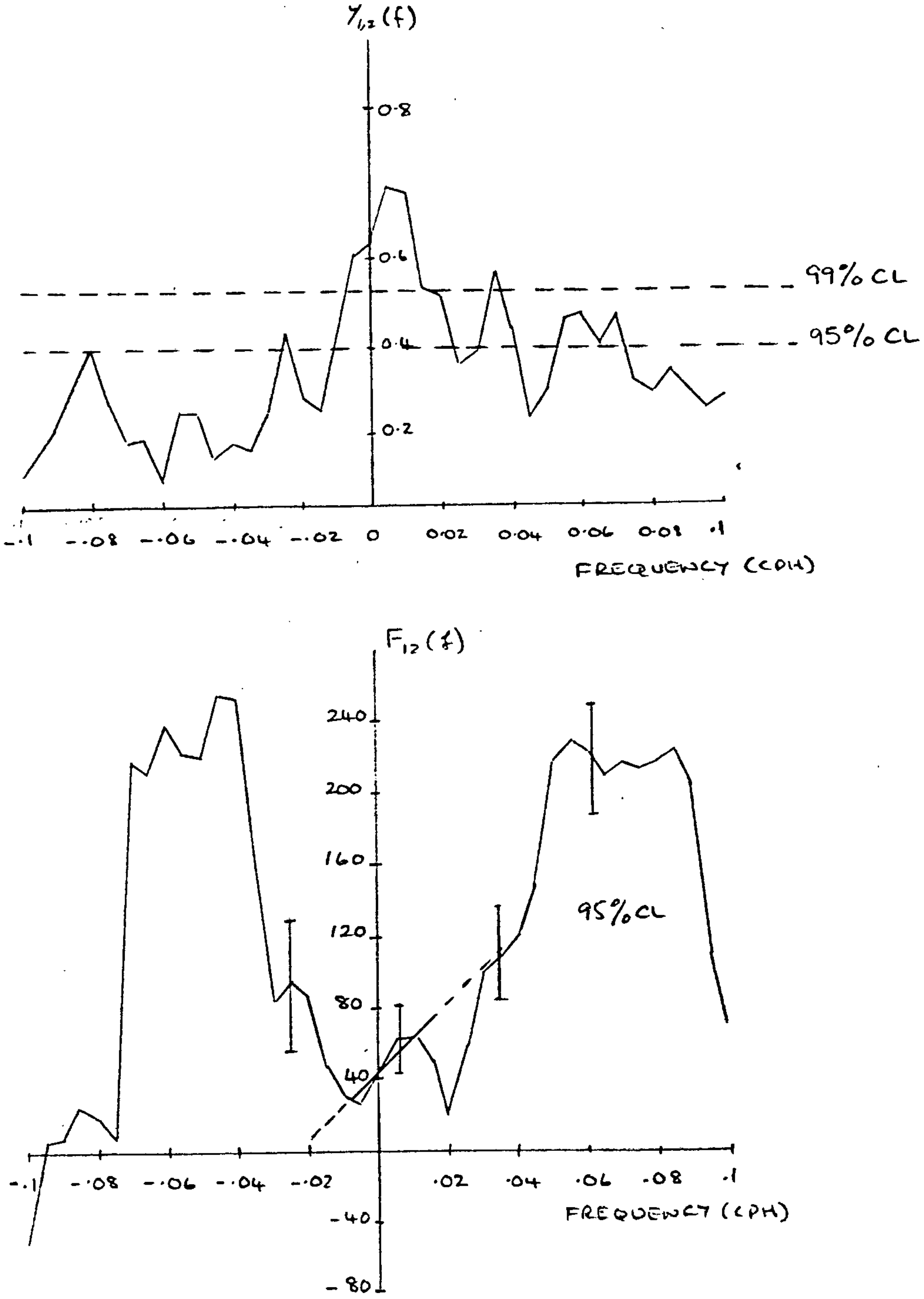

Fig 39: Vector coherence and phase for winds at Stompneus Point Weather station and upper currents at mooring A.

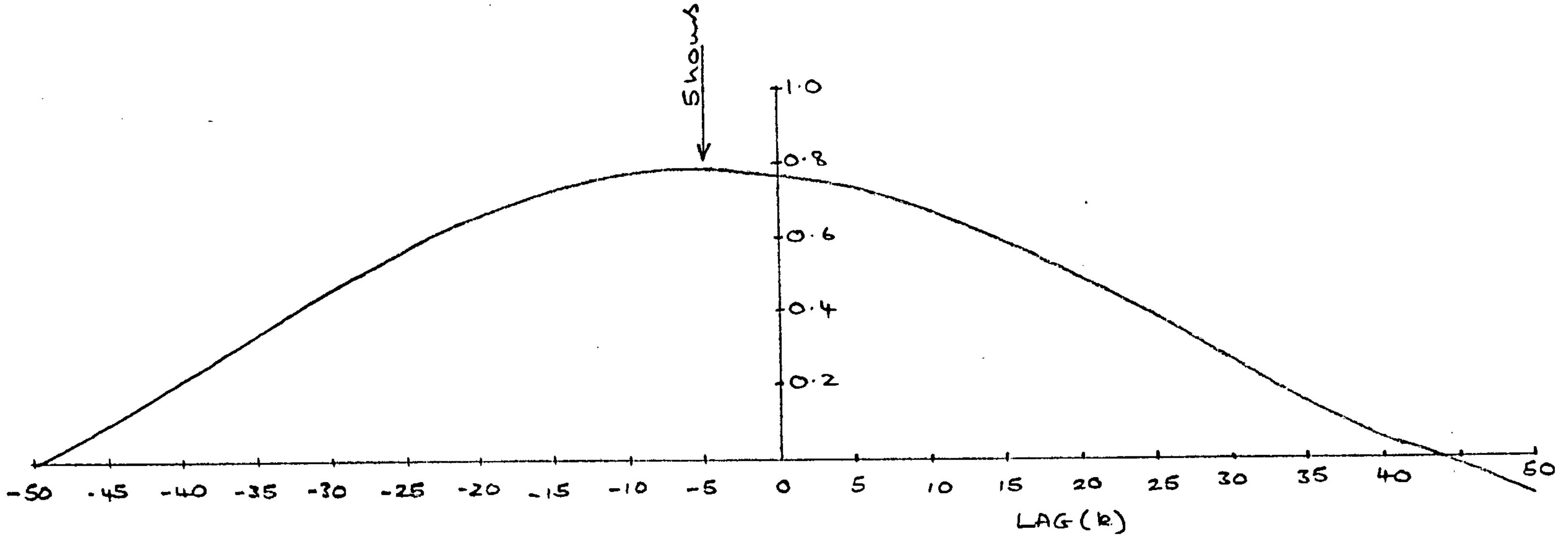

Fig 40: Cross correlation function (ccf) for low frequency winds at Stompneus Point weather station and upper currents at mooring A. Lag number K=-5 indicates that currents lead winds by about 5 hours.

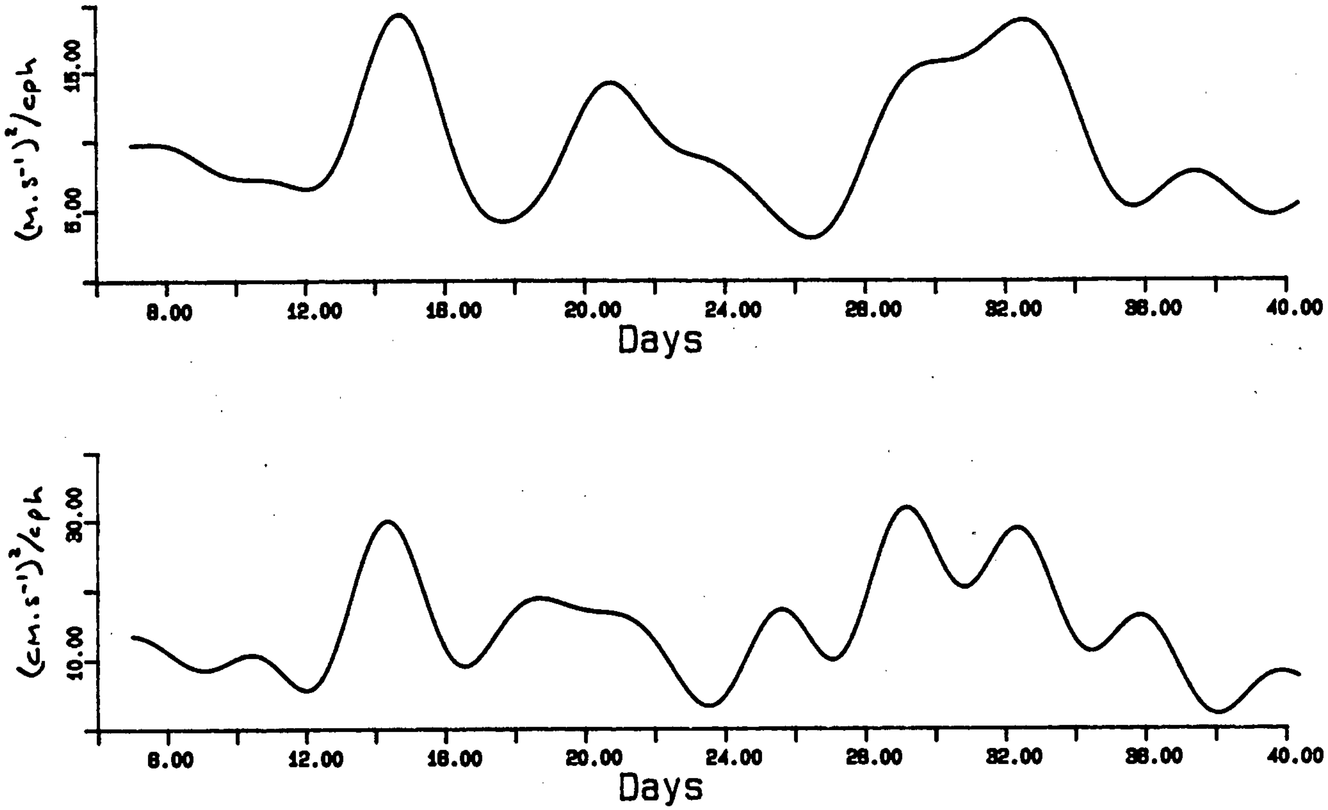

Fig 41: Demodulated N'/S' wind time series and upper N/S current measurements at mooring A. Demodulation at 5.5 days.

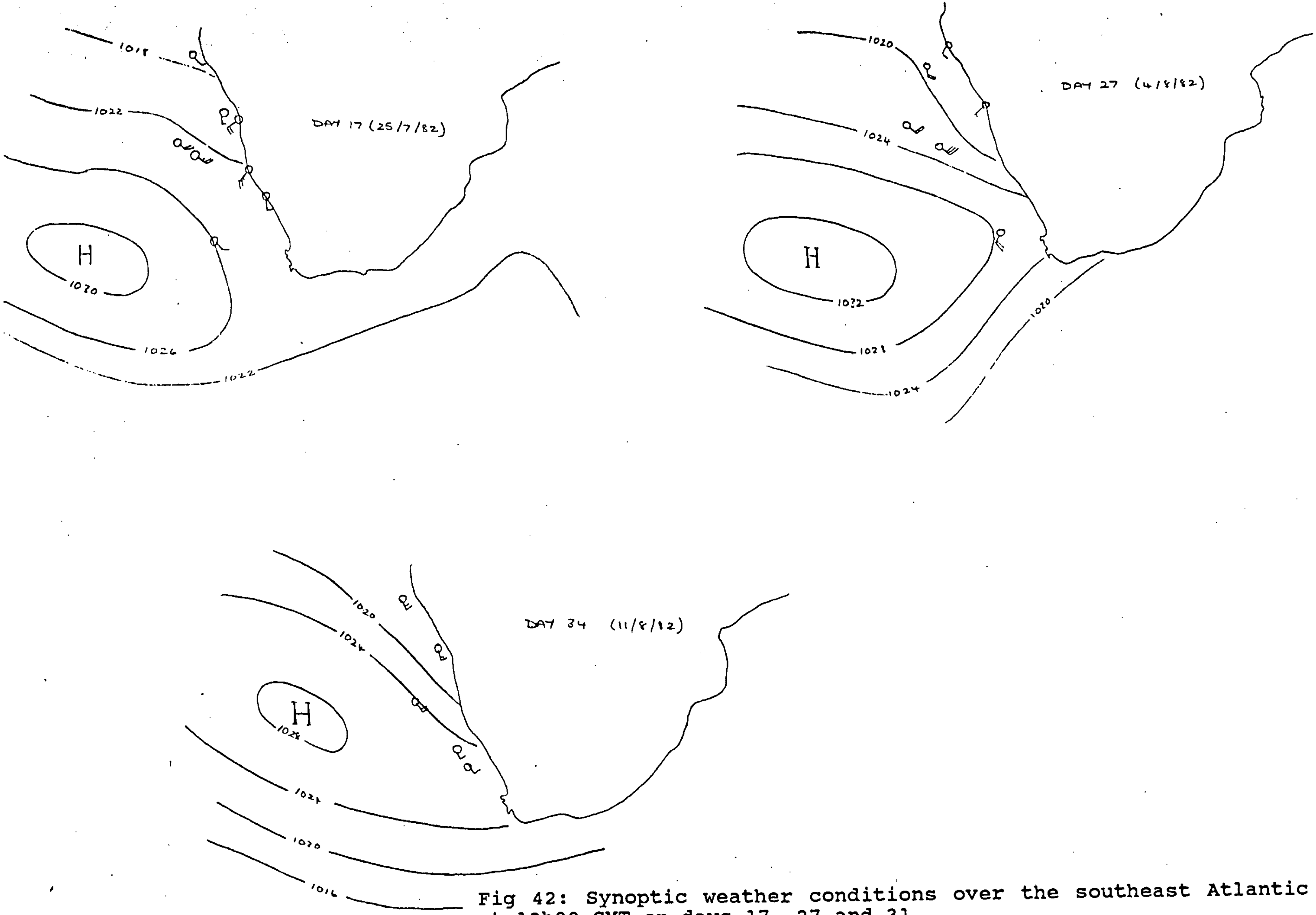

Fig 42: Synoptic weather conditions over the southeast Atlantic at 12h00 GMT on days 17, 27 and 31.

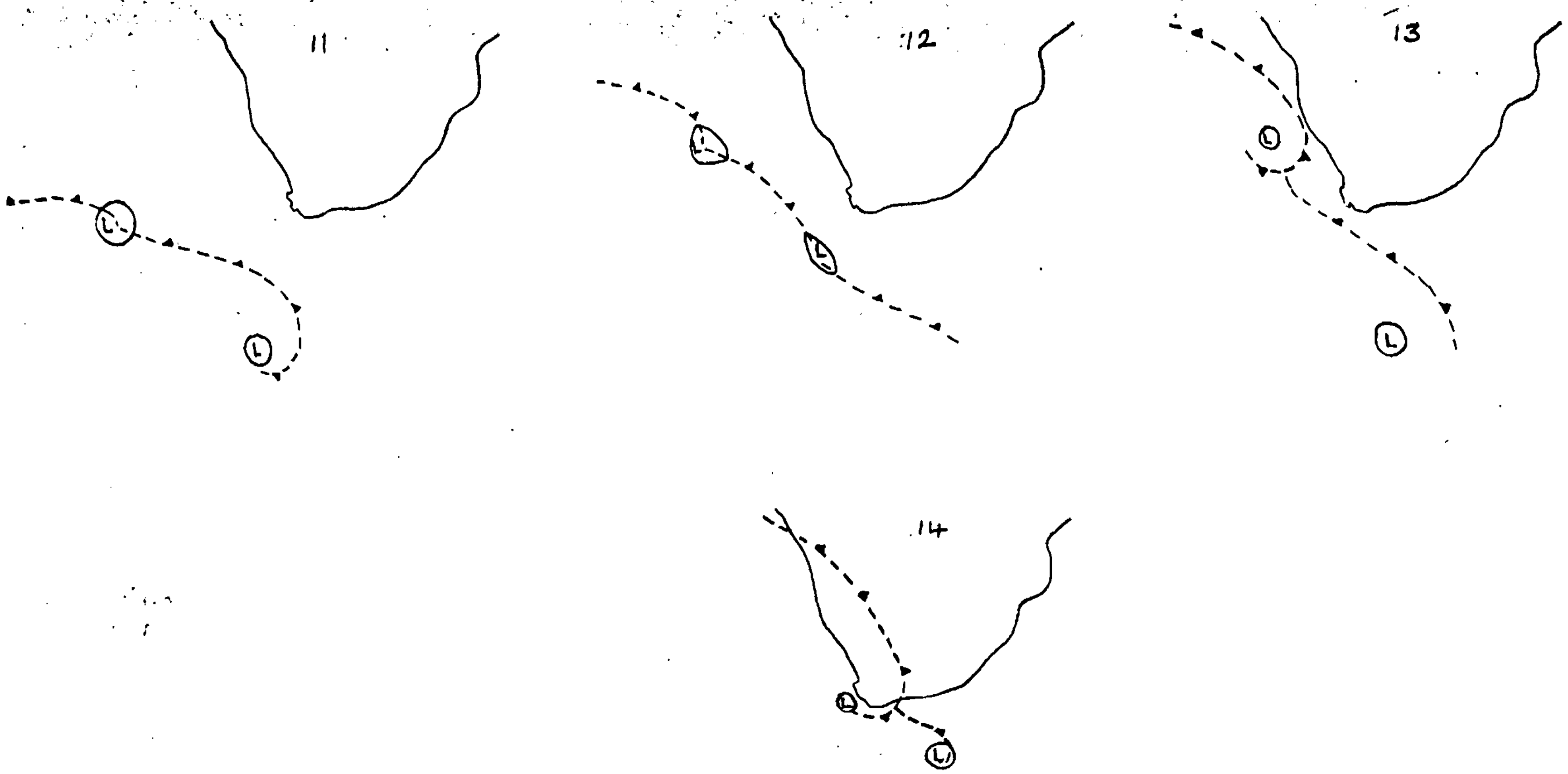

Fig 43: Frontal system active off the west coast of southern Africa, days 11 to 14.

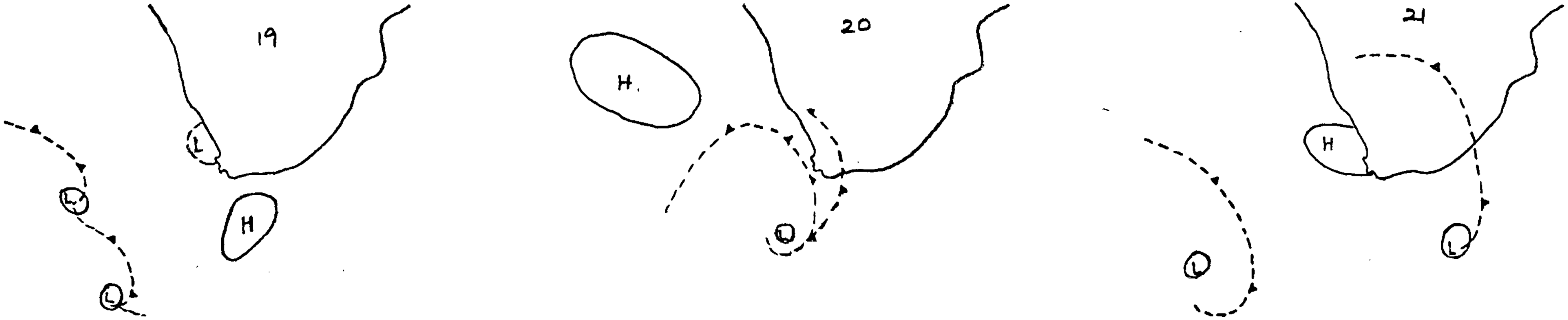

Fig 44: Frontal system active off the west coast of southern Africa, days 19 to 21.

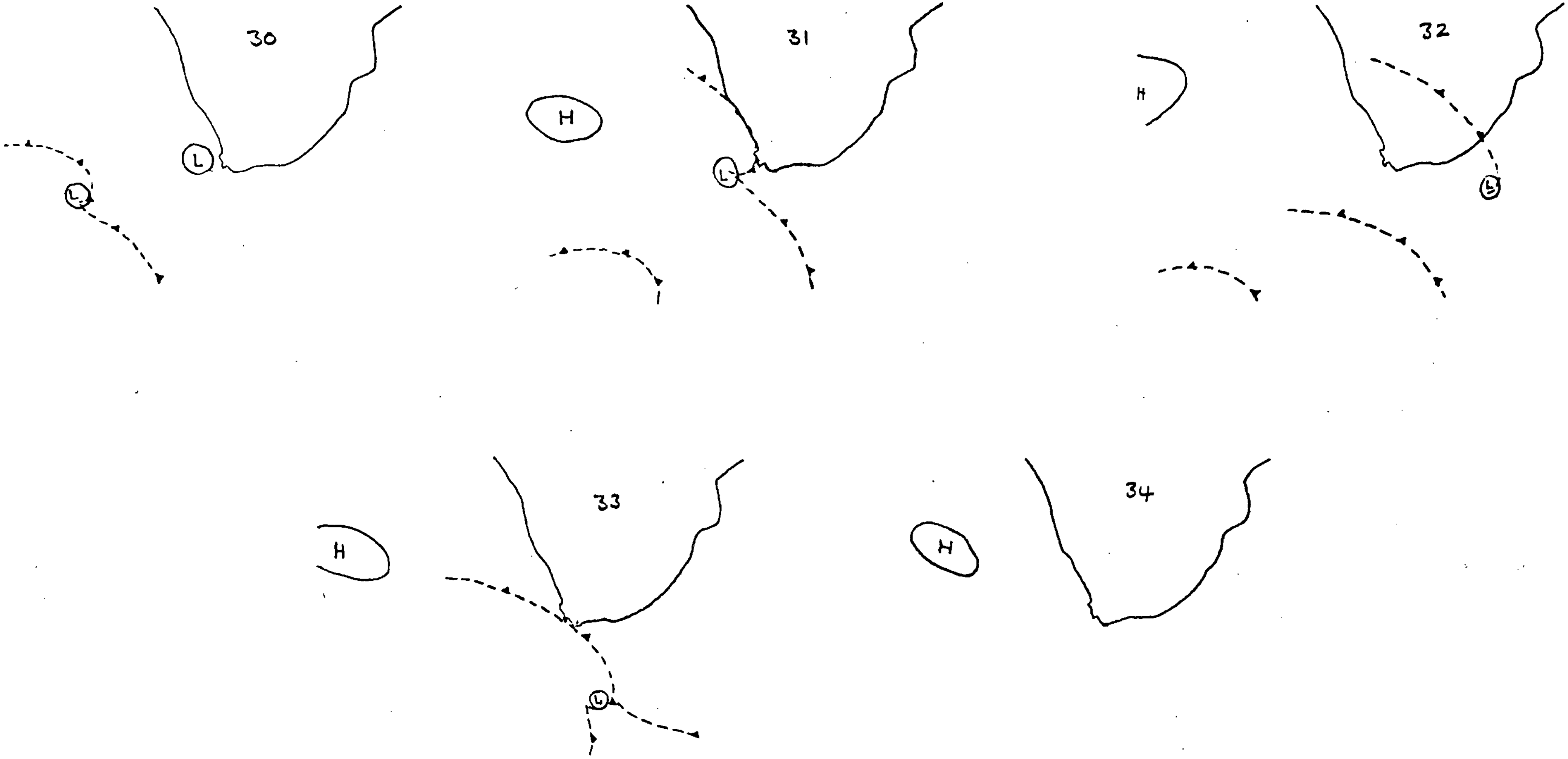

Fig 45: Frontal system active off the west coast of southern Africa, days 30 to 34 .

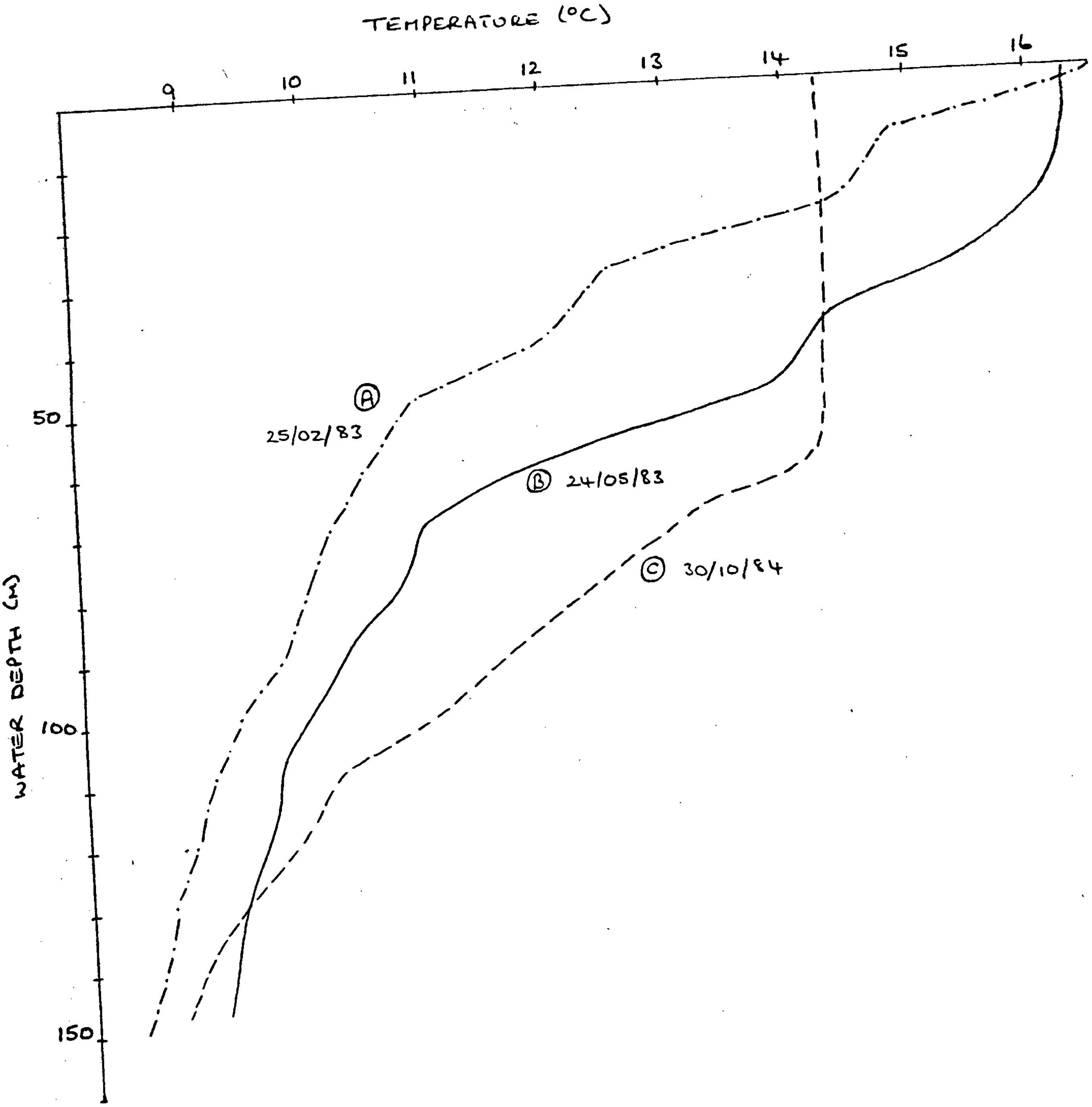

Fig 46: Water temperature profiles obtained in the near vicinity of mooring C on 25-02-83, 24-05-83 and 30-10-84.

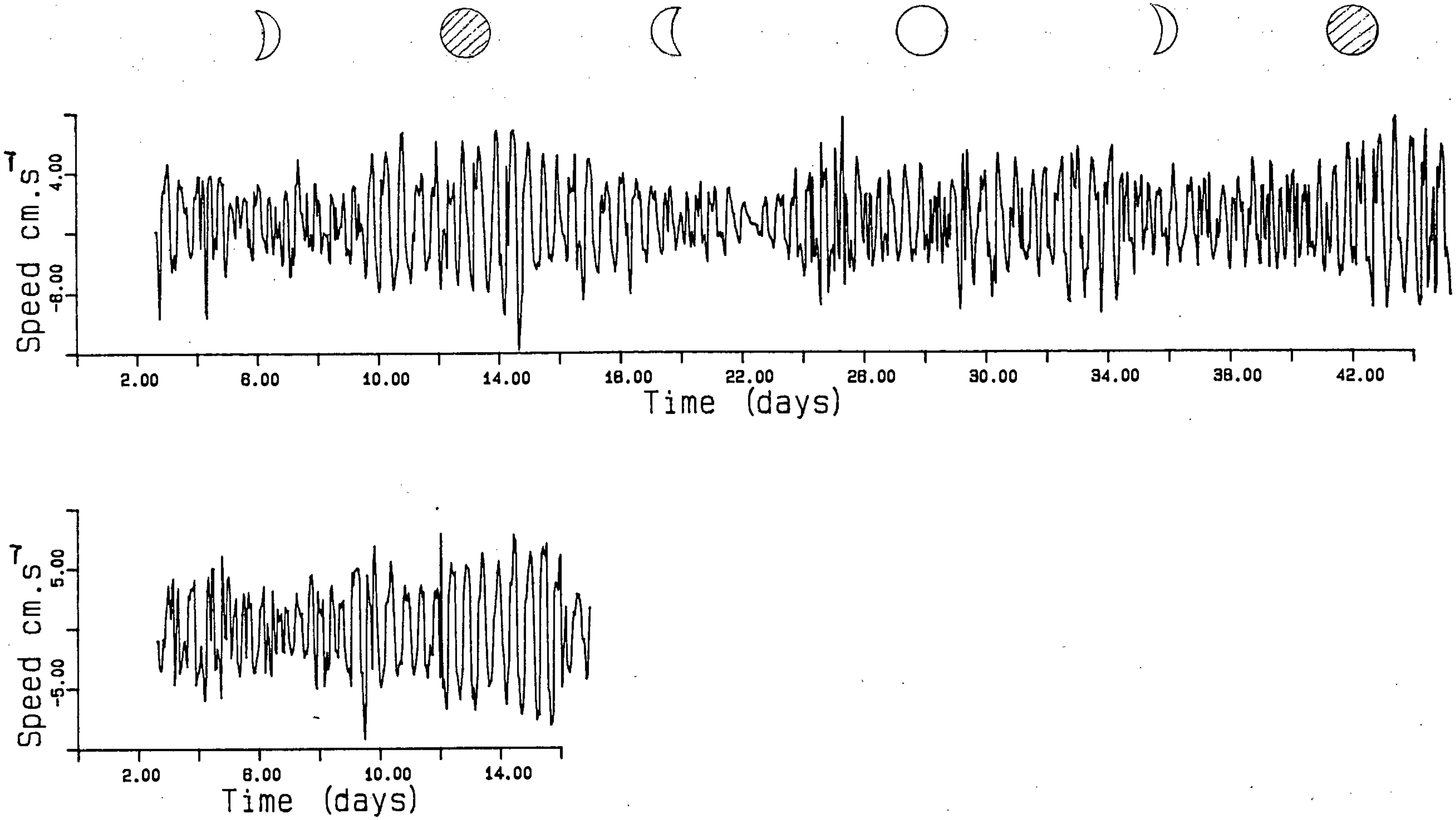

Fig 47: Semi-diurnal current speeds showing the effect of the baroclinic and barotropic tidal components in the upper and lower layers at mooring A.
Phases of the moon: ▨ New moon, ☾ First quarter, ○ Full moon
☽ Last quarter.

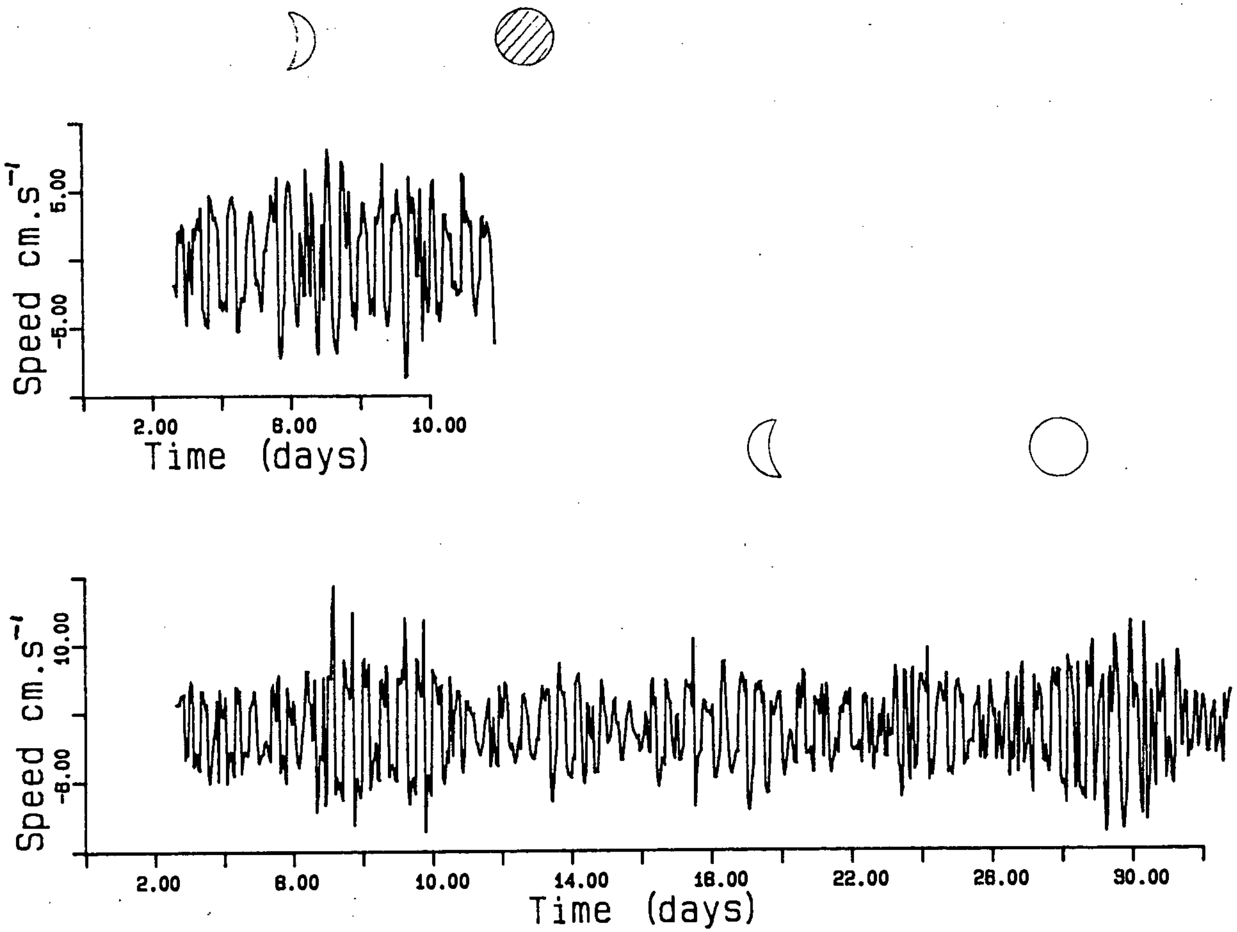

Fig 48: Semi-diurnal current speeds showing the effect of the baroclinic and barotropic tidal components in the upper and lower layers at mooring B.
Phases of the moon: ▨ New moon, ☾ First quarter, ○ Full moon ☽ Last quarter.

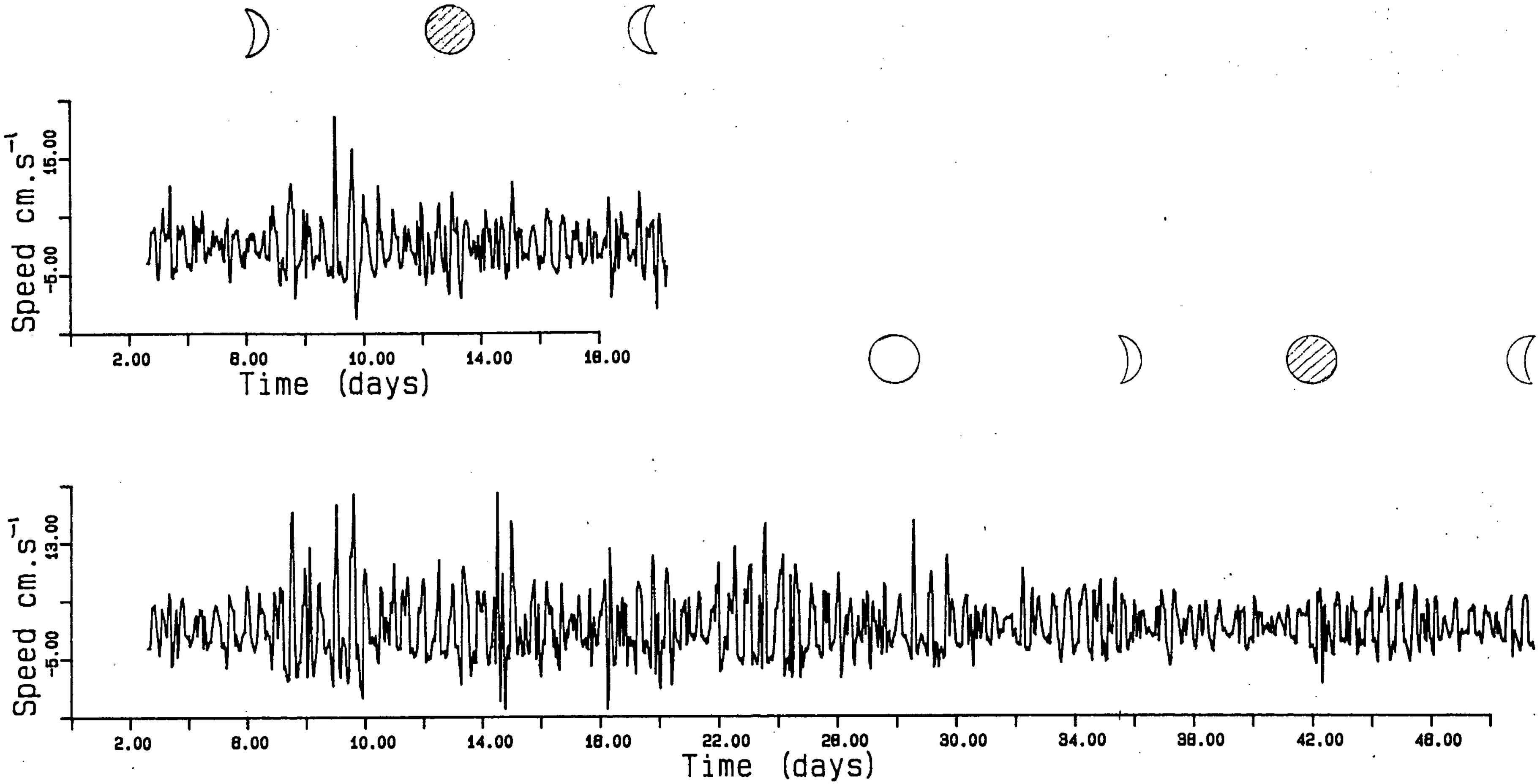

Fig 49: Semi-diurnal current speeds showing the effect of the baroclinic and barotropic tidal components in the upper and lower layers at mooring C.
Phases of the moon: ▨ New moon, ☾ First quarter, ○ Full moon
☽ Last quarter

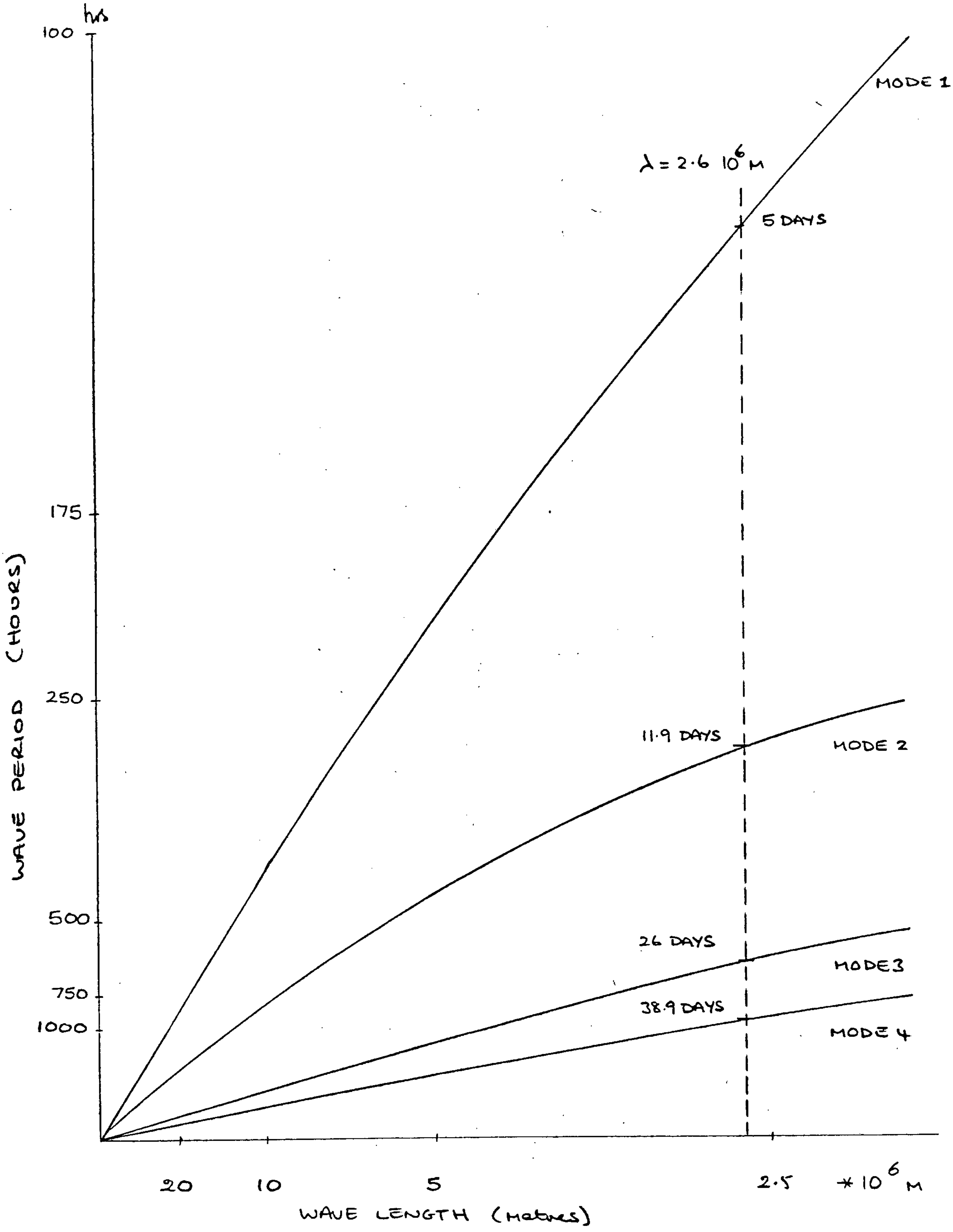

Fig 50: Dispersion curves obtained from the barotropic shelf wave model of Buchwald and Adams (1968).

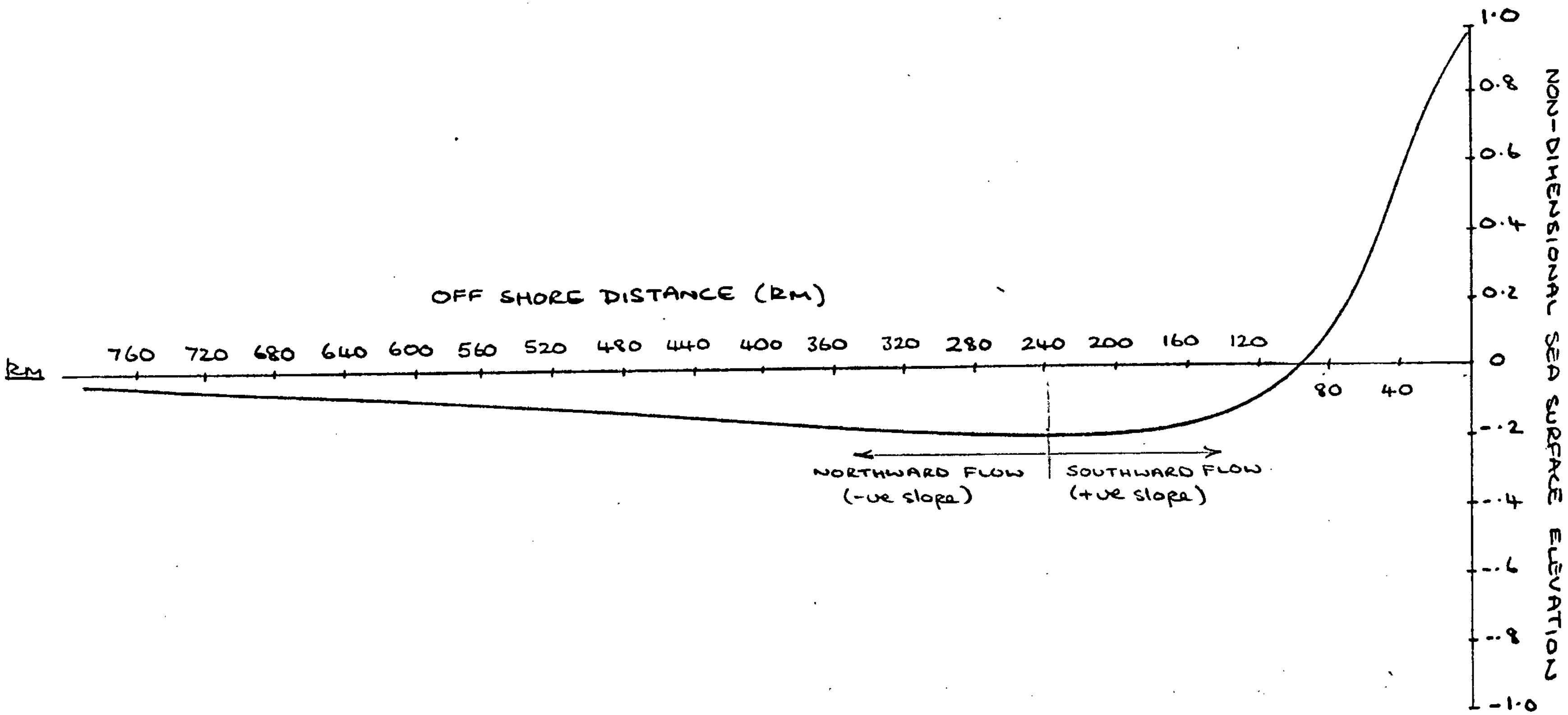

Fig 51: The non-dimensional sea surface elevation for the first mode barotropic shelf wave. Turning point at about 240 km off shore.

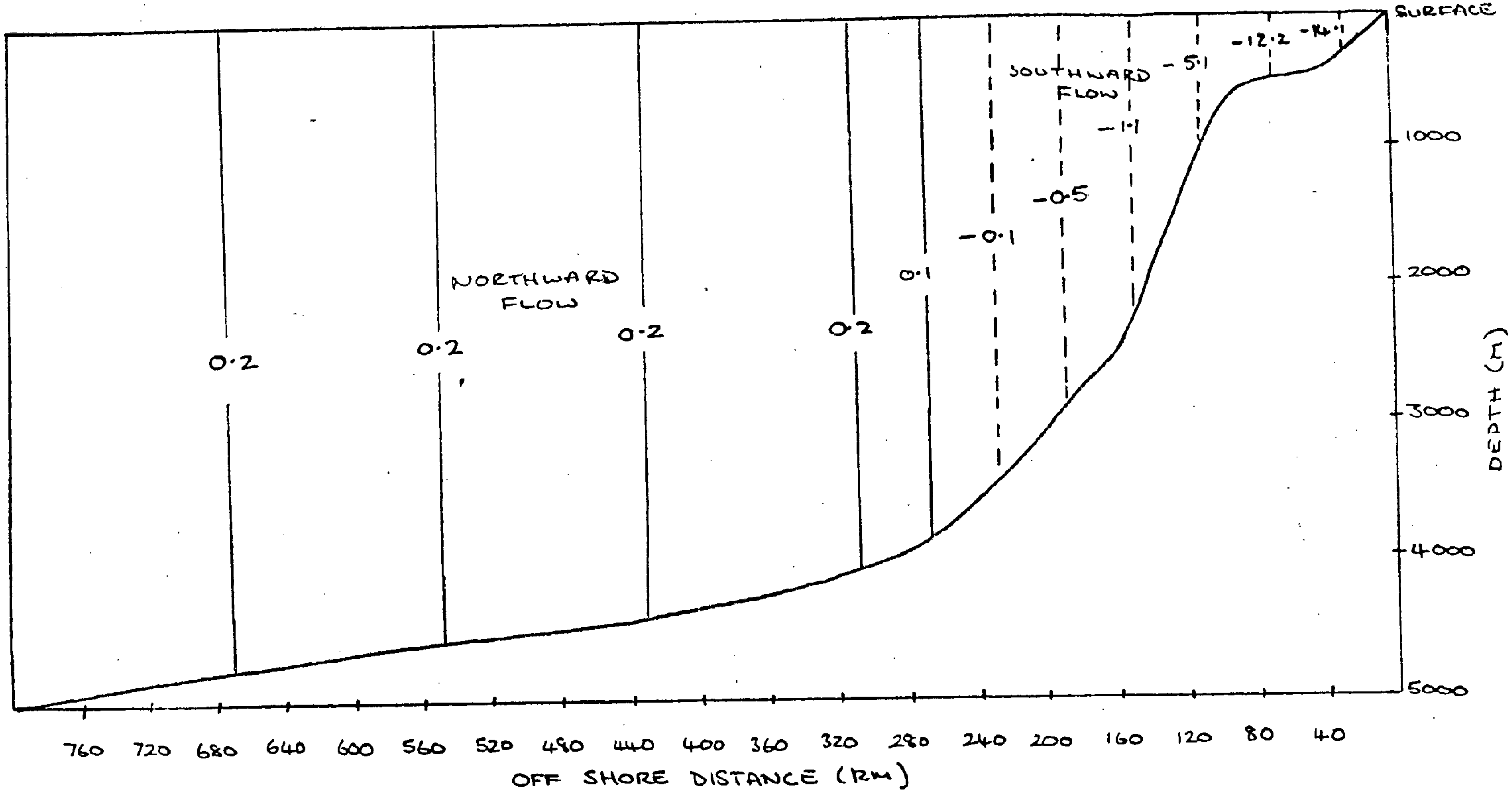

Fig 52: Longshore current isotachs for the first mode barotropic shelf wave. Southward flow shown inshore off about 240 km.

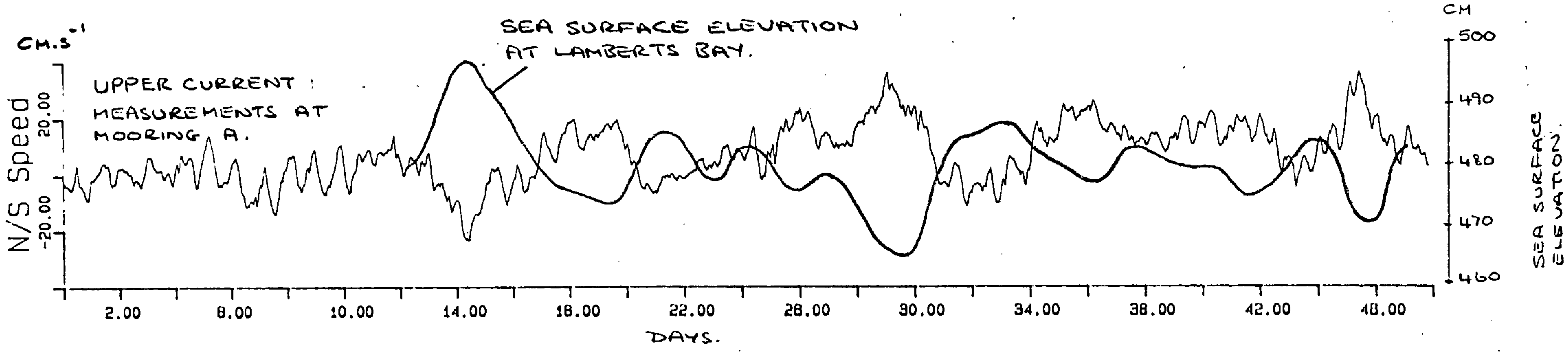

Fig 53: Upper North/South current speeds at mooring A, with observed sea surface elevations at Lamberts Bay superimposed.

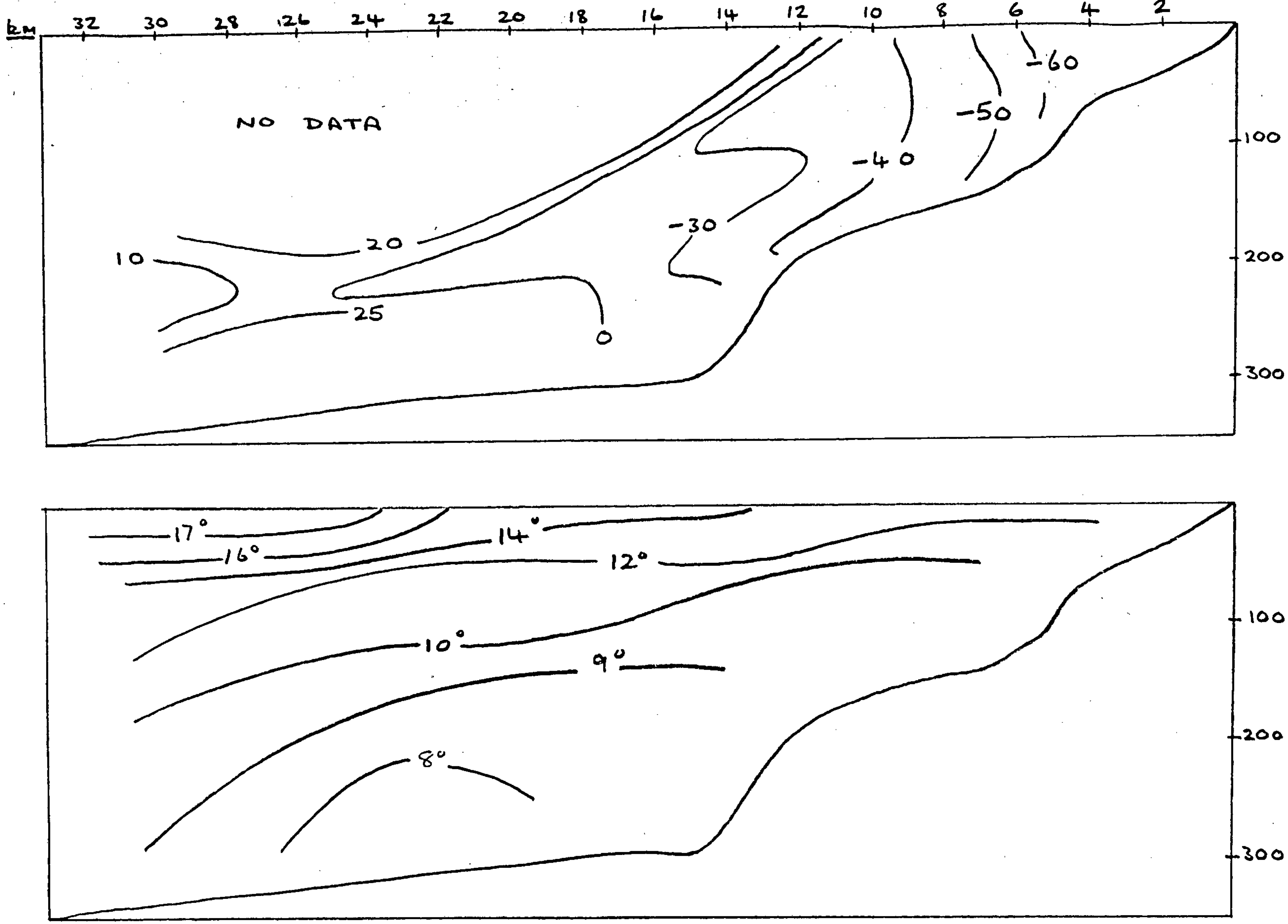

Fig 54: a) Longshore current isotachs along a line west of Cape Columbine obtained during a current profiling experiment in May 1983. b) Temperature section along current profiling line, May 1983.

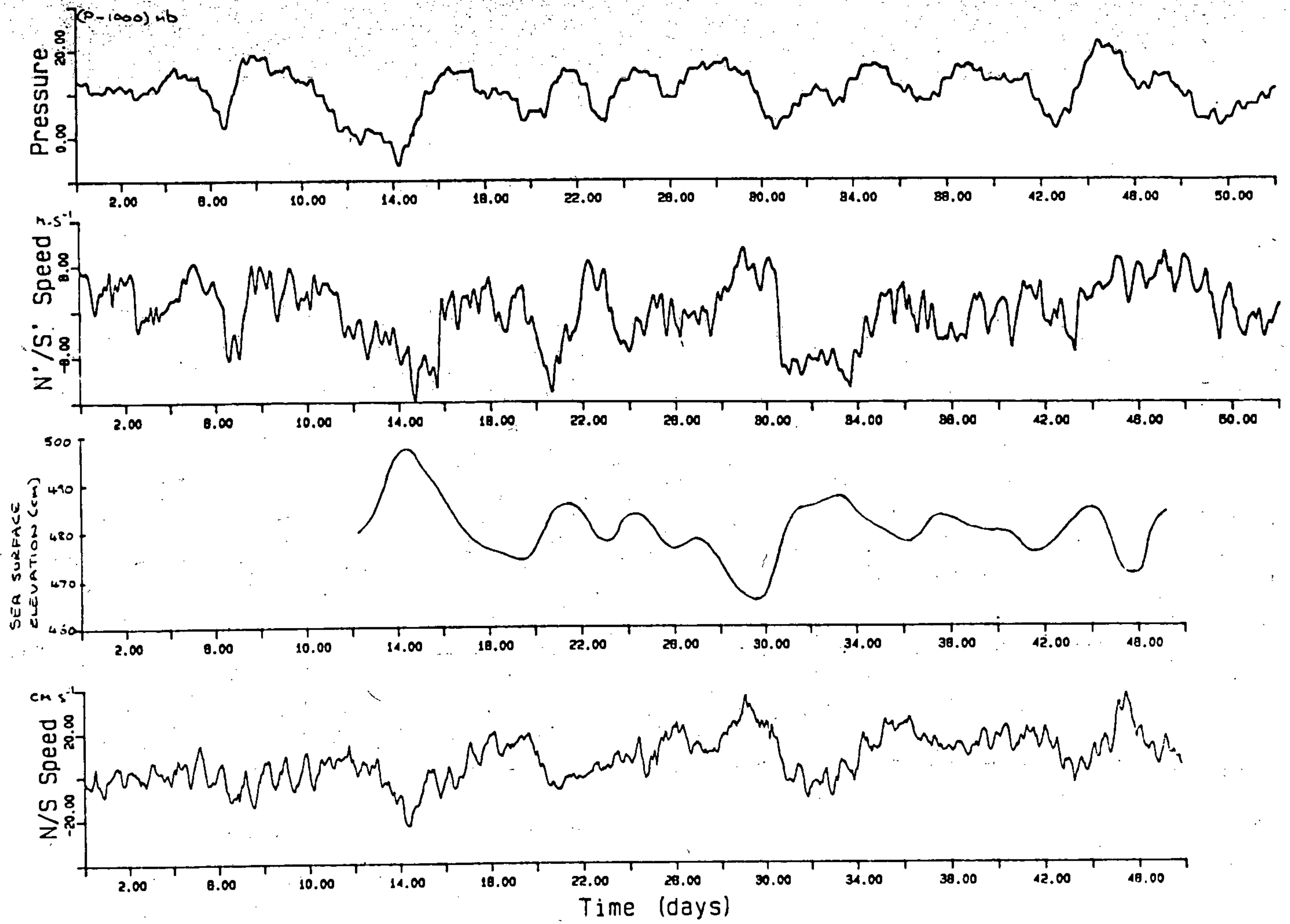

Fig 55: Composite time series records of concurrent meteorological and hydrological data. From top to bottom - atmospheric pressure (Stompneus Point), N'/S' winds (Stompneus Point), sea surface elevation (Lamberts Bay) and upper N/S currents (mooring A).